[redacted]

WT-1465

UNCLASSIFIED

This document consists of 116 pages.

No. 163 of 215 copies, Series A

OPERATION PLUMBBOB

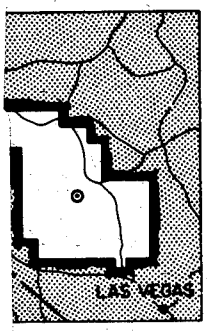

NEVADA TEST SITE

MAY-OCTOBER 1957

AUG 8 1974

Project 32.4

FALLOUT STUDIES AND ASSESSMENT OF RADIOLOGICAL PHENOMENA

Issuance Date: October 30, 1959

CIVIL EFFECTS TEST GROU

[redacted]

[redacted]

[redacted]

1059152

When no longer required, this document may be destroyed in accordance with applicable security regulations.

DO NOT RETURN THIS DOCUMENT

DISCLAIMER NOTICE

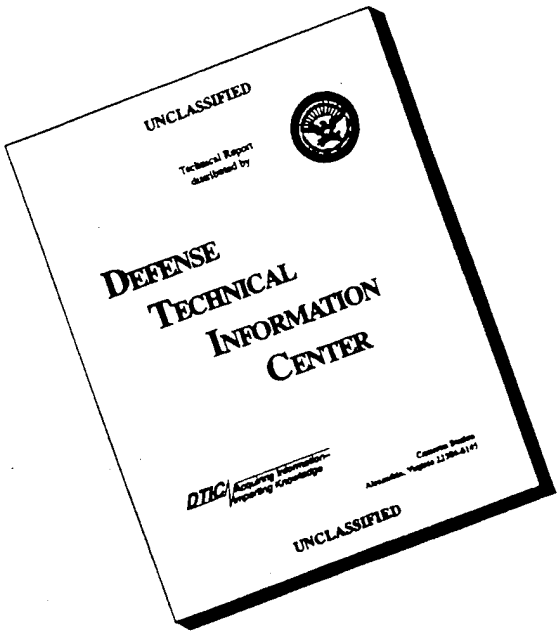

THIS DOCUMENT IS BEST QUALITY AVAILABLE. THE COPY FURNISHED TO DTIC CONTAINED A SIGNIFICANT NUMBER OF PAGES WHICH DO NOT REPRODUCE LEGIBLY.

Defense Nuclear Agency
6801 Telegraph Road
Alexandria, Virginia 22310-3398

SSTS

7 November 1995

MEMORANDUM FOR DEFENSE TECHNICAL INFORMATION CENTER
ATTENTION: OCD/Mr. Bill Bush

SUBJECT: Declassification of WT-1465 and Withdrawal of AD-A995003

The Defense Nuclear Agency Security Office (ISTS) has declassified the following report:

WT-1465 (no DTIC accession number available)

Distribution statement "A" applies.

Since the original report has been declassified, the extracted version (AD-A995003) is no longer applicable.

Therefore, this office requests that the extracted version be withdrawn from the DTIC system. A copy of the original report is enclosed to be entered into your system. This office would appreciate notification of your accession number, once it is assigned.

FOR THE DIRECTOR:

JOSEPHINE B. WOOD
Chief, Technical Support

Enclosure:
A/S

[redacted]

Report to the Test Director

FALLOUT STUDIES AND ASSESSMENT OF RADIOLOGICAL PHENOMENA

By

E. A. Schuert

Approved by: C. F. MILLER
Director
Program 32

Approved by: R. L. CORSBIE
Director
Civil Effects Test Group

U. S. Naval Radiological Defense Laboratory
San Francisco, California
November 1958

[redacted]

[redacted]

[redacted]

Blank Pages

ABSTRACT

Several related fields important to fallout reclamation research were investigated.

A comparison of the ionization from an infinite-plane photon source to that of a real surface having attenuating irregularities was made. The results for Nevada desert soil surfaces show terrain attenuation of the photon source to be as high as 40 per cent when measured with a T1B survey meter at 3 ft. This attenuation was found to be a function of time since detonation and to fall off rapidly with height, becoming small at 50 ft above the terrain. A technique for rapidly evaluating this factor is presented.

Comparisons were made on fallout particles resulting from one tower-supported and one balloon-detonated shot in order to evaluate the effect of shot towers on the nature of fallout particles. The inclusion of the iron from the shot tower into the fireball caused a significant increase in the amount of gamma activity deposited in the local fallout, suggesting a means of controlling the balance of activity between local and world-wide fallout, as well as questioning the representativeness of tower-shot fallout to operationally delivered low air-burst phenomenology.

Several prototype collecting instruments were evaluated, and the results of their applicability to future experimentation were discussed.

The results of the technical measurements on several fallout events are given for reference to the work presented in the final report of Project 32.3.

ACKNOWLEDGMENTS

Although this report represents the work of many investigators, major contributions were made by the following:

L. E. Egeberg, Project Officer of the field phase of this experiment.

The Analytical and Standards Branch, USNRDL, for the sample analyses described in Appendix B.

Carl F. Miller for over-all assistance and, especially, for the theoretical treatment of the gamma spectral analysis.

I would also like to thank C. E. Adams for his support in the study of fallout particles, N. Farlow for assistance in particle density determinations, Miss M. Sandomire with respect to statistical procedures, and Miss J. Sanderson and C. Ellis for invaluable help in data reduction.

CONTENTS

CONTENTS (Continued)

ILLUSTRATIONS

CHAPTER 2 TERRAIN ATTENUATION FACTOR

ILLUSTRATIONS (Continued)

TABLES

TABLES (Continued)

TABLES (Continued)

[redacted]

Chapter 1

OBJECTIVES

This project was designed to investigate several related fields important to research in the reclamation of areas contaminated by fallout. Certain of the experiments were aimed at answering specific questions wherein prior knowledge was insufficient; whereas others took advantage of new circumstances to extend the knowledge of fallout phenomenology. Specifically, Chap. 2 evaluates the effect of natural terrain on the attenuation of the gamma source materials as compared to the theoretical smooth plane where no roughness or terrain attenuation exists. Chapter 3, by taking advantage of balloon and tower-supported detonations, describes the effect of shot towers on the physical and chemical properties of fallout material. Chapter 4 documents the fallout in support of Project 32.3, wherein a detailed knowledge of the time-dependent phenomena around the radiological shelter was required. Chapter 5 describes the results of a study of prototype instrumentation developed for the collection of countermeasures data.

The objectives of Project 32.4 were then to (1) study the terrain attenuation factor for gamma fields; (2) study the effect of shot towers on the physical, chemical, and radiochemical properties of fallout material; (3) provide documentary support to Project 32.3; and (4) field test prototype instrumentation developed for the collection of countermeasures data.

[redacted]

Chapter 2

TERRAIN ATTENUATION FACTOR

2.1 BACKGROUND

Under present theory, if the absolute photon-emission rate from a smooth plane and the gamma-energy spectrum of the photons are known, the gamma-field intensity at any height above this plane can be calculated.[1] Such calculations are frequently used in the reduction of field data when it is desired to know from the gamma-field measurements the quantity or fraction of the device deposited in that area.[2] These conversions for a real or rough surface require a correction for the attenuation of gamma activity by the soil surface. This attenuation effect was first demonstrated at Operation Jangle.[3] Subsequent studies[4] were made using data obtained for other purposes at later test operations; however, certain pertinent data were missing, and thus the quality of the results obtained left the conclusions questionable. Measurement of all necessary parameters was attempted at Operation Plumbbob to increase the accuracy of such an experimentally determined correction factor. The terrain attenuation factor is defined as the ratio of the observed ionization rate to that calculated for a smooth plane.

If the absolute photon-emission rate of the deposited material is determined, the absolute ionization rate at some height above this plane can be calculated using the methods derived for a smooth plane.[1] This calculated value can then be directly compared with an accurate measurement of the actual ionization rate over the fallout area at the same height. The difference between the measured reading and that calculated will be a measure of the reduction due to attenuation by surface irregularities.

Another method for determining the effect of terrain on radiation intensity may be possible: It is assumed that, when measurements of gamma ionization are made at heights much greater than 3 ft, the effect of soil attenuation is minimized as the measuring instrument approaches the altitude where the path of the gamma photons is not obstructed by irregularities in the earth's surface. Therefore at some altitude the calculated intensity values for an ideal smooth plane should approach the measured intensity values over a real plane. If this is true, the evaluation can be accomplished without determining the absolute photon-emission rate per unit area by simply taking relative readings as a function of altitude at a time when the gamma-energy spectrum of the source is known. Then, by assuming a photon-emission rate of, say, 10^6 photons/sec/sq ft and using the computations of Werner[5] and Van Lint,[6] one can determine for the measured spectrum the air ionization rate in milliroentgens per hour as a function of altitude. This calculated curve can be compared to the measured data by normalizing at an altitude above which the ratio of calculated to measured is a constant. The ratio of the measured value at 3 ft to that calculated for 3 ft will be a determination of the terrain attenuation factor for the 3-ft measurement. Comparison of this approach to the absolute method will de-

termine whether absolute radiation measurements need to be made or whether the only requirement is that the measurements be relative to each other.

2.2 PROCEDURE

Major participation for Project 32.4 for this objective was in shot Shasta. A limited number of measurements were also made in shots Priscilla and Diablo.

2.2.1 Shasta Shot

On the morning of D+2 day, a satisfactorily flat radiation field was found in the vicinity of the Project 32.3 radiological shelter. This underground shelter was used as the center of a 1000-ft-radius 43-point gamma survey made at a height of 3 ft. An AN/PDR/T1B survey meter was used which had been calibrated with a set of Co^{60} standards the day of the measurements. At each of the 43 points the meter was first zero set; then four readings were taken at azimuths 90° apart.

Coincident with this survey, a fallout sample collected over 2.68 sq ft at the center of the circular area was being analyzed at the U. S. Naval Radiological Defense Laboratory (USNRDL) to determine, by gamma spectroscopy,[7] the absolute photon-emission rate per unit area emanating from the fallout radiation field within the area. The sample had been collected in the open-close collector (OCC) installed on the top of the shelter.

Also, during the morning of D+2 day, a determination of radiation intensity as a function of height above the center of the area was made. Measurements were taken from a helicopter by suspending the same survey meter employed in the surface measurements 1 ft below the aircraft. Readings were taken at 100-ft intervals from 100 to 1500 ft above the surface.

Documentary photographs of the area were taken to define the roughness of the terrain for comparison with other soil types and surface environments.

2.2.2 Priscilla and Diablo Shots

Limited measurements made on these detonations employed the same general techniques described for Shasta shot, with the exception that few measurements above an altitude of 3 ft were obtained. Attempts were made to suspend instruments from latex balloons, having a free lift of approximately 25 lb, to obtain gamma-intensity measurements as a function of altitude. The survey meter, equipped for remote readout, was suspended from the balloon harness. The meter was raised to predetermined heights, and readings were taken via a cable to a remote meter on the ground. Because of adverse wind conditions and the delicate nature of the balloons, this phase of the study failed. In lieu of the balloons a 60-ft boom crane was used on shot Diablo.

2.3 RESULTS

2.3.1 Shasta Shot

Figure 2.1 shows the gamma-radiation field over the area studied. Readings (in milliroentgens per hour) were made with survey meter AN/PDR/T1B-146. Four readings at 90° azimuths were taken at each point, the meter being zero set before each set of readings. In no case did any of these individual readings at any one point vary by more than 5 mr/hr. This amounts to a variation of from 2.5 to 5 per cent. Measurements are listed in Table 2.1. Table 2.2 lists the radiation measurements made over the selected area as a function of altitude. The shelter was located at an elevation of 4540 ft above mean sea level. All readings were again taken with survey meter AN/PDR/T1B-146, the meter being zero set before each reading.

The surface survey-meter readings were corrected for meter-scale calibration. In addition, such readings required correction for directional shielding by the instrument relative to the Co^{60} calibration direction and for shielding due to the presence of the monitor. These cor-

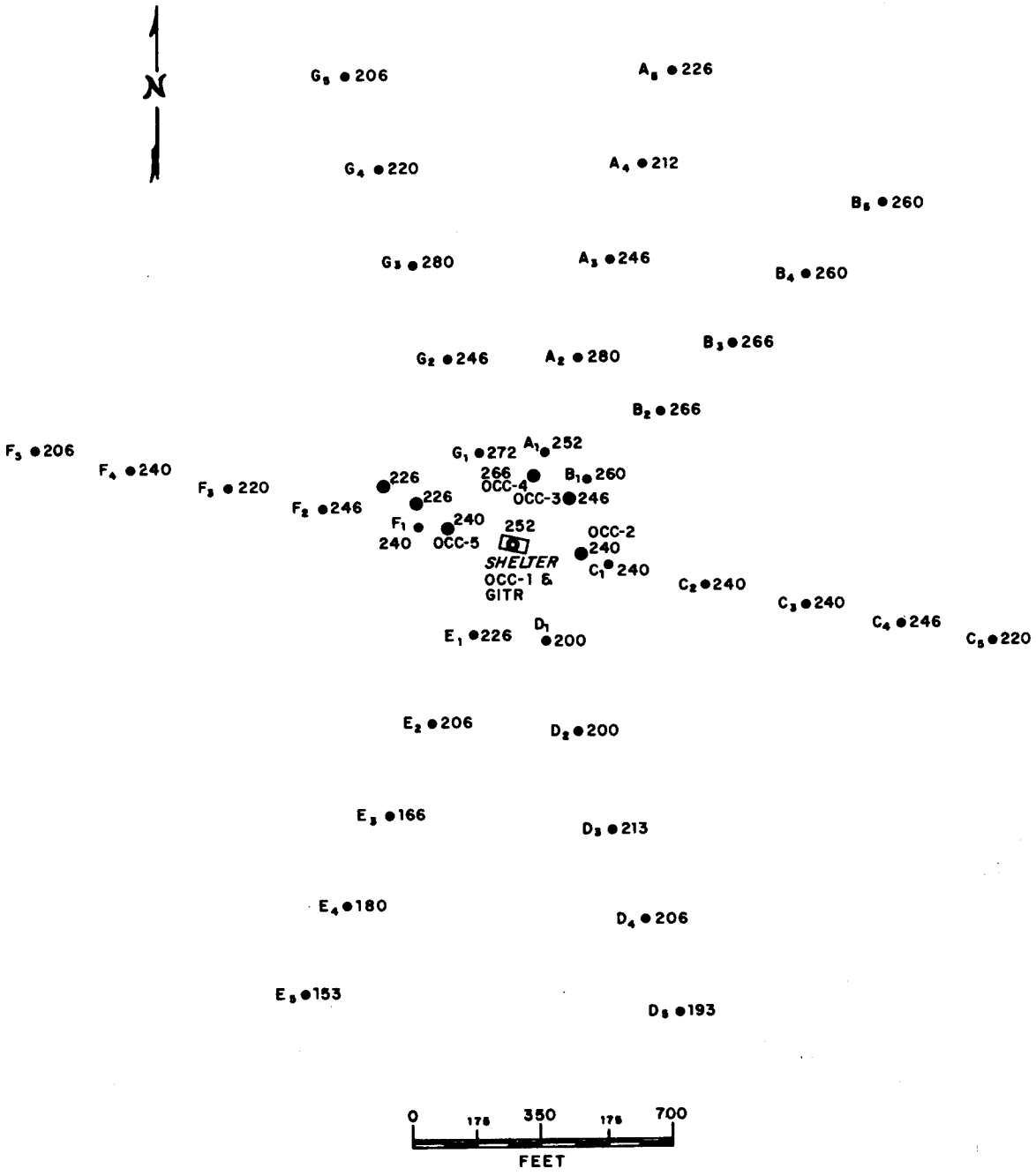

Fig. 2.1—Corrected gamma-radiation field at 3 ft around the radiological shelter, shot Shasta. (Readings in milliroentgens per hour at H+54 to H+56 hr.)

TABLE 2.1—CORRECTED GAMMA-RADIATION SURVEY AT 3 FT AROUND RADIOLOGICAL SHELTER

Station	Intensity, mr/hr	Time (Aug. 20, 1957)	Station	Intensity, mr/hr	Time (Aug. 20, 1957)
OCC-1	252	1050	D-1	200	1142
OCC-2	240	1055	D-2	200	1143
OCC-3	246	1053	D-3	213	1145
OCC-4	266	1051	D-4	206	1147
OCC-5	240	1057	D-5†	193	1148
GITR* (field)	226	1059	E-1	226	1155
OCC-6	226	1100	E-2	206	1157
Rad-Safe stake N879-E663.5	232	1057	E-3	166	1200
			E-4	180	1200
			E-5	153	1202
			F-1‡	240	1206
A-1	252	1105	F-2	246	1207
A-2	280	1107	F-3	220	1210
A-3	246	1109	F-4	240	1213
A-4	212	1112	F-5	206	1215
A-5	226	1114	G-1	272	1221
B-1	260	1118	G-2	246	1223
B-2	266	1120	G-3§	280	
B-3	266	1122	G-4	220	1226
B-4	260	1124	G-5	206	1228
B-5	260	1125			
C-1	240	1130			
C-2	240	1121			
C-3	240	1133			
C-4	246	1135			
C-5	220	1137			

*GITR, gamma-intensity time recorder.
†Rad-Safe survey stake N878-E664.
‡Near GITR.
§Center of 1000-ft smoothed circle.

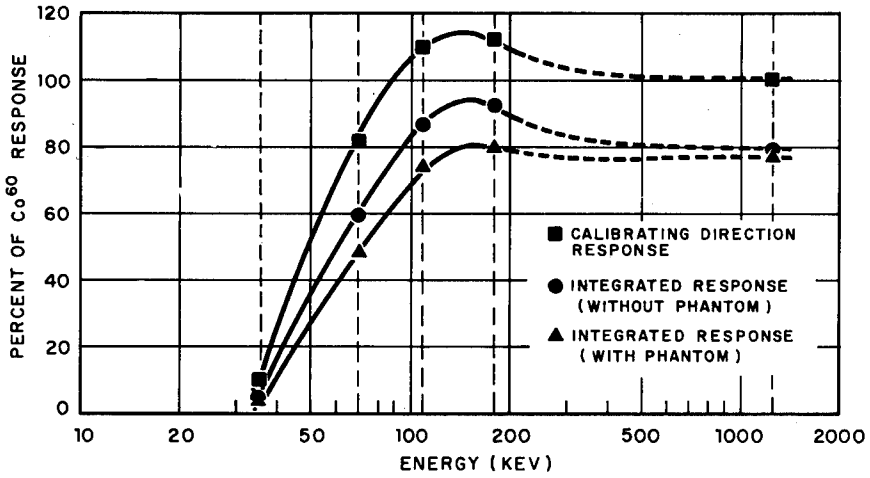

Fig. 2.2—Response characteristics of the AN/PDR/T1B survey meter.

rections were made by employing the results of a study made at Operation Teapot.[8] After correction for meter-scale calibration, all measured surface readings were multiplied by a factor of 1.33.* Figure 2.2 describes the response of the T1B survey meter as a function of the incident photon energy relative to a 1.25-Mev photon.

For the readings taken as a function of altitude, several variable parameters had to be considered in determining the meter correction. As the distance between the source and the detector increases, the photon spectrum experiences degradation due to air absorption; and, at distances of several mean free paths, the contribution from direct radiation approaches insignificance. Should the spectrum at altitude be so degraded that the major contribution is from energies of less than 100 kev, a radically different correction factor, relative to the 1.25-Mev calibration source, would have to be applied. An evaluation of this effect was made for several photon energies at 1 and 2 mean free paths by considering the preferred scattering angle for the Compton effect and computing the photon energy given to the recoil electron. This qualitative study suggested that the resultant degraded spectrum at distances as great as 1000 ft was still within the flat response range for the T1B survey meter. The multiplication factor of 1.33 used in correcting the surface readings did not appear reasonable for application to the measurements made at altitude for several reasons. First, the effect of shielding due to the presence of the monitor, or phantom, was absent because the survey meter was suspended below the aircraft hull. Second, to heights of at least 50 ft, the radiation was essentially unscattered and directed into the base of the meter. Therefore to this altitude, the effect of instrument-component shielding, relative to the calibration source direction, must have been negligible. Although scattered radiation becomes prominent at higher altitudes, it probably had its major component in a forward direction. Because of these factors, no correction (other than for meter-scale calibration) was applied to these measurements.

The fallout collected at the center of the array, OCC-1, was shipped to USNRDL and analyzed by gamma-ray spectroscopy to determine the absolute photon-emission rate as a function of area.[7] This analysis was done at 0900 on Aug. 20, 1957, coincident with the related field surveys. Table 2.3 characterizes the gamma spectrum from a 1-sq ft area as a function of energy. This fallout sample, used to determine the photon-emission rate, was also counted in the doghouse (DH) counter (see Appendix B for a description of the instrument). Since the DH counter had a known calibration between counts per second and photons per second as a function of energy and counter efficiency, a check was made on the reduced absolute photon-emission rate by converting it to DH counts per second and comparing it with that measured. The computed value was within 1 per cent of that measured.

Decay data, as well as comparison by radiochemical analysis of the fallout and cloud samples, showed the close-in fallout to be fractionated with certain of the radionuclides depleted. Such fractionation required that the photon-emission rate be determined experimentally and precluded the use of any classical fission-product mixture data previously computed[9] since no quantitative determinations of the fractionation were made.

Figure 2.3 shows the terrain characteristics of the measured area, which was typical of the Nevada desert, consisting of rocky soil covered with scrub brush to heights of 2 ft. Occasional dry washes were observed.

A theoretical study was made from the work of Werner[5] and Van Lint[6] to evaluate the gamma intensity as a function of altitude for various initial photon energies emitting from an infinite-plane surface. These data are tabulated in roentgens per hour per photon per second per square foot in Table 2.4 and are shown graphically in Figs. C.1 and C.2. Values were computed for an energy range from 0.06 to 4.0 Mev and a height range from 3 to 1500 ft.

With the known photon-emission rate from the spectral analysis and with Table 2.4, the theoretical gamma-field radiation rate in milliroentgens per hour for a smooth plane was computed and plotted in Fig. 2.4. For comparison with the theoretical curve, the measured values were also plotted.

*Private communication with C. F. Miller.

TABLE 2.2—CORRECTED GAMMA-IONIZATION MEASUREMENTS AS A FUNCTION OF ALTITUDE OVER RADIOLOGICAL SHELTER

Height above ground, ft	Gamma intensity, mr/hr	Time (Aug. 20, 1957)
1660	2.1	0855
1560	3.0	0856
1460	3.5	0858
1360	4.0	0900
1260	5.2	0902
1160	6	0903
1060	7	0904
960	11	0905
860	14	0907
760	19	0908
660	23	0850
660	23	0910
660	23	0919
560	26	0911
460	36	0912
360	50	0914
260	80	0915
160	120	0916

TABLE 2.3—ABSOLUTE PHOTON-EMISSION RATE AS A FUNCTION OF ENERGY, SHOT SHASTA
(Station OCC-1; time, 0900; Aug. 20, 1957)

Energy, Mev	Photon-emission rate, $4\text{-}\pi$ photons/sec/sq ft
0.030	1.76×10^7
0.055	6.95×10^5
0.100	4.65×10^7
0.135	1.92×10^7
0.225	5.46×10^6
0.285	1.31×10^7
0.520	1.11×10^7
0.662	2.78×10^7
0.745	2.97×10^7
0.960	1.14×10^6
1.04	1.89×10^6
1.13	1.10×10^6
1.28	6.35×10^5
1.38	1.22×10^6
1.59	2.74×10^6

TABLE 2.4—COMPUTED INTENSITY AS A FUNCTION OF ALTITUDE FOR VARIOUS INITIAL PHOTON ENERGIES FROM A CONTAMINATED INFINITE-PLANE SURFACE

[(Gamma dose rate, r/hr/photon/sec/sq ft ($\times 10^9$)]

Energy, Mev	Height, ft																		
	3	10	15	20	30	40	50	60	70	80	90	100	150	200	300	400	500	1000	1500
0.06	0.35	0.21	0.18	0.15	0.12	0.10	0.091	0.081	0.071	0.064	0.057	0.051	0.032	0.015	0.0063	0.0032	0.0017	0	0
0.08	0.48	0.31	0.26	0.22	0.19	0.16	0.14	0.12	0.11	0.096	0.086	0.078	0.050	0.027	0.013	0.0069	0.0039	0	0
0.1	0.60	0.39	0.34	0.29	0.24	0.21	0.18	0.16	0.14	0.13	0.12	0.11	0.071	0.043	0.022	0.012	0.0074	0	0
0.2	1.20	0.87	0.78	0.69	0.59	0.52	0.46	0.42	0.38	0.35	0.32	0.30	0.22	0.17	0.11	0.074	0.049	0	0
0.3	1.82	1.39	1.29	1.18	1.05	0.920	0.838	0.774	0.722	0.674	0.632	0.600	0.479	0.396	0.289	0.213	0.152	0	0
0.4	2.45	1.88	1.75	1.59	1.41	1.24	1.13	1.05	0.980	0.924	0.863	0.822	0.653	0.537	0.392	0.288	0.231	0.03	0
0.5	3.08	2.37	2.20	2.00	1.78	1.57	1.43	1.34	1.25	1.18	1.10	1.04	0.828	0.680	0.495	0.364	0.294	0.05	0
0.6	3.66	2.82	2.62	2.38	2.11	1.88	1.71	1.60	1.49	1.41	1.32	1.25	0.992	0.810	0.590	0.436	0.349	0.1	0
0.7	4.22	3.25	3.02	2.76	2.44	2.18	1.97	1.85	1.73	1.64	1.54	1.46	1.15	0.938	0.683	0.504	0.402	0.11	0
0.8	4.76	3.66	3.40	3.11	2.76	2.45	2.24	2.10	1.97	1.86	1.74	1.66	1.30	1.06	0.771	0.569	0.458	0.14	0
0.9	5.27	4.05	3.76	3.44	3.06	2.73	2.48	2.33	2.20	2.08	1.94	1.85	1.45	1.18	0.855	0.632	0.502	0.16	0
1.0	5.76	4.44	4.12	3.77	3.35	2.98	2.72	2.55	2.40	2.29	2.14	2.04	1.60	1.30	0.939	0.693	0.554	0.18	0
1.2	6.67	5.13	4.76	4.39	3.90	3.47	3.15	2.97	2.82	2.67	2.50	2.38	1.86	1.51	1.09	0.803	0.641	0.22	0.02
1.4	7.51	5.77	5.36	4.95	4.39	3.93	3.56	3.35	3.18	3.03	2.84	2.70	2.11	1.70	1.23	0.908	0.730	0.25	0.05
1.6	8.25	6.34	5.89	5.46	4.85	4.34	3.91	3.70	3.51	3.34	3.14	2.98	2.34	1.88	1.36	1.00	0.801	0.28	0.08
1.8	8.93	6.86	6.38	5.91	5.25	4.69	4.25	4.02	3.83	3.65	3.42	3.25	2.55	2.04	1.48	1.09	0.868	0.30	0.10
2.0	9.56	7.35	6.82	6.33	5.62	5.03	4.55	4.33	4.12	3.94	3.70	3.50	2.73	2.19	1.58	1.17	0.937	0.35	0.14
2.2	10.2	7.86	7.28	6.80	6.00	5.40	4.86	4.63	4.41	4.21	3.97	3.75	2.93	2.34	1.69	1.25	1.00	0.37	0.14
2.4	10.8	8.31	7.70	7.20	6.35	5.71	5.17	4.91	4.70	4.48	4.22	3.99	3.11	2.48	1.80	1.34	1.06	0.40	0.15
2.6	11.4	8.78	8.14	7.60	6.75	6.03	5.45	5.20	5.00	4.75	4.47	4.24	3.30	2.62	1.89	1.40	1.12	0.43	0.17
2.8	12.0	9.25	8.57	8.00	7.10	6.39	5.76	5.50	5.28	5.04	4.72	4.49	3.48	2.76	2.00	1.48	1.18	0.45	0.19
3.0	12.6	9.71	9.00	8.40	7.45	6.70	6.05	5.78	5.55	5.31	4.98	4.73	3.67	2.90	2.10	1.56	1.24		0.20
3.2	13.2	10.2	9.43	8.79	7.81	7.02	6.34	6.08	5.84	5.57	5.23	4.96	3.84	3.04	2.20	1.63	1.30		
3.4	13.8	10.7	9.85	9.20	8.16	7.34	6.63	6.35	6.10	5.85	5.50	5.20	4.03	3.19	2.31	1.71	1.36		
3.6	14.5	11.2	10.3	9.60	8.51	7.66	7.00	6.68	6.44	6.14	5.80	5.49	4.27	3.36	2.42	1.80	1.44		
3.8	15.1	11.6	10.7	10.1	8.86	7.98	7.29	6.99	6.71	6.42	6.06	5.74	4.44	3.49	2.53	1.87	1.50		
4.0	15.7	12.1	11.1	10.4	9.21	8.30	7.58	7.26	7.00	6.67	6.32	5.99	4.64	3.64	2.64	1.95	1.55		

The attenuation of the gamma flux due to the roughness of the terrain was found to be 40 per cent at an altitude of 3 ft for the H+54 hr photon spectrum. This is equivalent to a terrain attenuation factor of 0.6. It can be seen from Fig. 2.4 that the gross differences between the observed and calculated gamma-ionization rates exist in the first 50 ft of altitude, with the effect of terrain attenuation becoming unnoticeable above this height.

The effect of terrain attenuation was also looked at qualitatively for several locations by employing the following technique. Assume an unfractionated fission-product mixture and compute the fissions per square foot for a sample based on the radiochemical analysis of Mo^{99}. Determine for the sample the contribution from induced activities by determining the capture to fission ratios for the important nuclides. From the work of Miller and Loeb,[10] determine, again for unfractionated fission products, the roentgens per hour per fission per square foot at

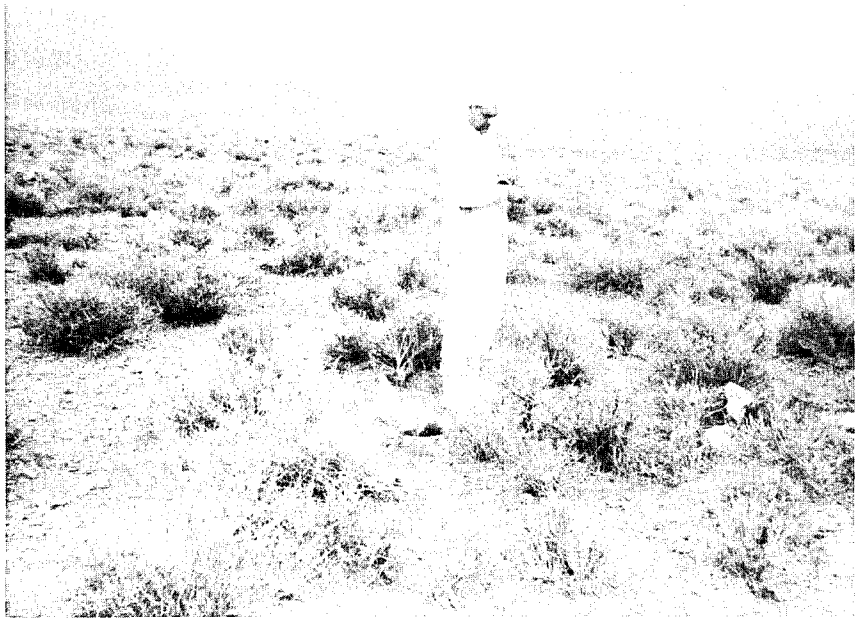

Fig. 2.3 — Typical terrain in the Shasta-Diablo close-in fallout area.

time t by considering the contribution from the fission products and induced products. From the decay data presented in the final report of Project 32.3, Operation Plumbbob,[11] as compared to theoretical fission-product decay, determine a depletion factor at time t due to fractionation. The product of these three factors will determine a calculated infinite-plane ionization rate at 3 ft for comparison with that measured and will allow a determination of the terrain attenuation. Results of such computations are shown in Table 2.5.

This technique results in poor agreement when compared with the more detailed approach of calculating the ionization rate from an absolute photon-emission rate. At station OCC-1 the two computed terrain-attenuation factors were 0.425 and 0.6, respectively. This discrepancy is probably introduced in the determination of the depletion factor as a means of determining fractionation. However, it is of interest to note from Table 2.5 the apparent dependency of the terrain factor on time since detonation. There is much less attenuation at H+14 hr than at H+54 hr, suggesting an energy shift (see Sec. 2.4).

2.3.2 Priscilla and Diablo Shots

No suitable flat gamma field could be found after shot Priscilla. Because of the steep gradients, it was decided not to attempt to make this study on this shot.

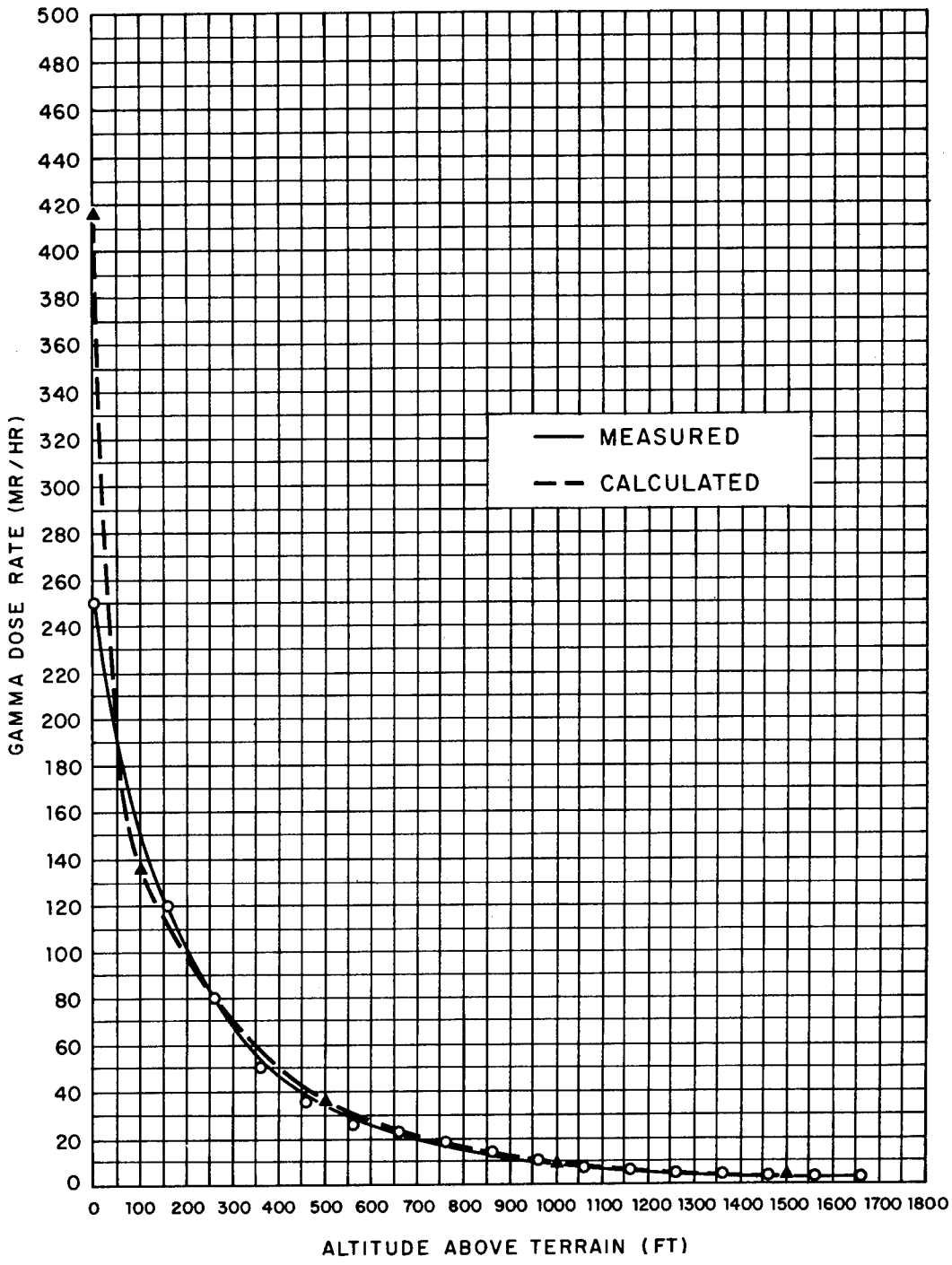

Fig. 2.4—Comparison of measured and calculated gamma dose rate as a function of altitude at H+54 hr, shot Shasta.

On shot Diablo a flat fallout field was located on D+5 day, and measurements were made with some variation of the technique employed on Shasta shot.

A 200-ft-diameter circular area was surveyed with a calibrated AN/PDR/T1B survey meter at a height of 3 ft. Corrected gamma measurements varied from a minimum of 350 mr/hr to a maximum of 380 mr/hr. Terrain characteristics of the area measured were similar to those found on the Shasta experiment and described in Sec. 2.3.1.

TABLE 2.5—TERRAIN ATTENUATION FACTORS DETERMINED FROM RADIOCHEMICAL APPROACH, SHOT SHASTA

Station	Time	Terrain factor
OCC-4	H+14	0.86
OCC-6	H+14	0.81
OCC-9	H+14	0.88
OCC-1	H+54	0.425
OCC-4	H+54	0.460
OCC-6	H+54	0.420

Since no helicopter was available, a 60-ft boom crane was used, and measurements as a function of altitude were made from the boom of this crane after locating it in the center of the surveyed area. Two runs were made, one with the boom facing west and one with the boom facing east (Table 2.6).

TABLE 2.6—CORRECTED GAMMA-RADIATION MEASUREMENT AS A FUNCTION OF ALTITUDE OVER SHOT DIABLO FALLOUT FIELD, D+5 DAY

	Gamma, mr/hr		
Height, ft	Boom facing east	Boom facing west	Mean
3	366	360	363
10	386	312	347
20	340	280	310
30	286	272	279
40	272	266	269
50	250	266	258
58	250	252	251

Again, since the survey meter was suspended from the boom and had an unobstructed 2-π view of the surface, no correction was applied to these measurements other than for meter-scale calibration.

Although the data from Diablo shot were not nearly so complete as those from Shasta shot, a study of the terrain attenuation factor can be attempted using the alternate approach suggested in Sec. 2.1.1. If this is done, it is necessary to assume that the gamma spectrum obtained on Shasta shot was the same as that which might have been obtained from Diablo shot since no spectral data were obtained in this case. Since the two devices and their environments were very similar and the radiochemical analysis of the respective fallout samples indicated similar fractionation of the fission-product mixture, it was assumed that employment of the Shasta spectrum for analysis of the Diablo fallout could be made. Because of the differ-

ence in intensity between the Shasta and the Diablo fallout fields, the relative spectrum of the fallout from shot Shasta was employed, and an arbitrary absolute photon-emission rate was assumed such that a calculated curve in milliroentgens per hour as a function of altitude could be plotted for comparison to that measured. The calculated curve was computed such that the dose rate at 3 ft was arbitrarily set at 1000 mr/hr. Comparison of this curve with that measured is shown in Fig. 2.5. The points on the calculated curve were multiplied by a constant such that there was coincidence with the measured curve at an altitude of 58 ft. Since the ratio of the calculated to measured values is not yet a constant at the higher altitudes and since the curves theoretically cannot cross each other, comparison of the calculated and measured values at 3 ft must indicate the minimum difference in intensity due to terrain attenuation. This value of the terrain factor at 3 ft was found to be 0.61 at a corrected time of H+54 hr.

2.4 DISCUSSION

It was hypothesized that the effect of terrain attenuation was a function of altitude, becoming insignificant at some height above the ground. This theory was verified from the data plotted in Fig. 2.4. It can be shown (since this phenomenon is purely a shielding effect) that, for a given surface roughness and fallout particle size, the amount of shielding is a function of the angle the incident photons that are seen by the detector make with the ground. When the detector is at a height of 3 ft, it is seeing ionization over an area of approximately 100 ft radius, 50 per cent of which is originating within a 50-ft radius. As close as 10 ft the photons are reaching the detector from an angle of 17° with the horizontal and are experiencing shielding by a rough surface. When the detector is raised to higher altitudes, the effect would be expected to be the same if the geometry were proportional. However, regardless of the altitude, the source area approaches that of an infinite field[6] at a radius of 1000 ft. Therefore the contribution to a detector originates from a source area having less shielding between detector and source as the height is increased, or the effective angle of the direct incident radiation with the horizon increases with increasing detector height.

The results of the experiment on the shot Shasta fallout agree very well with the theory. The effect of terrain attenuation falls off rapidly with increasing altitude and becomes small at approximately 50 ft. Since all the required data were obtained on the Shasta shot, an absolute evaluation could be made between the calculated and measured values at altitude. Above approximately 50 ft the ratio between calculated and measured values was constant; in addition, the computed values were within 10 per cent of those measured. This excellent agreement substantiates the method of computation and contributes to the over-all accuracy of the experiment.

It has been common practice to refer to terrain attenuation factors as having a constant value and being dependent only on the nature of the surface roughness. The qualitative work done on the Shasta fallout at H+14 and H+54 hr suggests that such attenuation is also a function of time. This is to be expected when the phenomenon is considered from a straightforward shielding point of view. Comparison of the mean photon energy of a fission-product mixture as a function of time, as described by Miller,[12] shows the mean energy (Mev) per photon to drop from 0.7 at H+14 hr to 0.51 at H+54 hr. This lowering of mean energy would suggest an increase in attenuation, as was observed in Table 2.5. The effect of energy dependence would be most pronounced from 1 to 100 hr for a pure fission-product mixture.

The photon emission from the fallout field was attenuated 40 per cent at 3 ft at H+54 hr when measured with a calibrated AN/PDR-T1B survey meter whose readings were corrected for instrument and monitor shielding. This rather large loss due to the shielding of the terrain for an H+54 hr photon spectrum must be corrected for in any calculation wherein an attempt is made to determine, from survey data, the fraction of the bomb debris deposited.

Most postshot analyses of fallout patterns are based on observed readings from T1B survey meters. If it is assumed that such measurements are made using a calibrated instrument, correction for instrument and monitor shielding and terrain attenuation must be made if the fraction of the device deposited is to be inferred from these measurements. In the specific

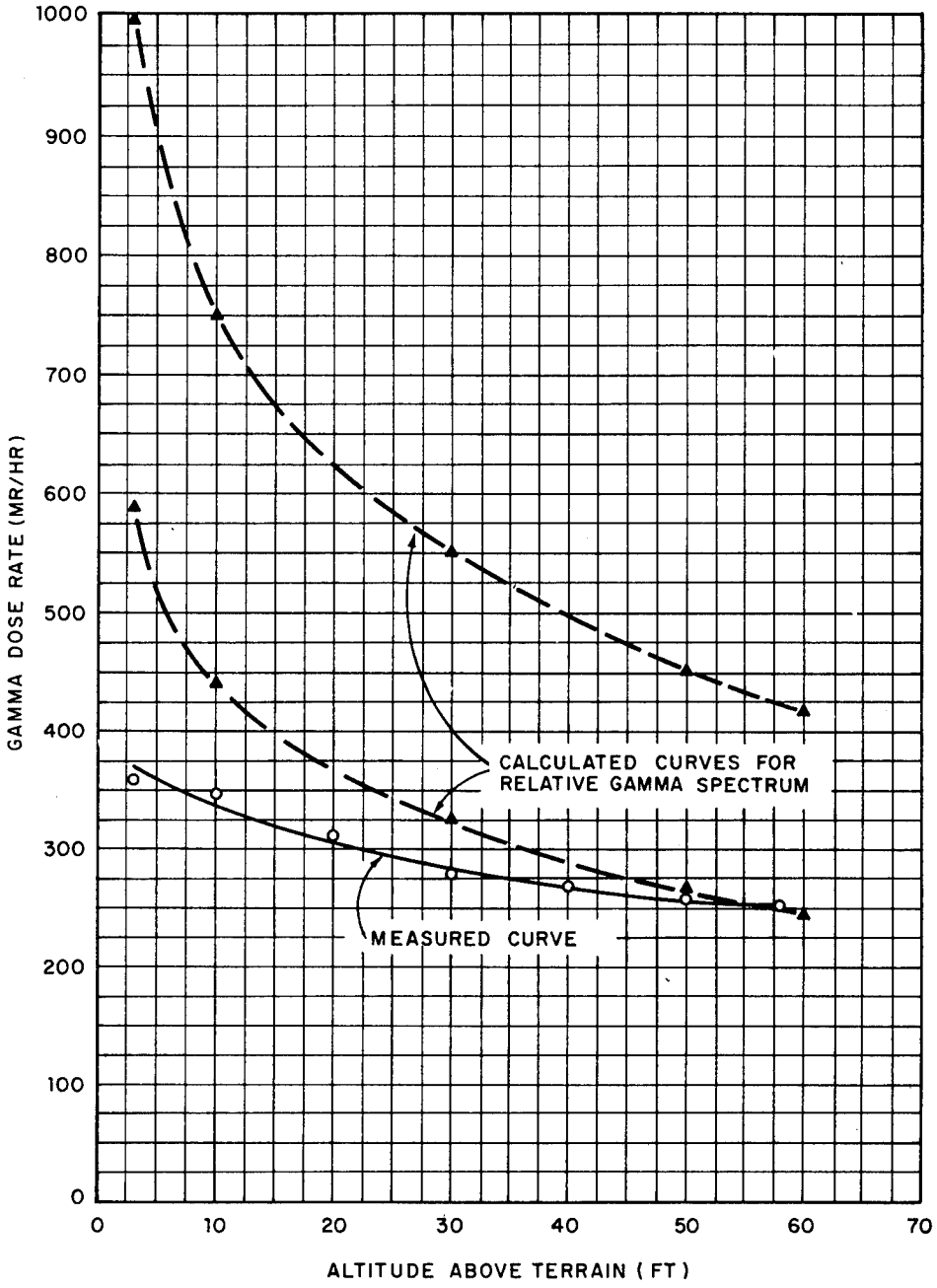

Fig. 2.5—Comparison of measured and calculated gamma dose rate as a function of altitude on D + 5 day, shot Diablo.

case for Shasta, for example, a measured dose rate of 100 r/hr at 3 ft at H+54 hr would, in reality, have an absolute photon-emission rate equivalent to 186 r/hr from an infinite smooth plane.

It might be argued that the effect measured is not due to terrain attenuation but rather due to the instrument's seeing less of the low-energy portion of the spectrum at increasing altitudes. However, an examination of the percentage of ionization contributed as a function of energy band and altitude negates this argument. Less than 1 per cent of the ionization is contributed by photon energies of less than 0.1 Mev, and the spectrum seen is approximately independent of altitude over the range of interest for energies above 0.2 Mev; below 0.2 Mev the contribution is approximately 11 per cent at 3 ft, 6 per cent at 100 ft, and 2 per cent at 500 ft.

The data from both Diablo and Shasta suggest a quick technique for the determination of the effect of terrain attenuation, the required input parameters being a measured curve of gamma dose rate as a function of altitude to approximately 50 ft and the relative energy spectrum of the photons at the time the determination is to be made.

2.5 CONCLUSIONS AND RECOMMENDATIONS

The attenuation of photons deposited on a rough surface is real, and such attenuation significantly reduces the measured ionization rate from a source of given strength. Such attenuation is a function of time since detonation, being least for a high-energy photon spectrum. For desert areas like those at the Nevada Test Site, attenuation was found to be as high as 40 per cent for readings taken at 3 ft with a T1B survey meter. Unless this parameter is taken into account in determining the fraction of the device deposited per unit area from measurements made at 3 ft, gross errors will result in such integration.

The results obtained agree with the proposed theory and offer a rapid solution to the determination of the terrain attenuation factor for unfractionated fission-product mixtures. This can be accomplished by normalization of a calculated curve with that measured at an altitude above 50 ft. The ratio of the calculated to measured values at 3 ft will then determine the effect of terrain attenuation for the specific soil-surface and energy-spectrum photon of interest. The same can be determined for any mixture if the relative photon spectrum is measured as well.

It is recommended that a well-controlled field experiment be run to determine this effect for a fission-product mixture distributed over a wide range of surface conditions such that corrections can be made in the calibration procedure for any given survey instrument.

REFERENCES

1. L. D. Gates, Jr., and C. Eisenhaur, Spectral Distribution of Gamma Rays Propagated in Air, Report AFSWP-502A, January 1954.
2. T. R. Folsom and L. B. Werner, Distribution of Radioactive Fallout by Survey and Analysis of Contaminated Sea Water, Operation Castle Report, WT-935.
3. C. F. Ksanda et al., Gamma Radiations from a Rough Infinite Plane, U. S. Naval Radiological Defense Laboratory, Report TR-108, Jan. 18, 1956.
4. W. W. Perkins, Variation of Gamma Intensity with Height from the Ground Before and After Clearing the Surface Area, U. S. Naval Radiological Defense Laboratory, in preparation.
5. L. B. Werner, Percent of Weapon Debris Removed by Local Fallout, paper presented at Fallout Symposium, Rand Corporation, March 5–7, 1957.
6. Victor A. J. Van Lint, Gamma Rays from Plane and Volume Source Distributions, Operation Redwing Report, ITR-1345, September 1956.
7. W. E. Thompson, Spectrometric Analysis of Gamma Radiation from Fallout from Operation Redwing, U. S. Naval Radiological Defense Laboratory, Report TR-146, Apr. 29, 1957.
8. George A. Work, Evaluation of Military Radiac Equipment: Accuracy of Military Radiacs, Operation Teapot Report, WT-1138, May 1955.

9. R. C. Bolles and N. E. Ballou, Calculated Activities and Abundances of U^{235} Fission Products, Report NRDL-456, Aug. 30, 1956.
10. C. F. Miller and P. Loeb, Ionization Rate and Photon Pulse Decay of Fission Products from the Slow-neutron Fission of U^{235}, U. S. Naval Radiological Defense Laboratory, Report TR-247, Aug. 4, 1958.
11. W. E. Strope, Evaluation of Countermeasure System Components and Operational Procedures, Project 32.3, Operation Plumbbob Report, WT-1464.
12. C. F. Miller, Gamma Decay of Fission Products from the Slow-neutron Fission of U^{235}, U. S. Naval Radiological Defense Laboratory, Report TR-187, July 11, 1957.

Chapter 3

EFFECT OF SHOT TOWERS ON THE NATURE OF FALLOUT PARTICLES

3.1 BACKGROUND

A large majority of the continental test detonations from which fallout has been documented and on which fallout models have been developed have been fired from steel towers. At Operation Plumbbob the use of balloon-supported detonations gave an opportunity for a comparison of the physical and chemical composition of the fallout particles from a true low air burst (balloon detonated) with that from a tower shot. The results of such an investigation should describe the nature of the fallout from an operational near-surface burst, which, in turn, may improve the development of a fallout model for such a detonation.

A knowledge of the source of fallout particles is mandatory for an adequate understanding of the mechanism of fallout[1] as well as for the development of reclamation procedures.[2] The inclusion of foreign materials in the fireball, such as shot-tower iron, may influence the characteristics of the fallout particles. Such particles, through differences in size, shape, and chemical characteristics, will influence the presently developed theories on fallout formation and deposition.

For comparison purposes two shots of equal scaled height, one tower supported and one balloon supported, are required. The influence of a shot-tower-free environment can be determined by collecting and analyzing fallout particles from these detonations.

3.2 PROCEDURE

On-site fallout was collected from shots Priscilla, Diablo, Shasta, and Owen. Priscilla and Owen were balloon-supported shots, and Diablo and Shasta were tower shots. Sample analyses were performed on shots Priscilla and Diablo only.

3.2.1 Instrumentation

Three types of ground-level collectors were employed in the field. These were the open-close collector (OCC), the always-open collector (AOC), and the incremental collector (IC).

Figure 3.1 shows the OCC and typical installation. The OCC consists of a framework covered by an air-operated sliding cover. This framework holds a polyethylene-lined tray $21\frac{1}{2}$ by 18 by 2 in. deep. An aluminum hexcell insert coated with an Apon resin completely fills the tray with honeycomb openings of $\frac{3}{4}$-in. cell size. This insert acts as a trap for the fallout particles. Each instrument was installed flush with the ground to ensure maximum efficiency of collection and to eliminate bias due to projections in the air stream. The collectors were timed to open at H+0 hr by an Edgerton, Germeshausen & Grier, Inc. (EG&G), Mark IV Blue

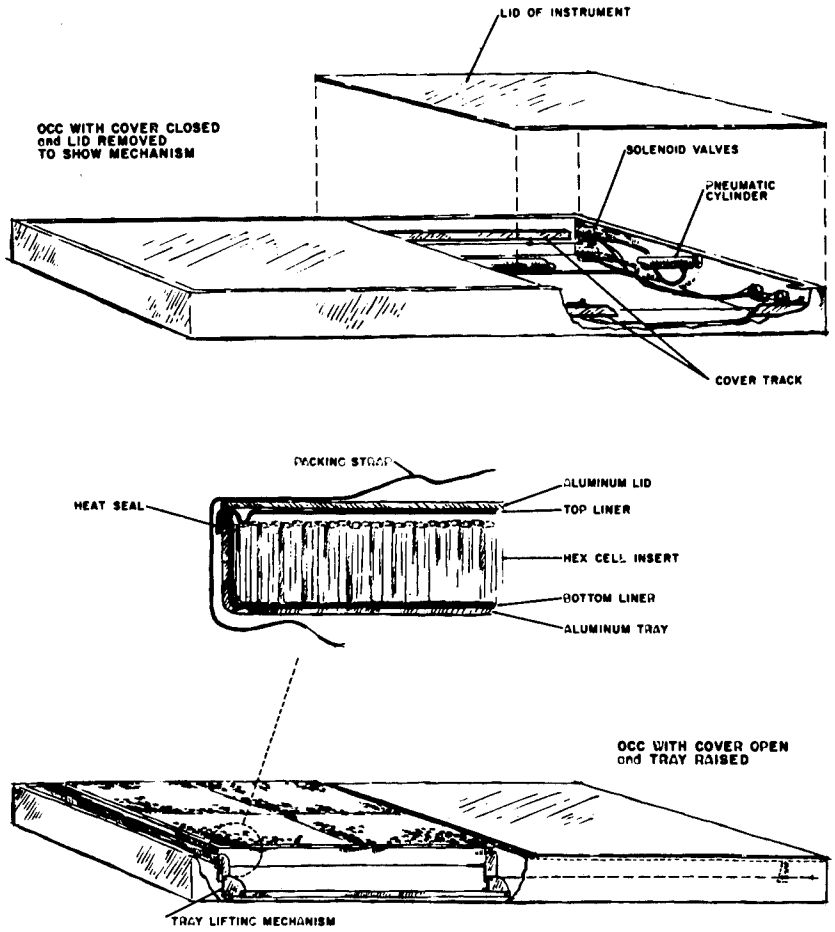

(a)

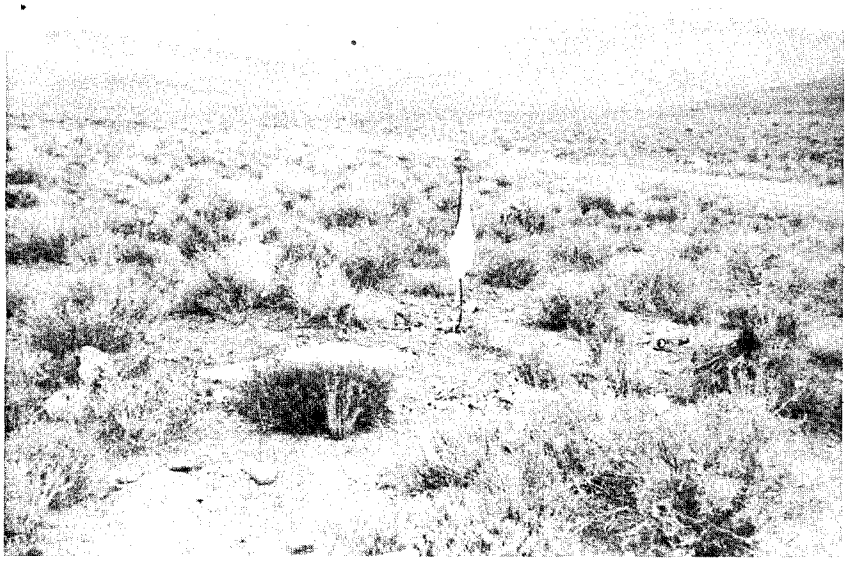

(b)

Fig. 3.1—(a) Diagram of the OCC; (b) typical installation.

Box, backed up by a type 44518 Giannini pressure trigger. A time-delay mechanism closed the covering lid at H+1 hr.

The AOC instruments are identical to the OCC in collecting area and installation; however, they have no covering mechanism and remain exposed from the time when last checked and cleaned to recovery.

Samples from both instruments were recovered by removing the tray, covering it with a polyethylene lid, and subsequently banding and boxing it at the project's Forward Area trailer.

Figure 3.2 shows a typical IC. This instrument exposes a series of 60 trays incrementally for 1-min sampling periods. The trays are cycled by a self-contained pneumatic indexing system and are stacked on a compensated tray elevator arrangement. Each sample-tray collecting area was $3\frac{1}{4}$ in. in diameter, the surface consisting of a grease layer for positive retention of the collected particles. The instruments were mounted in a pit with the collecting orifice flush with the ground; triggering was initiated in this case by a hard wire signal from the USNRDL shelter.

3.2.2 Sampling Array

The locations of the samplers were predetermined from fallout predictions and off-site safe firing requirements as determined by the Test Organization. Station arrays for the four shots are shown in Figs. 3.3 through 3.7. The relation of the collectors to the measured fallout field is also indicated by the superposition of the Test Organization Rad-Safe surveys for each of these detonations on the station-array diagrams.

3.2.3 Disposition of Samples

All samples were shipped to USNRDL from Indian Springs by special carrier aircraft.

3.2.4 Sample Analysis

(a) *Fallout Particle Identification.* Only radioactive particles were examined, thereby ensuring that all particles measured were true fallout. It was necessary to do this because the OCC collectors had collected extraneous soil particles from the dust raised by the shock wave. This was especially true on those stations close to Ground Zero (GZ).

On shot Diablo radioactive particles were easily isolated visually because of their black color and melted surface. This technique was verified by radioautographing a gross sample and finding no particles other than the black ones exhibiting any activity.

Since the shot Priscilla particles were the color of the natural desert soil particles, their isolation was accomplished by radioautographic techniques. The OCC gross sample was sieved into 10 fractions, and these fractions were then spread on the back of single-emulsion X-ray film and fixed thereto with Krylon. After exposure for approximately 60 hr starting at D+4 day, the films were developed with the particles attached; those particles exhibiting radioactivity were removed and washed in acetone.

All particles from both shots were placed in vials and assigned identifying numbers (see Sec. B.2.1).

(b) *Particle Surface Characteristics.* Each particle was observed under a low-power stereomicroscope having a 15× wide-angle eyepiece with reticle and a 3× objective. The reticle scale had a least count of 16.5 μ per division.

The particles were classed into five groups as follows: spheres, spheroidal, irregular smooth, irregular angular, and elongated. The maximum dimension of each particle and the maximum dimension at right angles to the first measurement were recorded (major and minor axes). In addition, the particle color and surface characteristics were documented.

(c) *Particle Internal Characteristics.* Thin sections were made of spheres and irregular particles from both Diablo and Priscilla[3]. The particles were embedded in plastic, one side was ground flat to the center of the particle and mounted on a microscope slide. The other side was then ground until a 30-μ-thick section was obtained. Radioautographs made of the sections

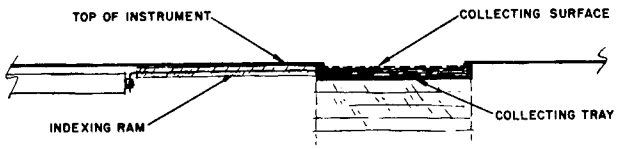

DETAIL OF COLLECTING AREA

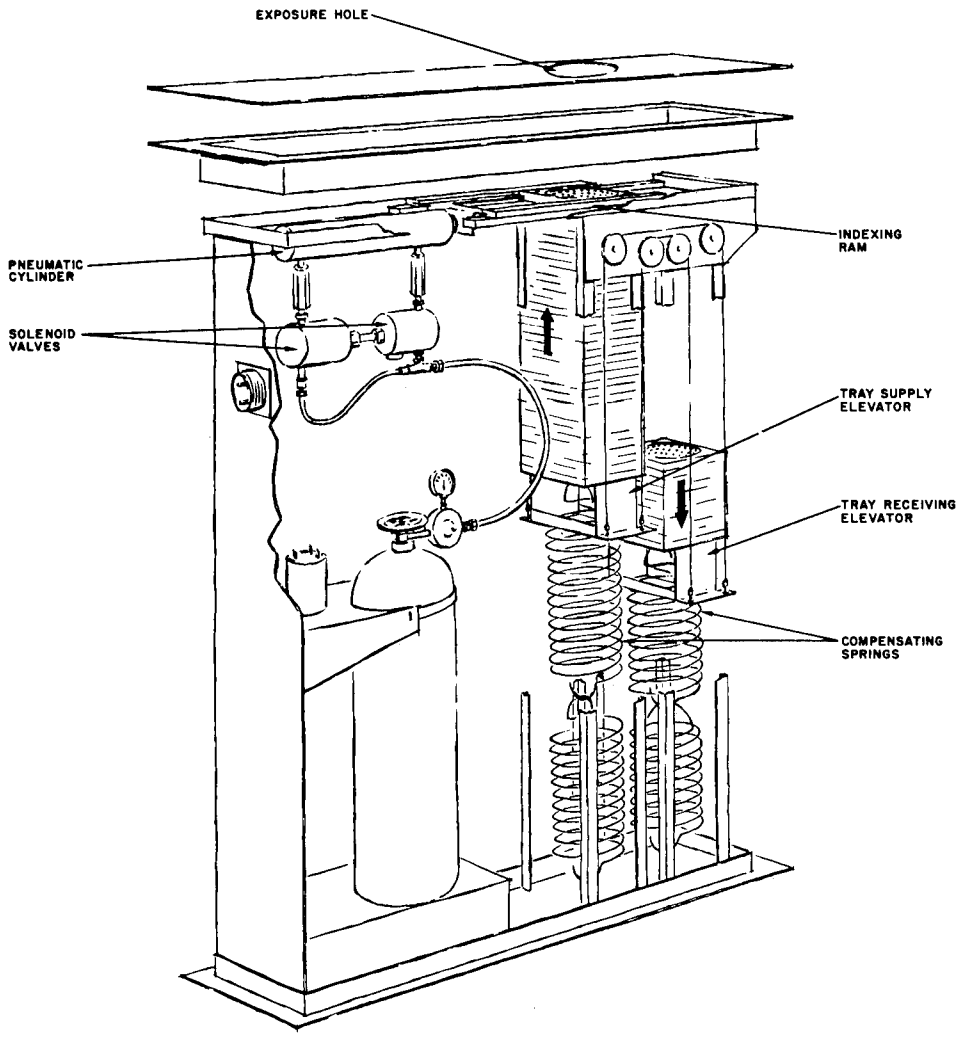

Fig. 3.2—Diagram of the IC.

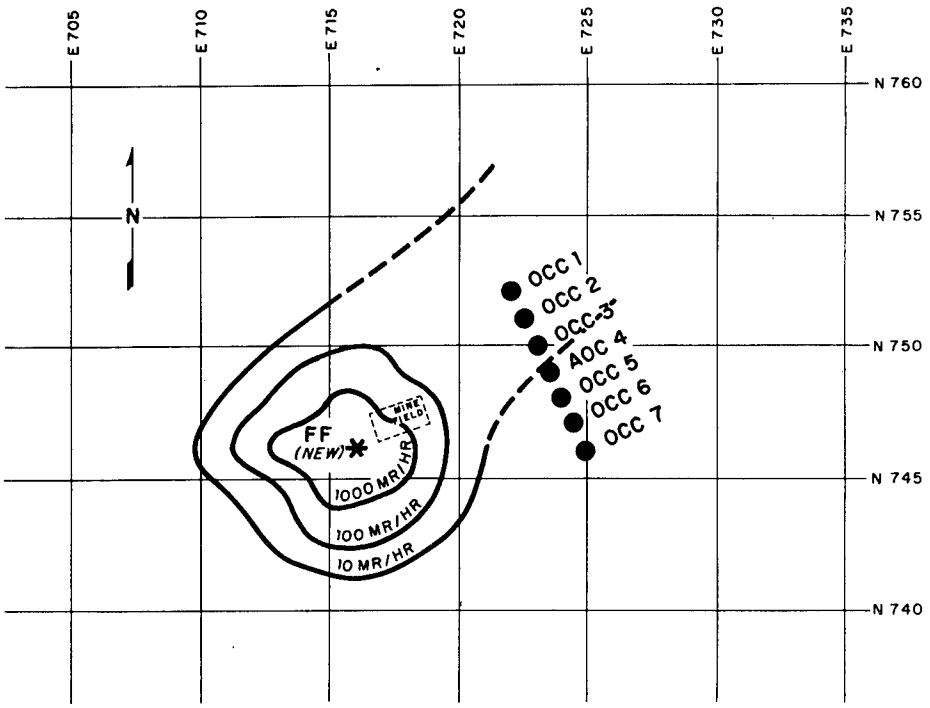

Fig. 3.3—Station array and gamma dose rate contours at H+6 hr, shot Priscilla.

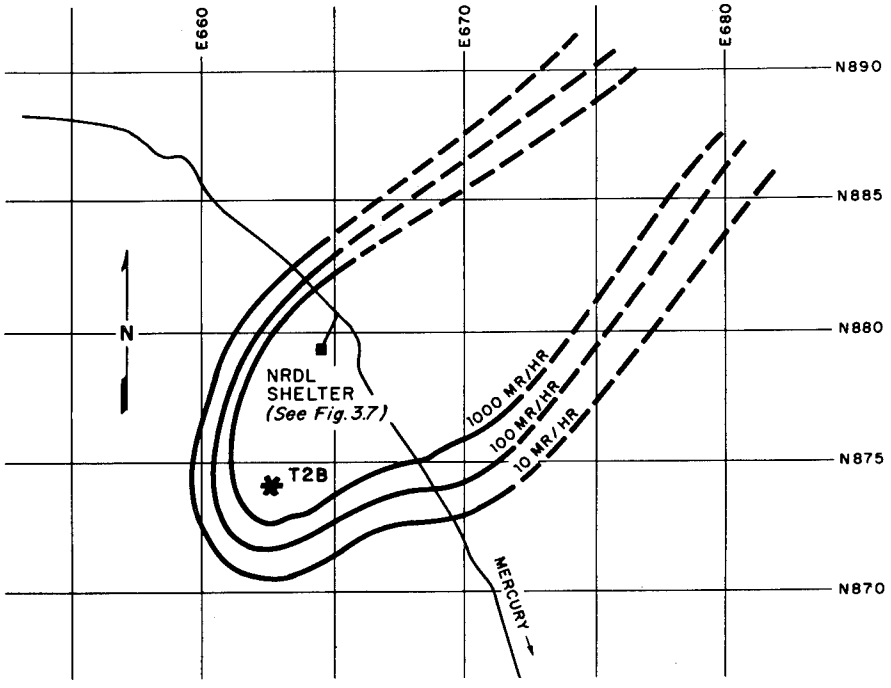

Fig. 3.4—Station array and gamma dose rate contours at H+6 hr, shot Diablo.

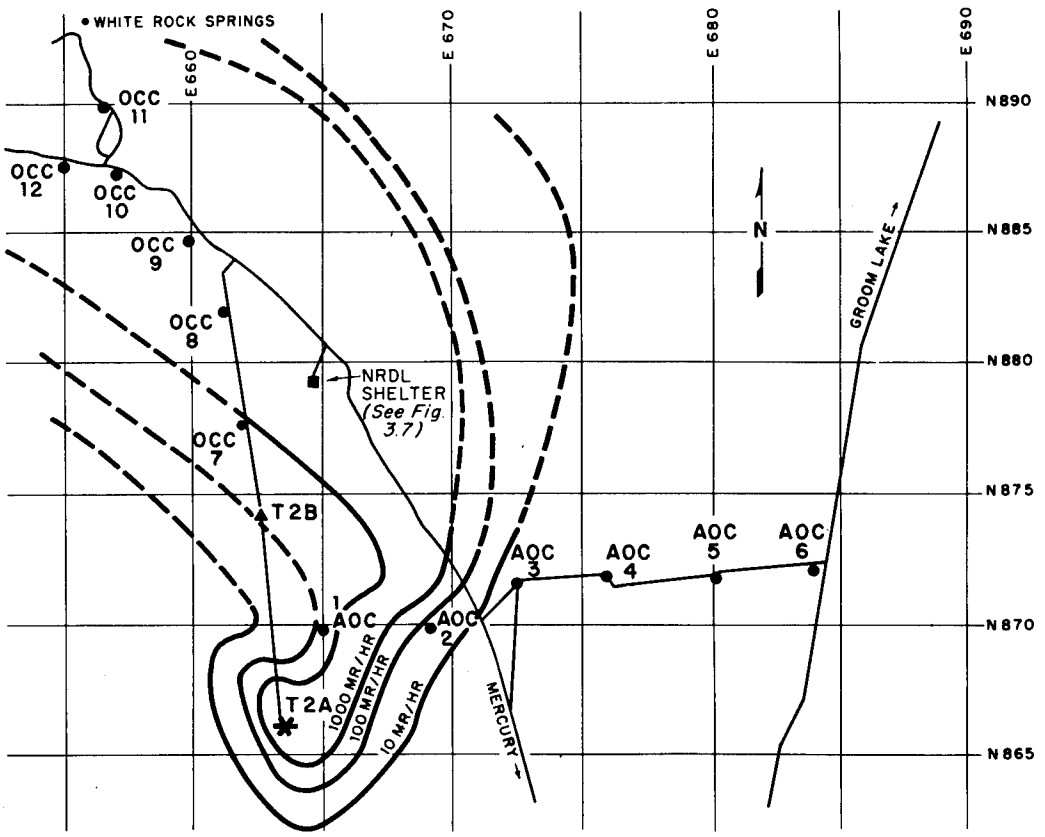

Fig. 3.5—Station array and gamma dose rate contours at H + 6 hr, shot Shasta.

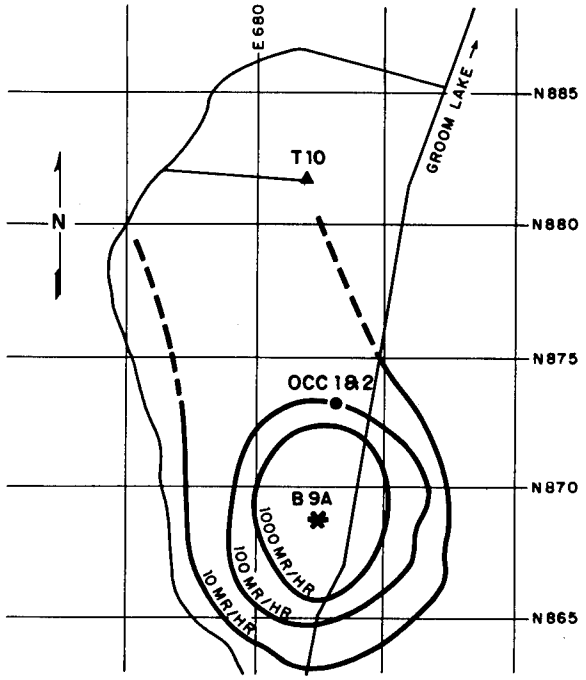

Fig. 3.6—Station array and gamma dose rate contours at H + 6 hr, shot Owen.

were mounted on microscope slides for comparison. The sections were studied under a stereomicroscope.

(d) *Particle Density.* Two techniques were employed in determining the apparent density of the particles. Apparent density is that density relative to the entire particle complete with any internal voids and not the true density of the solids.

Eighteen spheres were selected from the Diablo fallout, and their volume was computed. These particles were then weighed on a quartz-fiber microbalance to 0.1 μg. Their density was then calculated from their known volume and weight (see Table A.3).

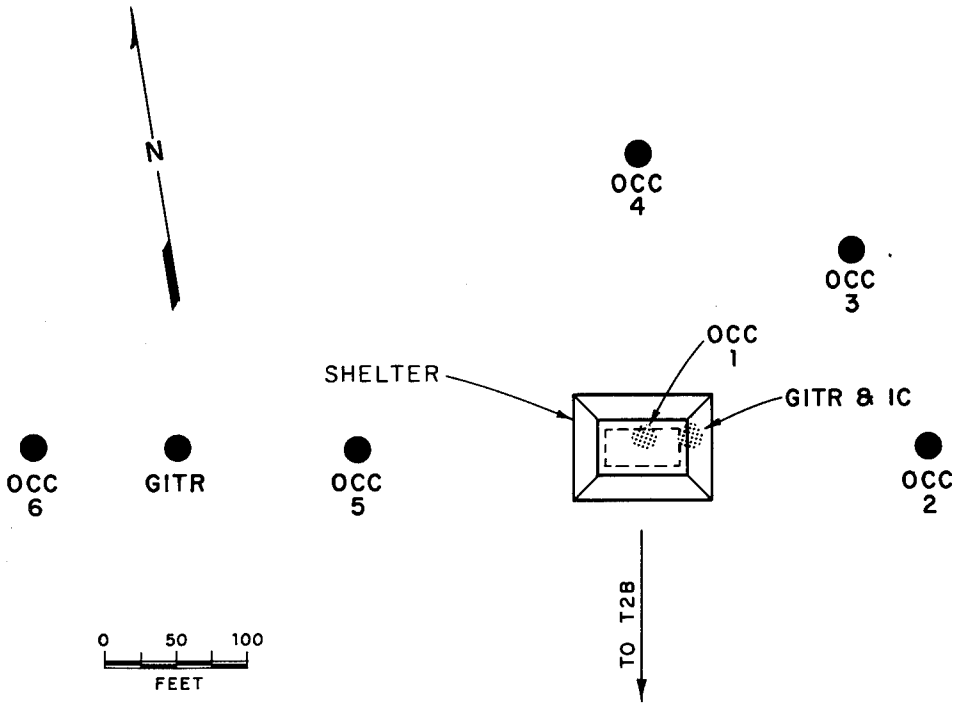

Fig. 3.7—Station array around the radiological shelter for shots Diablo and Shasta.

The density of 34 particles from Diablo and Priscilla, including five spheres from the above group, was determined by a flotation technique using bromoform-bromobenzene mixtures of known specific gravities. Because of the irregular shapes of many of the particles, it was necessary to employ this secondary technique. Ten bromoform-bromobenzene mixtures were made up having specific gravities from 1.9 to 2.8. These mixtures were standardized by measuring their index of refraction on a refractometer and using a calibration curve relating the specific gravity to the index of refraction of the mixtures. Each particle was dropped in successive mixtures until it would float in one and sink in the mixture having the next lowest specific gravity. The particles were washed in acetone and dried between mixtures.

Comparison of the two techniques was made by observing the density measurements made on the five spheres using both systems. Agreement was found to within two significant figures.

(e) *Chemistry of Particles.* Several particles from each shot were analyzed by X-ray diffraction for compound identification.

Eight particles from Diablo and six from Priscilla were analyzed for iron and lead. These analyses were done colorimetrically using *o*-phenanthroline for the iron and dithizone for the lead. The iron and lead content of the preshot soil was also determined for each shot (see Table A.4).

(f) *Magnetic Properties.* The particles were tested by passing a small Alnico magnet over them.

(g) *Radioactivity Determinations.* Those particles whose activity had been determined were all gamma counted in a well scintillation counter. The particles were placed in a Lusteroid tube and inserted in the well under constant geometry. The count rate was linear for most particles, however; for some of the most active particles, a correction for coincidence loss was necessary. The Priscilla particles were counted at H+340 hr after detonation, and the Diablo particles were counted at H+1000 hr. All activity measurements were corrected to a common time of H+340 hr, using experimentally determined decay curves for the counters in question.

3.3 RESULTS

3.3.1 Instrumentation

Mechanically the fallout collectors (OCC, AOC, and IC) functioned very well. The instruments operated 95 per cent successfully, with the one apparent failure being on shot Shasta where an OCC failed to open. The use of compressed air for power rather than batteries was well justified and is recommended.

On those collectors placed closer than 2 miles to GZ, the ground shock wave caused two problems that have subsequently been eliminated. On shot Priscilla the OCC and AOC hexcell inserts were not fastened to the tray, and several were blown out. This was remedied for the remainder of the operation by fastening them in place. A more serious problem that eliminated the usefulness of the OCC and AOC collections for mass measurements was the ability of extraneous material to deposit in the collectors from the dust raised by the shock wave. In one case, where the mass per unit area could be computed from the IC trays, an adjacent OCC was in error by having collected 20 times the true amount of material. All this excess was deposited by the shock wave. This condition exists only at close-in stations and can be remedied by using a 2-min time delay on the OCC opening mechanism. Of course, this problem will always exist for the AOC.

TABLE 3.1—MAJOR CONSTRUCTION MATERIALS USED IN TOWER AND CAB SUPPORTING THE DIABLO DEVICE

Material	Weight, lb
Iron	766,628
Lead	71,120
Concrete foundation	1,833,600

3.3.2 Diablo and Priscilla Fallout

(a) *Shot Characteristics and Environment.* Diablo was detonated at 4:30 a.m. (PDT), July 15, 1957, on a 500-ft steel tower in Yucca Flat (location T-2b). The yield as determined by fireball estimate was 23.8 ± 1 kt, and by radiochemistry, 18.7 ± 1.5 kt. Table 3.1 shows the breakdown of the major tower and cab materials used in construction. It is understood that in this detonation the device was also shielded with approximately 100 tons of a density-4 lead-polyethylene mixture.

Priscilla was detonated at 6:30 a.m. (PDT), June 24, 1957, from a balloon, the device being 700 ft above the terrain. The shot was located in Frenchman Flat (location FF-new). The yield as determined by fireball estimate was 36.2 ± 1.1 kt, and by radiochemistry, 37.1 ± 1.5 kt. Because the device was balloon detonated, there was very little extraneous environmental material associated with the firing.

(b) *Fallout Samples.* Diablo particles were collected for analysis from OCC-4, from the IC at the USNRDL shelter, and from the ground about the shelter. These particles were col-

lected within a circle of 100-ft radius, 1 statute mile north of GZ. A total of 352 particles was analyzed. All the particles were radioactive. A tabulation of these data is given in Table A.1.

All the particles analyzed from shot Priscilla were collected in AOC-4, located 1.3 statute miles from GZ. A total of 93 radioactive particles was documented (see Table A.2 for a tabulation of the particle characteristics).

(c) *Particle Parameters.* (1) Geometry. The particles were classed into five groups as follows: spheres, spheroidal, irregular smooth, irregular angular, and elongated. Figure 3.8 shows characteristic particles from each of these groups.

TABLE 3.2—DIABLO PARTICLES GROUPED BY SHAPE

Shape	No. of particles
Spheres	162
Spheroidal	92
Irregular smooth	43
Irregular angular	13
Elongated	42
Total	352

Table 3.2 shows the Diablo particle group breakdown by number of particles. Of the total, 72 per cent was spheroidal (sum of spheres and spheroidal), and 98 per cent had a melted appearance on their surface.

TABLE 3.3—PRISCILLA PARTICLES GROUPED BY SHAPE

Shape	No. of particles
Spheres	15
Spheroidal	13
Irregular smooth	33
Irregular angular	28
Elongated	4
Total	93

Table 3.3 shows the Priscilla particle group breakdown by number of particles. Of the total, 30 per cent was spheroidal, and 90 per cent appeared to be melted.

(2) Color. All the Diablo particles were black on the surface; many were quite shiny, and some were dull with discolorations. The Priscilla particles were all brown, the color of the desert sand.

(3) Internal Characteristics. Ten Diablo particles were thin sectioned and observed under an optical microscope. The sections were also radioautographed. In general, for both spheroidal and irregular particles, the sections indicated a layer of black opaque material on the surface of the particles, the inside being transparent glassy material. Many bubblelike voids were observed inside the particles; however, some were solid. The number of voids tended to increase with the irregularity of the particle. The radioautographs showed the activity to be concentrated on the surface of the particles, with some indication of a lesser amount

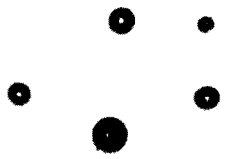

Spheres

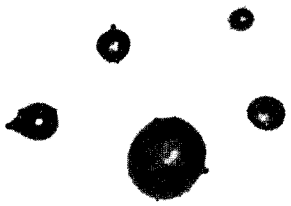

Spheroidal

Irregular smooth

Irregular angular

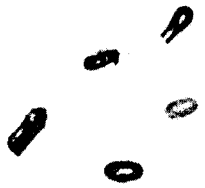

Elongated

Fig. 3.8—Typical fallout particles (magnification, 2×).

within the particles in some cases. It can be stated generally that the black color and the radioactivity were related.

Seven Priscilla particles were thin sectioned as described above; however, no radioautographs were made because of the low level of activity at the time of analysis. These particles had no distinguishing surface characteristics, and in this sense they differed from the Diablo particles. They were made up of a vitreous material, glassy with internal voids.

(4) Apparent Density. Eighteen Diablo spheres, ranging in size from 297 to 924 μ in diameter, were weighed, and their volumes were computed. Density computations were made from these data. In addition, the apparent density of 5 of the above spheres and 10 irregular-shaped particles was determined by a flotation technique in bromoform-bromobenzene mixtures of known specific gravities (see Table A.3 for a tabulation of these data). No correlation could be found between sphere diameters and apparent density.

For the spheres the mean density was 2.72 ± 0.295 g/cm^3, and for the irregular-shaped particles the density was 2.25 ± 0.425 g/cm^3. Since the standard error of the difference approximately equaled the difference of the means, the data do not allow one to conclude that there was a significant difference between densities for spheres and irregular particles. It is interesting to note, however, that physical observations on the particles indicated more internal voids in the irregular-shaped particles than in the spheres; perhaps because of the lower temperatures to which these irregular particles may have been subjected. Presumably the spheres, being in a molten state for longer periods of time, had more opportunity to vent any trapped gas. Therefore, from a purely observational point of view, the spheres would be expected to be more dense.

TABLE 3.4—IRON AND LEAD CONTENT OF DIABLO AND PRISCILLA PARTICLES

Sample	Content, wt.% Iron	Lead*
	Diablo	
Particles	6.03 ± 1.7	0.78 ± 0.33
Background soil	1.90 ± 0	0.018 ± 0.0146
	Priscilla	
Particles	3.01 ± 1.43	2.27 ± 1.30
Background soil	2.7 ± 0	0.0054 ± 0.0012

*Questionable results; see Table A.4.

The densities of 19 Priscilla particles (9 spheres and 10 irregular particles) were measured by the flotation technique. Table A.3 tabulates these data. For the spheres the mean density was 2.19 ± 0.22 g/cm^3, and for the irregular particles it was 1.84 ± 0.33 g/cm^3. Here again no significant difference was observed between the two groups.

(5) Chemistry of Particles. Two particles from each shot were analyzed by X-ray diffraction. The surface material on the Diablo particles was found to be magnetite, Fe_3O_4. Internally the particles were vitreous. The Priscilla particles were completely vitreous.

Eight Diablo particles and six Priscilla particles were analyzed for iron and lead. In addition, the natural soil background for the two detonation locations was examined for these elements. Table 3.4 tabulates the results in percentage by weight. The analytical data are given in Table A.4.

(6) Magnetic Properties. The majority of the Diablo particles collected were magnetic, whereas none of the Priscilla particles indicated magnetic properties when tested with a small Alnico bar magnet.

(7) Particle-size Distribution. The 352 Diablo particles analyzed ranged from 250 to 4500 μ in diameter; the mean size was 1000 μ. Figure 3.9 is a histogram of the size distribution. Figure 3.10 is a plot of the same group on logarithmic probability paper. The distribution is best described by a log-normal function.

The 93 Priscilla particles ranged from 46 to 2940 μ in diameter. In this case the mean size was 943 μ. Figure 3.11 shows the size distribution for these particles, and Fig. 3.12 is a plot of the particles on arithmetic probability paper. In this case the distribution appears to be skewed normal.

(8) Relation of Activity to Particle Size. It is well known that for a given particle size the range of activity can be very large; i.e., if 100 particles having the same diameter were collected, their individual activities might vary by several orders of magnitude. This is to be expected because certain of these particles undoubtedly saw more or less of the fireball at early times.

The particle sizes were determined by observing each particle under an optical microscope and measuring the major and minor axes. The diameters, then as reported, were computed by taking the square root of the product of these two measurements. With the exception of the elongated particles, the remainder, and majority, were reasonably symmetrical about their centers of gravity.

On shot Diablo each of the five particle groups, classed by their shape, was examined by plotting activity as a function of size. It appeared reasonable to fit a straight line through these data when plotted on log-log paper. Least-square lines were fitted to each group as shown in Fig. 3.13. The resulting equations for the lines are as follows:

Spheres	$A = 3.41D^{1.94}$	$n = 162$	(3.1)
Spheroidal	$A = 7.58 \times 10^{-3}D^{2.75}$	$n = 92$	(3.2)
Irregular smooth	$A = 2.09 \times 10^{-2}D^{2.43}$	$n = 43$	(3.3)
Irregular angular	$A = 9.84 \times 10^{9}D^{4.21}$	$n = 13$	(3.4)
Elongated	$A = 6.74 \times 10^{1}D^{1.43}$	$n = 42$	(3.5)

where A is the gamma activity in counts per minute at H+340 hr, D is the particle diameter in microns, and n is the number of particles in the group. With the exception of the irregular-angular particles, which were very few in number, the groups tended to merge.

Figure 3.14 is a plot of all Diablo particles combined. Figure 3.15 plots the best fit to these points as determined by a regression line. The equation for the line is:

$$A = 1.07D^{2.03} \qquad n = 3.52 \qquad (3.6)$$
$$S_y = \pm 396\%$$
$$S_b = 57\%$$

where S_y is the standard deviation of activity about the line and S_b is the standard deviation of the slope of the line. The parallel band about the line in Fig. 3.15 shows the error in activity about the line for a 95 per cent confidence interval; whereas the curved lines indicate for the same confidence interval the error of the mean activity for any given particle size.

Of the 93 particles documented on shot Priscilla, 21 were counted for gamma activity. This group had a size range of from 560 to 2940 μ, with a mean diameter of 1230 μ. Because the sample was small, it was not broken up into groups by shape. Figure 3.16 is a plot of ac-

(Text continues on page 47.)

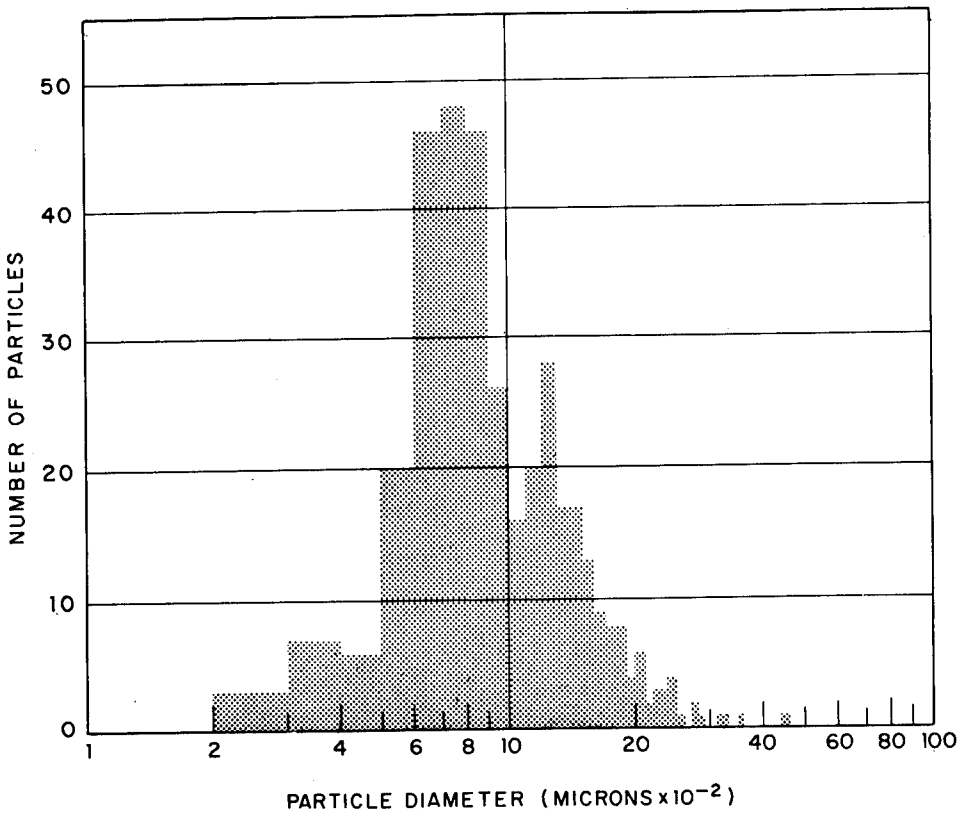

Fig. 3.9—Particle-size distribution, shot Diablo.

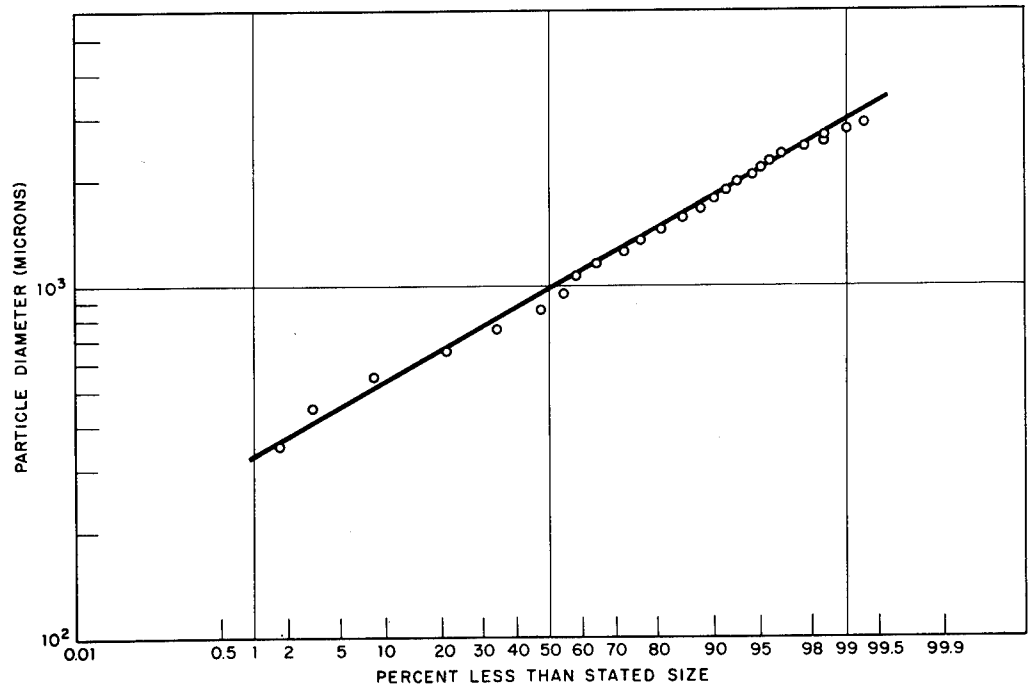

Fig. 3.10—Particle-size distribution, shot Diablo.

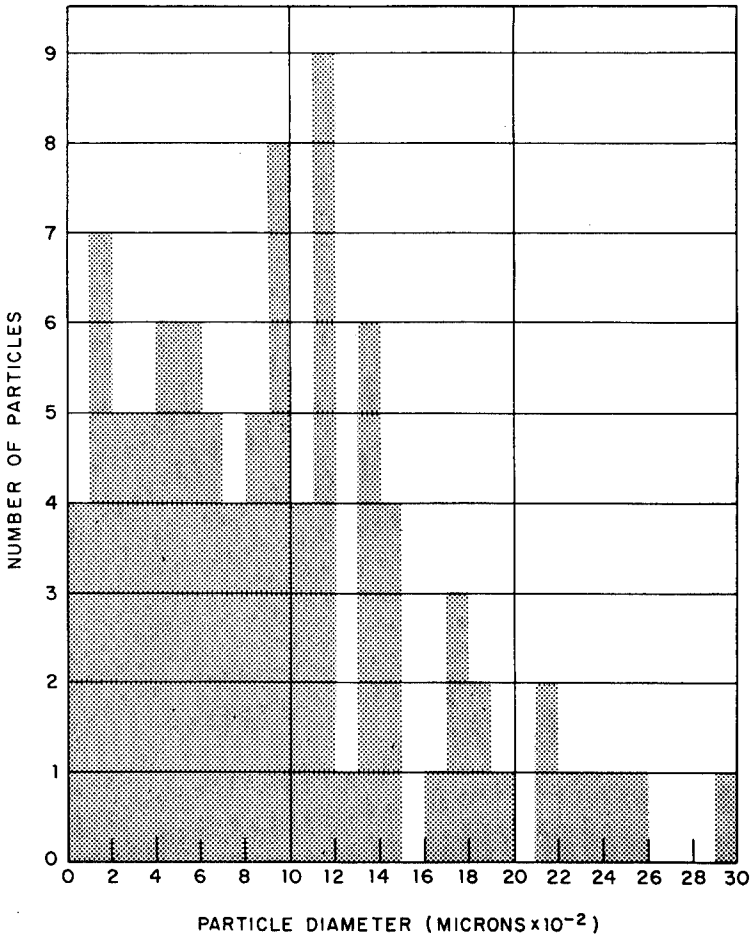

Fig. 3.11—Particle-size distribution, shot Priscilla.

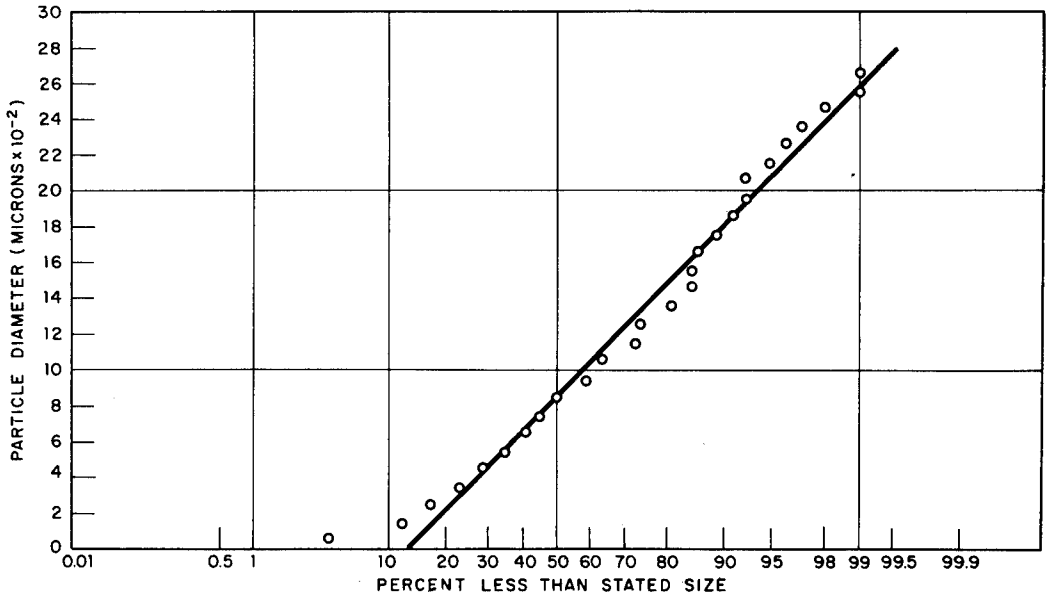

Fig. 3.12—Particle-size distribution, shot Priscilla.

[redacted]

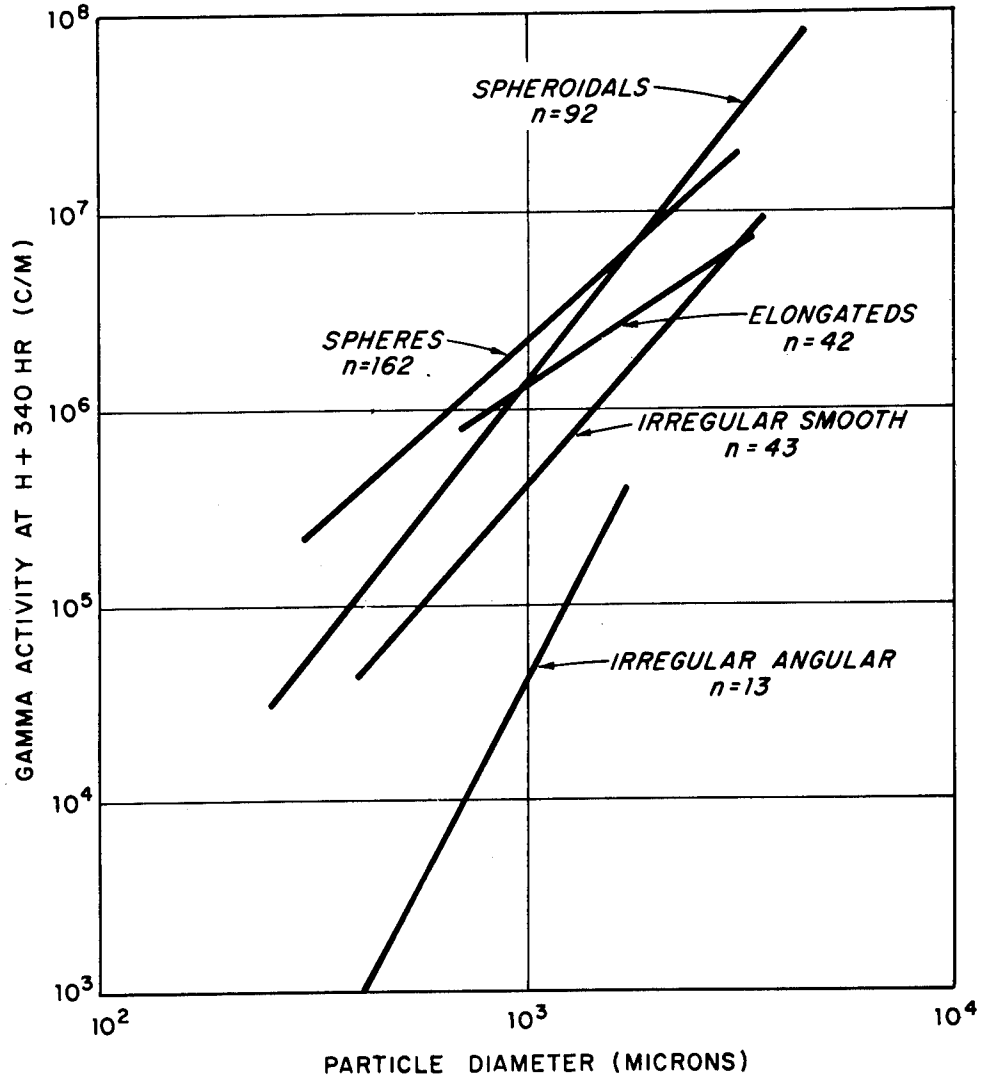

Fig. 3.13—Relation of activity to particle size as a function of particle geometry, shot Diablo.

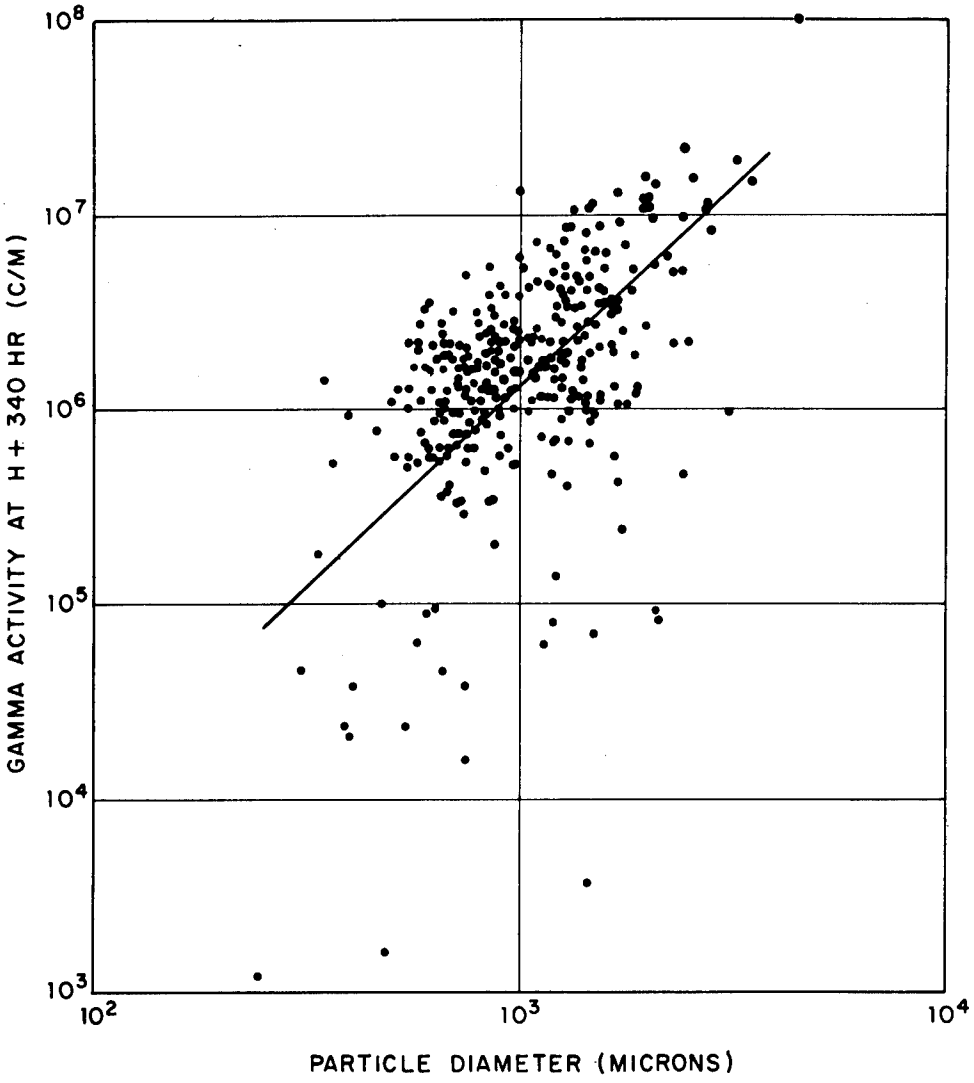

Fig. 3.14—Relation of activity to particle size for all particles, shot Diablo.

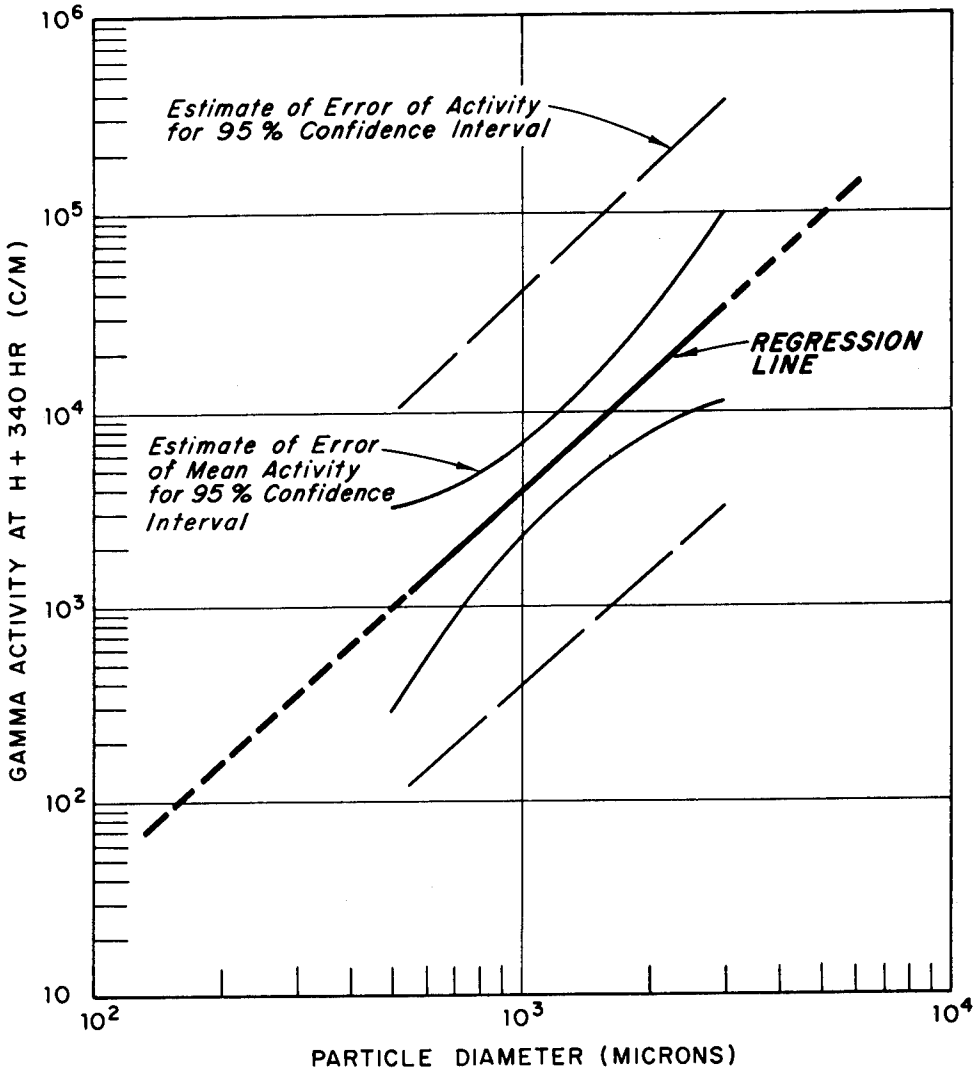

Fig. 3.15—Best fit of a straight line showing relation of activity to particle size, shot Diablo.

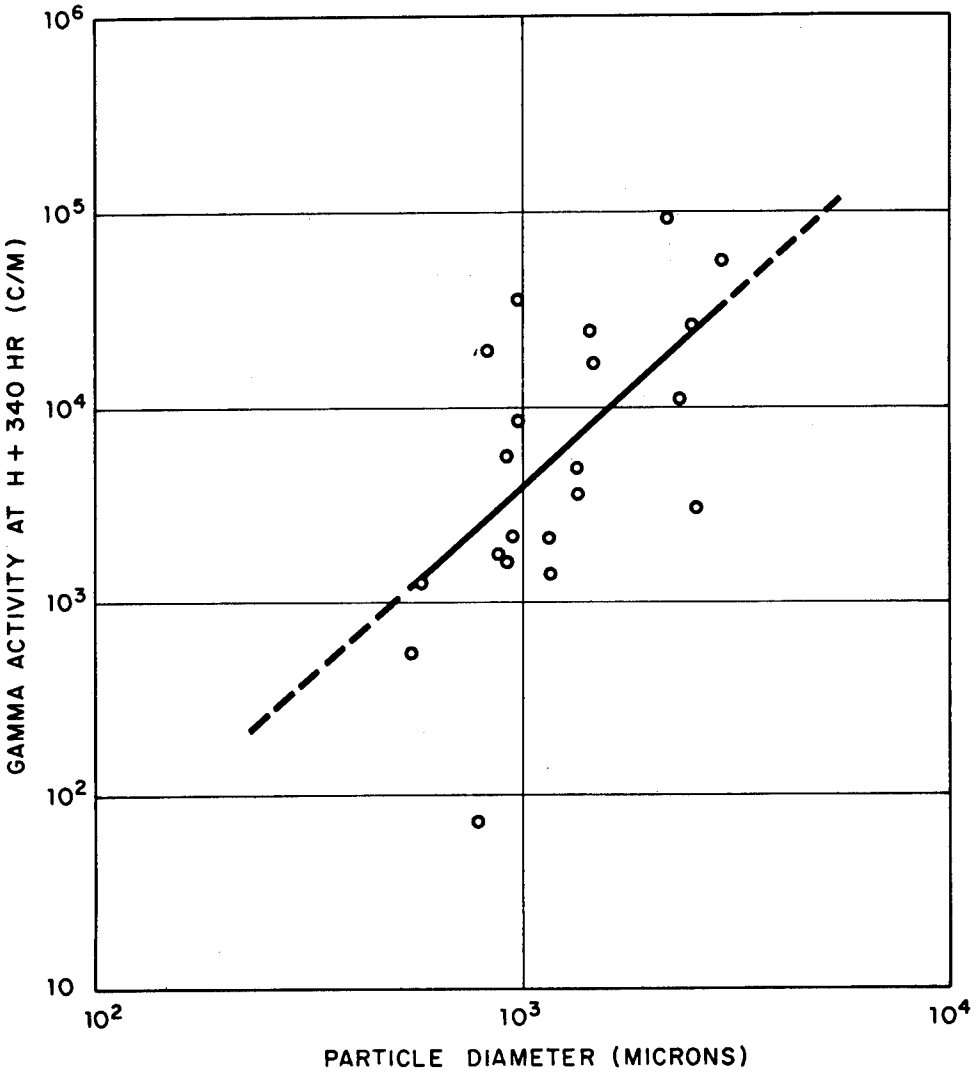

Fig. 3.16—Relation of activity to particle size, shot Priscilla.

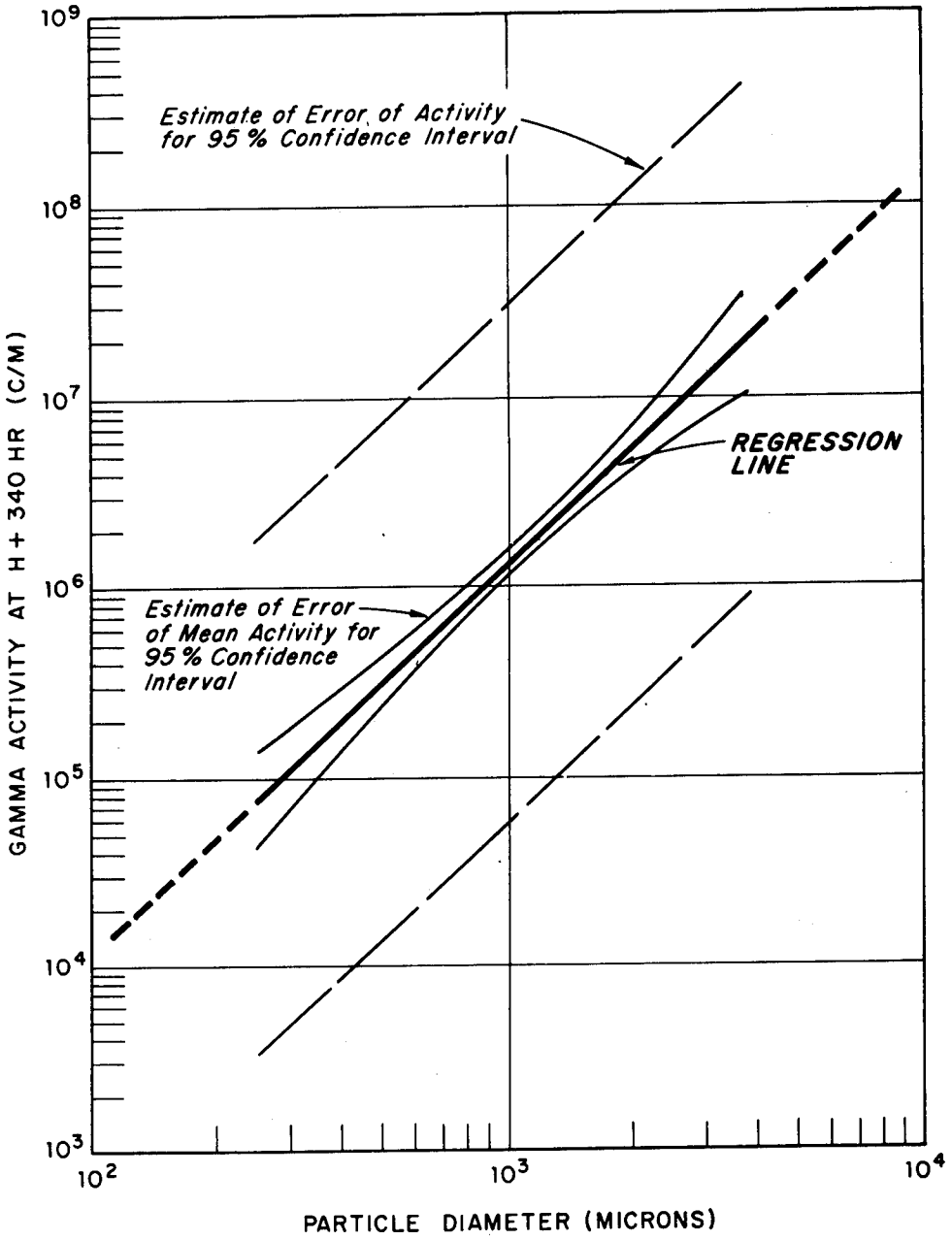

Fig. 3.17—Best fit of a straight line showing relation of activity to particle size, shot Priscilla.

tivity vs. size, and Fig. 3.17 shows the best straight line fitted through these points. The equation for the line is:

$$A = 4.33 \times 10^{-3} D^{1.98} \qquad n = 21 \qquad (3.7)$$
$$S_y = 226\%$$
$$S_b = 255\%$$

The graphed statistical estimates in Fig. 3.17 are for the same parameters as those discussed for Fig. 3.14.

(9) Decay. All particles were counted in a crystal well counter and corrected to a common time of H+340 hr. The well-counter decay curves for both shots are shown in Fig. 3.18.

TABLE 3.5—GAMMA ACTIVITY AS A FUNCTION OF SIEVE SIZE, SHOT DIABLO

Size range, μ	Mean size, μ	Activity, ma	Activity, %
>2,000	>2,000	$5{,}971 \times 10^{-11}$	4.6
841–2,000	1,420	$61{,}500 \times 10^{-11}$	47.7
591–840	715	$55{,}000 \times 10^{-11}$	42.6
421–590	505	$5{,}441 \times 10^{-11}$	4.2
<420	≪ 420	$1{,}325 \times 10^{-11}$	0.8

(d) *Activity as a Function of Particle Size by Sieving.* The shot Diablo sample OCC-4 was sieved into 10 fractions, and the relative gamma activity of each fraction was measured in a 4-π ionization chamber. These measurements, made Aug. 2, 1957, 0815 to 0840 Pacific Daylight Time, are shown in Table 3.5. No mass measurements were made because of the probable inclusion of extraneous material in the sample from the dust raised by the shock wave.

TABLE 3.6—COMPARISON OF GZ PRESHOT SOIL SAMPLES

Size range, μ	Mean size, μ	Sample, wt. %	
		Diablo	Priscilla
>2,000	>2,000	0	0
841–2,000	1,420	4.6	5.2
591–840	715	8.2	10.0
421–590	505	8.2	10.5
<420	≪ 420	79.0	74.3

(e) *Particle Size of Diablo and Priscilla GZ Preshot Soil Samples.* Approximately 25 lb of surface soil was collected at GZ locations for the two shots. These samples were rough-sieved in the field to remove the large rocks and organic matter. This sieving unfortunately removed all particles larger than 2000 μ. These samples were sieved, and the size distributions were compared as shown in Table 3.6.

3.4 DISCUSSION

The primary objective of this work was to study the effect of shot towers on the nature of fallout particles. The ideal case would be to document two identical devices fired under identical conditions, with the exception that one device would be tower-mounted and the other free of any tower or other materials. The best compromise to this situation which was compatible with other considerations within the project as well as the weapons test was to utilize shots Diablo and Priscilla. Comparison of these detonations appears to have eliminated the other

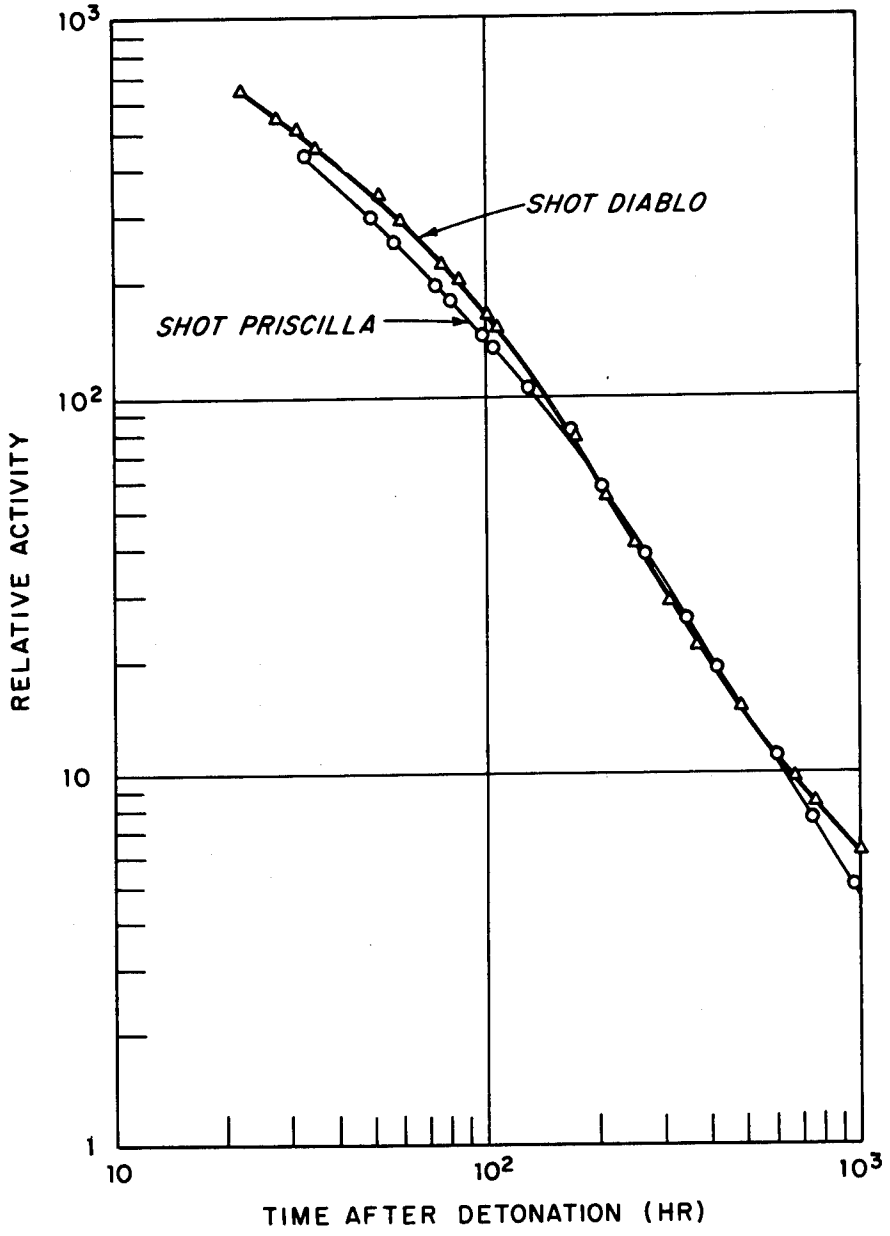

Fig. 3.18—Scintillation counter decay of fallout particles, shots Diablo and Priscilla.

variables to the extent that the major difference between the shots was the inclusion of the tower and shielding material about Diablo.

3.4.1 Instrumentation

In any collection of fallout (or, for that matter, precipitation), one factor to be considered is the sample bias introduced by the collecting instrument. This bias can be serious when the sample consists of a wide range of particle sizes. It is related to the wind speed past the collector. In most sampling arrangements the error is introduced by the instrument itself disrupting the flow lines about the collector. Theoretically, if the flow lines over the collecting orifice are in a plane parallel to the plane of the orifice, no sample bias will exist. This condition was achieved by installing the IC, OCC's, and AOC's at ground level with their openings flush with the surface of the terrain. With this ideal installation and with near-calm early morning surface winds, it is concluded that the instrument bias was negligible.

3.4.2 Shot Characteristics and Environment

With a known yield it is possible to estimate[4] the maximum fireball radius for an air burst to within ±20 per cent.

$$R = 180W^{0.4} \tag{3.8}$$

where R is the maximum fireball radius in feet and W is the total yield in kilotons. Table 3.7 tabulates these data for shots Diablo and Priscilla.

TABLE 3.7—VARIOUS ESTIMATES OF MAXIMUM FIREBALL RADIUS

Method	Yield, kt	Radius, ft
	Diablo	
Fireball	23.8 ± 1	640
Radiochemistry	18.7 ± 1.5	580
	Priscilla	
Fireball	36.2 ± 1.1	760
Radiochemistry	37.1 ± 1.5	765

These estimates indicate both fireballs had some intersection with the surface; however, on detonations such as these the effect of the reflected shock wave on the fireball must be considered. As the shock wave is reflected from the surface, it tends to flatten the base of the fireball and inhibit contact of the fireball with the ground.

High-speed motion pictures of the Diablo and Priscilla fireballs showed that shot Priscilla had no contact with the ground. A heavy opaque turbulent mass developed below the fireball; there was no indication of uptake into the fireball as late as 1-sec postdetonation. Shortly thereafter a great river of surface material was pulled into the rising fireball. Diablo, rather than having a classical smooth spherical fireball, developed a lumpy turbulent mass, the main body of which did not intersect the ground; there was contact within 60 msec by two projections that appeared to follow the shot-tower support cables to the ground. Diablo photography was much more difficult to analyze; however, it can be concluded that, contrary to the estimates in Table 3.7, neither fireball intersected the surface, although there did exist some contact by projections from the Diablo fireball.

Although the detonations were fired in different locations, the surface-soil characteristics were very similar in size distribution, as shown in Table 3.6. This is particularly true of the

large particle sizes. Although the sieve analysis indicates similar characteristics in percentage by weight of those particles less than 420 μ for both locations, a more rigorous analysis down to smaller sieve sizes might have shown the differences observed visually between the soil in Yucca Flat and the fine powdery deposits native to Frenchman Flat. The point to be brought out, however, is the fact that both sites have similar size distributions in the range of interest to close-in fallout studies. Chemically the two soils were probably different because the Priscilla location was in a dry lake bed, suggesting a higher concentration of salts.

The apparent overwhelming difference between the two detonation environments was the fact that Diablo was tower-detonated and heavily shielded whereas Priscilla saw little other than the natural environment.

3.4.3 Fallout Samples

In this study it must be remembered that the fallout-sample particle-size distributions are by no means a measure of the over-all size distribution for the fallout event. Any point-collected sample reflects the fallout relative primarily to its distance from GZ. For example, samples collected at 5 miles have a much larger mean size than those collected at, say, 50 miles. An attempt was made to collect particles from each detonation at approximately the same distance from GZ so that a relative comparison could be made over the same size range. For both Diablo and Priscilla this distance was approximately 1 mile. Because of the closeness of these collections to GZ, the fallout samples were made up of large particles, both having a mean size of approximately 1000 μ. The Diablo sample size distribution ranged between 4500 and 250 μ; whereas the Priscilla size ranged from 2940 to 46 μ. The smaller maximum size and minimum size observed for the Priscilla detonation could be explained by meteorological variables between the two shots, especially if the mean winds through the altitude layer to the top of the cloud were less for shot Priscilla.

Although the instrument collection bias was negligible, sample bias may exist if care is not taken in the selection of the particles analyzed. For shot Priscilla it can be concluded that the sample analyzed was unbiased since all radioactive particles collected were included in the population describing the size distribution. Of these 93 particles, 21 were selected for determining activity-size relations. In this selection the small particles were discriminated against because of the low specific activity of these particles when counted. Table 3.8 compares the Priscilla unbiased size distribution with the size distribution used in the activity-size determinations. A comparison of the two distributions suggests the main effect of this bias was to discriminate against the small particles. The frequency distributions above 500 μ are not significantly different.

Again for shot Diablo the instrument collection bias was negligible for both the OCC and IC. Of the 352 particles analyzed, however, 20 were obtained from the ground, 26 from the IC, and the remainder from the OCC. Table 3.9 compares the size distributions for each of these collections.

It can be concluded that, since the entire IC sample was analyzed, no particles smaller than 250 μ were selectively ignored. This size represents the smallest particle arriving at this station. The frequency distributions for the IC and OCC were quite similar; however, some bias is seen to exist in the total sample by the inclusion of the 20 large ground-collected particles. Their inclusion did not affect the total to any great extent, as can be seen by comparing the mean diameter for the IC (900 μ) and the total (1000 μ).

Table 3.10 tabulates the sample characteristics for the fallout samples collected at Diablo and Priscilla.

3.4.4 Particle Parameters

Examination of the various particle parameters that were investigated indicates certain basic differences between the Diablo and Priscilla fallout. The outstanding differences are (1) the much higher percentage of spheroidal particles obtained from Diablo, (2) the inclusion of a surface coating of magnetite on the Diablo particles, and (3) the much higher specific activity associated with the particles produced by the tower detonation.

TABLE 3.8—COMPARISON OF SHOT PRISCILLA UNBIASED PARTICLE-SIZE DISTRIBUTION WITH THAT SELECTED FOR COUNTING PURPOSES

	Mean diameter, μ	Maximum diameter, μ	Minimum diameter, μ	No. of particles
Unbiased size distribution	943	2940	46	93
Size distribution used for counting	1230	2940	560	21

TABLE 3.9—COMPARISON OF DIABLO PARTICLE-SIZE DISTRIBUTIONS FROM IC, GROUND, AND TOTAL COLLECTIONS

	Mean diameter, μ	Maximum diameter, μ	Minimum diameter, μ	No. of particles
IC	897	1650	250	26
Ground	2136	4500	980	20
Total	1000	4500	250	352

TABLE 3.10—SAMPLE CHARACTERISTICS

	Diablo	Priscilla	
Sample location, miles from GZ	1.0	1.3	
Collecting instrumentation	OCC, IC, ground	AOC	
Instrument collection bias	None	None	
Total number of particles analyzed	352 size distribution 352 size activity	93 size distribution 21 size activity	
Distribution characteristics:		Size distribution	Size-activity determination
Mean diameter, μ	1000	943	1230
Maximum diameter, μ	4500	2940	2940
Minimum diameter, μ	250	46	560
Bias due to particle selection from samples collected	Small, indeterminate	None	Discriminated against small particles

The high percentage of spheroidal particles in the Diablo fallout suggests that during the formation processes these particles were exposed to melting temperatures for a longer period of time than the Priscilla particles. Several mechanisms could explain this difference and are discussed below.

The reactions, both physical and chemical, that take place in the first few seconds after detonation leading to a particle formation theory have been hypothesized by Adams et al.[3] Also, the physics of fireball phenomena has been studied, and many of the thermal parameters have been determined.

For a low air burst or tower shot, the fireball reaches maximum diameter in less than 100 msec and at temperatures well above 5000°K. Consider the cases of Diablo and Priscilla where the fireballs approached tangency with the surface, then experienced a flattening and raising of the fireball base due to the reflected shock wave, and then hovered in this flattened shape several hundred feet above the surface for a period of several seconds. During this time the fireball cools to approximately 2000°K. Analysis of high-speed fireball photography during this period indicates the development of an opaque turbulent mass beneath the fireball, however, no positive updraft from the surface.

It is during this period that the particles are undergoing formation with temperatures being compatible with the melting point of the desert material and the evaporation and condensation temperatures of the tower iron. The fireball after the first few milliseconds is considered to be isothermal and radiating at a rate proportional to its radius squared and its temperature to the fourth power.

It may be argued that the inclusion of tower iron in the Diablo fireball lowered the viscosity of the vitreous melt comprising the particles, thereby producing more spheroidal particles than were observed in the tower-free Priscilla fallout. This hypothesis would appear valid if the iron were homogeneously mixed throughout the particle; however, in the particles that were thin sectioned, the magnetite was concentrated in a surface layer, suggesting a condensation process at some time later than the formation time of the melted vitreous internal portion of the particle. This would suggest two processes separated in time, with the basic particle make up, before the inclusion of the magnetite and fission products, identical with that observed from shot Priscilla.

The rate of thermal-energy emission from the fireball has been found to be a function of the type of detonation,[5] i.e., whether a true air burst, a tower shot, or a surface detonation. The temperature of the fireball can be expressed as

$$T = K\left(\frac{t}{t_{2max.}}\right)^{-0.4} \tag{3.9}$$

where T = temperature, °K
t = time since detonation, sec
$t_{2max.}$ = time to second maximum, sec
K = constant

The constant K has been found to drop as one goes successively from air bursts to tower shots to surface bursts of equal yields. Since the energy emission is proportional to the radius squared and the fourth power of the temperature, some of the thermal energy from a tower shot is not being radiated in the first few seconds.

Now the inability to account for a given percentage of the thermal energy from a tower shot, as compared to an air burst, at these early times suggests that this energy is being transferred through the fallout formation processes. Approximately 50 per cent loss in radiated thermal energy has been observed between equivalent-yield tower and air bursts. This energy could be relegated to any of the various phases of fallout formation from soil melting to tower vaporization.

If it is assumed that Diablo and Priscilla produced the same tonnage of fallout, then the additional energy required to vaporize the Diablo tower, cab, and shield can be computed. This amounts to 15 per cent of the total thermal energy produced. The above calculation was made

by considering the energy required to vaporize the tower, cab, and shield materials and to raise the vapor to 10,000°K.

It appears reasonable to hypothesize that the higher percentage of spheroidal particles formed in the Diablo shot was due to a slower energy emission rate for the Diablo fireball.

The Diablo particles analyzed had a net iron content of approximately 6 wt.%; of this, approximately 2 per cent is the natural iron background in the desert soil. Priscilla fallout, on the other hand, had very close to the natural soil background iron content. This additional 4 per cent of iron in the Diablo particles, determined to be in the form of magnetite and distributed on the surface of the fallout particles, undoubtedly originated from the shot tower. This inclusion of tower iron accounted for the black color of the Diablo particles.

Since the fission products were also a surface phenomena and, in general, related intimately with the magnetite, it is suggested that the two are related. Since the Diablo particles were very much higher in specific activity than those particles from Priscilla, it is concluded that the inclusion of a relatively small percentage of iron into the fireball has the action of a very efficient scavenging agent for the fission products.

The inclusion of the lead-polyethylene shield about the Diablo device was reflected in the lead content of the Diablo particles. However, an anomalous result can be seen by examination of the lead content of the Priscilla particles (see Table A.4).

Some quantitative determinations were made on the relation of activity to particle size. Since the majority of the particles examined by thin sectioning suggested the activity to be a surface phenomenon, it appeared that a qualitative statement to the effect that the activity was proportional to the surface area or diameter squared could be made. This was certainly not evident from examination of the very large spread in the plotted points as shown in Fig. 3.14, for example. In extreme cases the activity for a given particle size can be seen to vary over four orders of magnitude. A regression line was fitted to both the Diablo and Priscilla data, and equations for these were determined as follows:

Diablo

$$A = 1.07D^{2.03} \tag{3.10}$$

$$S_y = \pm 396\%$$

$$S_b = \pm 57\%$$

Priscilla

$$A = 4.33 \times 10^{-3} D^{1.98} \tag{3.11}$$

$$S_y = 226\%$$

$$S_b = 255\%$$

where A = the gamma activity at H+340 hr, counts/min
D = the particle diameter, μ
S_y = the standard deviation of activity about the line
S_b = the standard deviation of the slope of the line

Although the data for Priscilla are statistically very poor, it is interesting to note the close relation of the exponents in both equations. They both suggest a D^2 relation, which agrees with the physical observations of the distribution of the activity on the surface of the particles.

Of much greater interest, however, is the very significant difference in the intercepts of the two equations. The activity for the smallest Diablo particle is approximately 250 times that of an equivalent-size particle from Priscilla shot, and this ratio increases with larger particles. This difference in specific activity suggests much higher gamma fallout fields from tower shots than from air bursts of equivalent scaled height. Since most of the low-yield weapons-test detonations have been tower shots, it suggests any documentation of their resultant fallout

patterns be used with care if applied to true low air-burst situations. Apparently the fallout from a true low air burst is much less hazardous than that indicated from documentation of tower-shot fallout.

Certain applications of the data presented in Figs. 3.16 and 3.17 are of interest. It can be seen that, if it is desired to determine the activity of a given particle from the population by the use of the plots, the spread in the results makes the value of little use. Estimates of the error of the mean activity for any given particle size are much more useful and can be determined for 95 per cent confidence from the curved lines about the regression line.

3.5 CONCLUSIONS AND RECOMMENDATIONS

The influence of a relatively small amount of iron into the reaction processes that form the fallout particles can cause a significant increase in the amount of gamma activity deposited in the local fallout. This can be of importance in such problems as the control of the fallout phenomenon, especially with respect to the balance between close-in and world-wide deposition.

Tower shots are not representative of low air bursts, and documented effects must consider the influence of the tower if extrapolation is to be made to operationally delivered or received weapons.

Further studies should be made on the formation processes of fallout, especially the reactions that take place in the first few seconds postdetonation. The influence of the environment, either natural or artificial, on the fallout history needs explanation. Such work would best include the study of thermal-energy emission-rate differences as well.

REFERENCES

1. Stanley M. Greenfield et al., Transport and Early Deposition of Radioactive Debris from Atomic Explosions, Rand Corporation, July 1, 1954.
2. C. F. Miller, The Theory of Decontamination of Nuclear Weapon Debris, U. S. Naval Radiological Laboratory, in preparation.
3. C. E. Adams, N. H. Farlow, and W. R. Schell, The Compositions, Structures, and Origins of Radioactive Fallout Particles, U. S. Naval Radiological Laboratory, Report TR-209, Feb. 3, 1958.
4. Capabilities of Atomic Weapons, Armed Forces Special Weapons Project, Report TM-23-200, June 1, 1955.
5. R. W. Hillendahl, Character of Thermal Radiation from Nuclear Detonations, U. S. Naval Radiological Laboratory, in preparation.

Chapter 4

DOCUMENTARY SUPPORT TO PROJECT 32.3

4.1 BACKGROUND

The proper evaluation of the radiological situation at a shelter location requires measurements of the radiation field as a function of time, analysis of fallout collected at the location as a function of time, and knowledge of the types of radiation from the fallout. The measurements and sample collections for Project 32.3 (Report WT-1464) were made using standard equipment developed for this purpose.

4.2 PROCEDURE

Measurements for documenting the fallout events about the Project 32.3 radiological shelter were accomplished for shots Diablo, Kepler, and Shasta.

4.2.1 Instrumentation

Six OCC's, as described in Sec. 3.2.1, were placed in the vicinity of the shelter to collect the fallout as a function of area and to describe the deposited material about the installation. These instruments were manually triggered by hard wire from inside the shelter.

One IC was installed at the shelter to obtain the fallout phenomenon as a function of time. Triggering was accomplished manually from inside the shelter.

Two self-recording gamma intensity–time recorders (GITR) were also installed at the shelter to record the gamma-ionization rate as a function of time at the shelter. These recorders had a dynamic range of from 3 mr/hr to 400 r/hr and were capable of operating remotely for a period of 7 days. Readout equipment for these instruments was installed in the shelter. This instrument, because of its great bulk, is now obsolete; a discussion of its predecessor, however, is given in Sec. 5.4.3.

A recording anemometer was installed on the roof of the shelter, with readout equipment in the shelter.

Instrument installation was as described in Sec. 3.2.2, and the station array is shown in Fig. 3.7.

4.2.2 Sample Recovery and Analysis

The OCC samples were recovered and processed as described in Chap. 3. Detailed physical, chemical, and radiochemical analyses were performed on these samples at USNRDL.

The IC trays were shipped to USNRDL, and each tray was counted to determine the time of arrival of fallout, time to peak activity, and time of cessation of fallout.

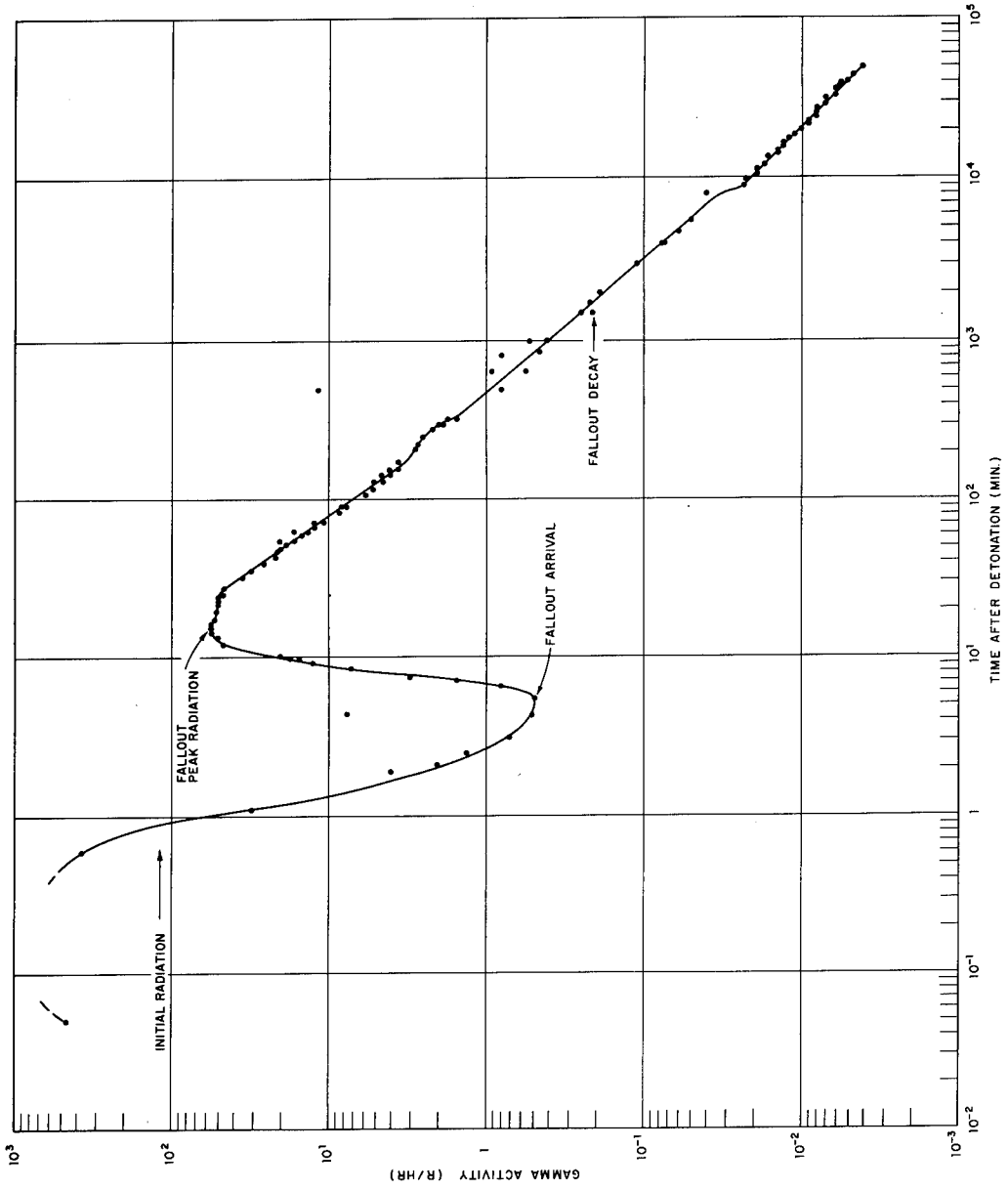

Fig. 4.1— Field gamma ionization rate as a function of time, shot Diablo.

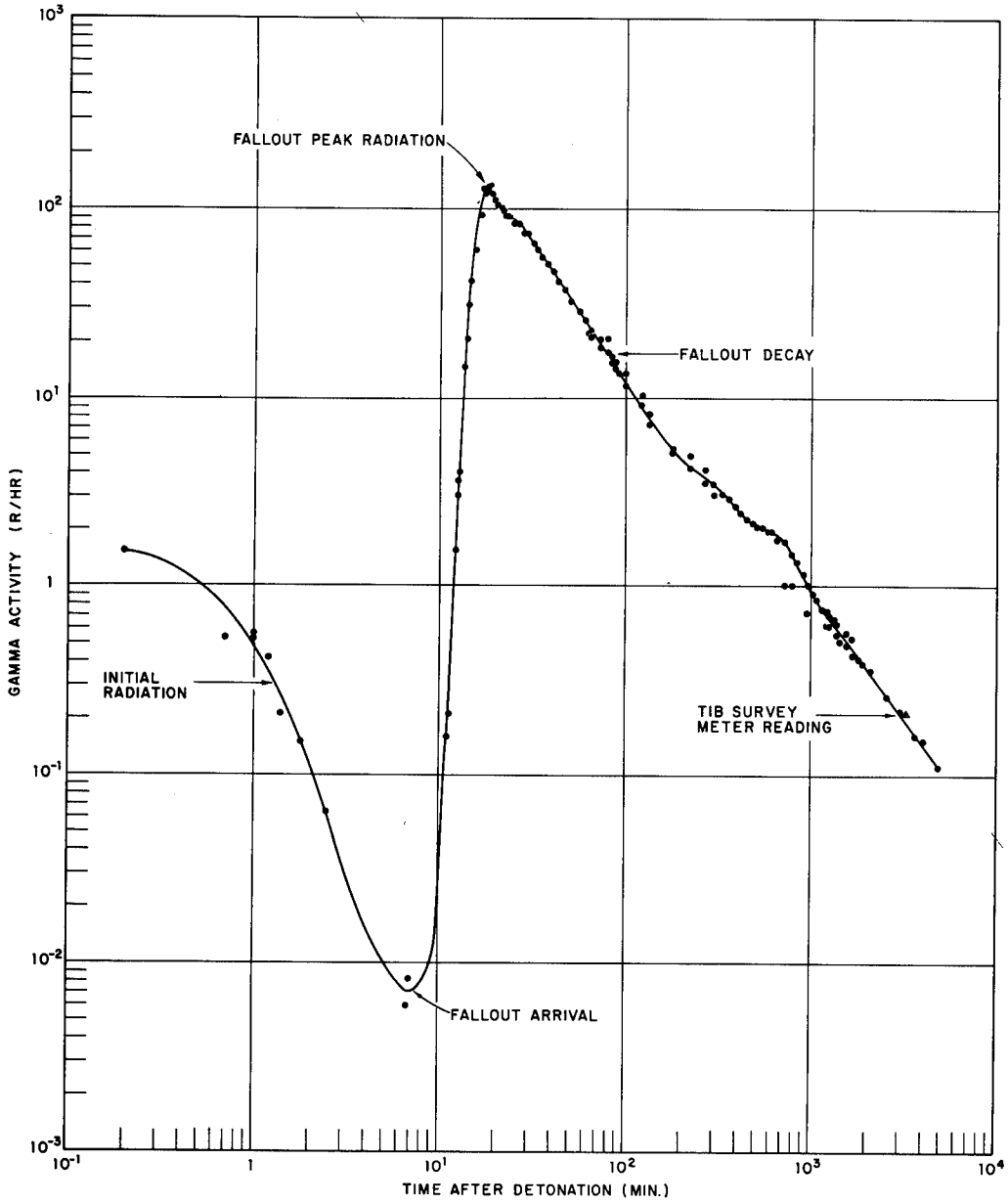

Fig. 4.2— Field gamma ionization rate as a function of time, shot Shasta.

Comparison of the above IC data was made with the radiation records from the GITR's. These recorders were also analyzed to determine the field decay for a period of several days postdetonation.

4.3 RESULTS

The instrumentation placed about the Project 32.3 radiological shelter experienced no failures throughout the operation. All requested data were obtained.

Figures 4.1 and 4.2 are plots of the gamma radiation as a function of time taken at the shelter during shots Diablo and Shasta.

Comparison of these measurements can be made with the spotted uncorrected field reading taken with an AN/PDR/T1B survey meter at the same location.

A complete history of the sample analyses accomplished for Project 32.3 is given in Appendix B.

4.4 DISCUSSION

This work was done as support to Project 32.3. Its application and evaluation are not pertinent to this report, and reference is directed to Report WT-1164 wherein the requested data were used.

Chapter 5

FIELD TEST OF PROTOTYPE INSTRUMENTATION

5.1 BACKGROUND

Continued weapons-test operations have dictated a continuing instrument prototype development program. Several new instruments and experimental techniques were evaluated for probable use at future test operations.

Many gamma-field measurements require data from various heights above the ground. Use of balloons as supporting devices for instrumentation was evaluated.

Measurement of gamma ionization as a function of time is of great value in understanding the dynamics of a fallout event at any location. A portable lightweight self-contained tape-recording instrument has been developed to satisfy this requirement.

A portable fallout collector is a primary requisite to gamma-field studies. A rugged power-operated self-contained fallout collector has been developed which permits maximum flexibility in installation and operation.

5.2 PROCEDURE

5.2.1 Use of Balloons as Instrument Platforms

Several captive latex balloons were tested under field conditions for use as platforms to support survey meters at various altitudes. Darex N4-24-1750, having a pay load of 22.9 lb at sea level, and Darex N4-28-2400, having a pay load of 36.2 lb, balloons were evaluated. The balloons were raised to a fixed altitude, and the survey meters were raised and lowered to the required altitudes by a pulley arrangement. The height of the instrument was determined by a log line from the instrument to the surface.

5.2.2 Fallout Collector

The OCC instrument was employed as the primary collecting device for this project because of its predicted performance. This instrument was tested on four shots, as described in Chap. 3.

5.3 RESULTS

5.3.1 Use of Balloons as Instrument Platforms

The use of balloons to suspend instrumentation failed in each attempt. The two main factors responsible were (1) the extreme delicacy of the latex bags, which ripped with little or no effort, and (2) the requirement for very still air for successful operation.

5.3.2 Fallout Collector

Of the 12 OCC's tested, 11 functioned perfectly. One instrument failed to open; the cause of failure is not known.

5.3.3 Gamma Intensity–Time Recorder

The newly developed portable GITR was completed at too late a date for testing at this operation. It has been laboratory tested and presently is being employed at Operation Hardtack.

5.4 DISCUSSION

5.4.1 Use of Balloons as Instrument Platforms

Unless field conditions are ideal, which they rarely are, the planned use of captive balloons of the type tested should be approached with caution. Better success could be obtained with plastic balloons and a design that employed airfoils to give additional lift under windy conditions.

5.4.2 Fallout Collector

The employment of a self-contained fallout collector proved highly successful, primarily because of its versatility and lack of need for a power line or triggering hard wire. This arrangement allowed rapid installation and complete mobility in planning the array. The use of compressed air as a power source proved successful and less troublesome than the wet-cell batteries employed in earlier instruments.

At any location, and especially close in, it is desirable to utilize a covering mechanism for such a collector. This prevents extraneous material from entering the collector as well as retaining the collected material after the fact. Although the mechanism functioned perfectly, the use of light- or blast-actuated triggers to open the OCC fallout collectors allowed blast-wave-raised surface dust to enter the collector, thereby negating accurate determination of mass of fallout per unit area. Use of either a radiation trigger or a delay mechanism on the lid-actuating mechanism is required to eliminate this problem. This problem exists only when collections are being made closer than a few miles from GZ.

5.4.3 Gamma Intensity–Time Recorder

The prototype GITR was not tested at this operation; however, since that time, it has been put into production and is being used at Operation Hardtack. Since the GITR appears to be potentially a very fine field instrument, reference is made to ITR-1621, Project 2.3, Operation Hardtack, in which this instrument is completely described and operational results are documented.

The instrument is 15- by 12- by 21-in. high, weighs approximately 50 lb, and consists of the following units: a radiation detector, an amplifier with time base, a recording system, a battery pack, and miscellaneous instrument control switches and associated circuitry. The detector unit can be mounted either inside the recorder case or as a separate unit connected by a cable not exceeding 25 ft in length. The detector is a low-range ionization chamber containing a concentric internal high-range chamber. Both chambers have a nearly 4-π response and are independent of incident gamma energy to within ± 20 per cent from 100 kev to 1.3 Mev. Recording is accomplished on a magnetic tape giving either 12 hr of operation with a range of dose rates from 10 mr/hr to 10^5 r/hr or 60 hr of operation with a range of 10 mr/hr to 2×10^4 r/hr. Tape readout is accomplished by a data-reduction device separate from the instrument in which the taped data are automatically plotted.

5.5 CONCLUSIONS AND RECOMMENDATIONS

5.5.1 Use of Balloons as Instrument Platforms

Latex balloons are not recommended. Plastic balloons will prove more favorable, especially if additional lift can be obtained from airfoils. The need for substantial amounts of helium and the difficulty of stabilizing any balloon in space make their potential as an instrument platform questionable.

5.5.2 Fallout Collector

Where many instruments are to be placed in a predicted fallout pattern, mobility is a prime requirement, and completely self-contained lightweight instrumentation is highly recommended. The use of compressed air for a power source is more favorable than batteries for field installations, especially where constant maintenance is difficult. It is essential to protect the fallout collecting tray from extraneous material wherever the instrument is located within the area affected by the shock wave.

Appendix A

TABULATED FALLOUT PARTICLE DATA

TABLE A.1—CHARACTERIZATION OF RADIOACTIVE FALLOUT PARTICLES COLLECTED 1.0 MILE FROM GZ, SHOT DIABLO

Particle No.	Size, μ (a) Maximum diameter	(b) Diameter at right angles to maximum	(c) $\sqrt{ab}$	Gamma activity at H + 340 hr, counts/min	Shape	Color
D-1	3130	2430	2760	10,600,000	Sphere	Black
D-2	2610	2150	2380	9,910,000	Spheroidal	Black
D-3	3360	2270	2760	11,500,000	Elongated	Black
D-4	4830	2630	3560	14,800,000	Irregular smooth	Black
D-5	2500	2140	2310	5,020,000	Irregular smooth	Black
D-6	1730	1550	1640	3,390,000	Sphere	Black
D-7	1540	1300	1410	6,600,000	Spheroidal	Black
D-8	1400	1370	1380	5,940,000	Sphere	Black
D-9	1510	1370	1430	991,000	Sphere	Black
D-10	2110	2040	2080	14,000,000	Irregular smooth	Black
D-11	1410	1370	1380	2,270,000	Sphere	Black
D-12	1580	1340	1455	4,050,000	Sphere	Black
D-13	1830	1340	1570	5,410,000	Spheroidal	Black
D-14	1010	858	930	1,160,000	Spheroidal	Black
D-15	1790	1610	1700	13,400,000	Sphere	Black
D-16	1970	1230	1560	3,460,000	Spheroidal	Black
D-17	2320	1260	1710	9,020,000	Elongated	Black
D-18	1270	1230	1250	862,000	Spheroidal	Black
D-19	1410	1370	1390	1,680,000	Sphere	Black
D-20	759	743	750	4,930,000	Spheroidal	Black
D-21	1370	1200	1280	1,760,000	Sphere	Black
D-22	1580	1090	1310	1,150,000	Spheroidal	Black
D-23	1870	1550	1700	7,560,000	Spheroidal	Black
D-24	1340	1100	1210	1,130,000	Spheroidal	Black
D-25	1020	990	1005	6,070,000	Sphere	Black
D-26	1410	1300	1350	3,340,000	Sphere	Black
D-27	1440	1440	1440	4,890,000	Spheroidal	Black
D-28	1760	1440	1590	6,400,000	Spheroidal	Black
D-29	1340	1230	1280	3,720,000	Sphere	Black
D-30	1160	1130	1140	1,690,000	Sphere	Black
D-31	1340	1200	1270	1,930,000	Spheroidal	Black
D-32	1510	1410	1460	8,040,000	Sphere	Black
D-33	2250	1060	1540	1,080,000	Elongated	Black
D-34	1870	1230	1515	708,000	Spheroidal	Black
D-35	2640	1300	1850	4,050,000	Elongated	Black
D-36	2040	1730	1870	1,930,000	Irregular smooth	Black
D-37	2530	1130	1690	3,660,000	Elongated	Black
D-38	1340	1090	1210	1,640,000	Sphere	Black
D-39	2460	1620	2000	2,660,000	Irregular smooth	Black
D-40	1160	1090	1125	7,080,000	Sphere	Black
D-41	1970	1090	1470	1,950,000	Elongated	Black
D-42	1340	1340	1340	10,200,000	Sphere	Black
D-43	1510	1230	1360	2,630,000	Spheroidal	Black
D-44	1410	1060	1220	3,350,000	Spheroidal	Black
D-45	1440	1270	1350	4,890,000	Sphere	Black

[redacted]

TABLE A.1 — (Continued)

Particle No.	Size, μ (a) Maximum diameter	(b) Diameter at right angles to maximum	(c) $\sqrt{ab}$	Gamma activity at H + 340 hr, counts/min	Shape	Color
D-46	2180	1230	1640	3,050,000	Elongated	Black
D-47	1650	1480	1560	3,580,000	Sphere	Black
D-48	1230	1130	1180	6,800,000	Spheroidal	Black
D-49	3200	1550	2230	6,730,000	Elongated	Black
D-50	2640	1130	1730	2,500,000	Elongated	Black
D-51	1580	1410	1490	11,400,000	Sphere	Black
D-52	1340	1200	1270	2,210,000	Spheroidal	Black
D-53	1340	1160	1250	4,040,000	Sphere	Black
D-54	1230	1230	1230	6,310,000	Sphere	Black
D-55	1270	1230	1250	1,300,000	Sphere	Black
D-56	1620	1410	1510	2,710,000	Spheroidal	Black
D-57	1650	1510	1580	4,120,000	Sphere	Black
D-58	1720	1650	1680	3,150,000	Spheroidal	Black
D-60	3130	1340	2050	9,540,000	Elongated	Black
D-63	1300	1020	1150	1,640,000	Spheroidal	Black
D-64	1690	1620	1660	3,410,000	Irregular smooth	Black
D-65	1060	1030	1050	2,200,000	Sphere	Black
D-66	1550	1340	1440	1,150,000	Spheroidal	Black
D-67	2850	1830	2280	2,470,000	Elongated	Black
D-68	1060	986	1020	2,080,000	Sphere	Black
D-69	1200	1020	1110	4,440,000	Sphere	Black
D-70	2010	1340	1640	3,570,000	Elongated	Black
D-71	2920	2010	2420	5,020,000	Elongated	Black
D-72	611	578	590	2,840,000	Sphere	Black
D-73	2010	1370	1660	1,980,000	Irregular smooth	Black
D-74	1550	1240	1390	1,800,000	Spheroidal	Black
D-75	1060	1020	1070	1,080,000	Sphere	Black
D-76	2080	1620	1440	1,070,000	Spheroidal	Black
D-77	2040	1510	1755	244,000	Irregular smooth	Black
D-78	1340	1200	1270	3,500,000	Spheroidal	Black
D-80	1340	1060	1190	1,710,000	Irregular smooth	Black
D-82	1440	1410	1425	2,400,000	Irregular smooth	Black
D-84	2010	1090	1480	862,000	Elongated	Black
D-86	1440	1020	1210	1,400,000	Irregular smooth	Black
D-87	2500	1130	1680	1,320,000	Elongated	Black
D-88	1160	1090	1125	1,120,000	Spheroidal	Black
D-89	2320	1480	1880	1,200,000	Elongated	Black
D-90	1090	1020	1050	4,230,000	Sphere	Black
D-91	2450	1340	1810	1,050,000	Elongated	Black
D-93	1760	1090	1390	3,400,000	Spheroidal	Black
D-94	1940	1200	1530	2,060,000	Irregular smooth	Black
D-95	915	880	900	2,100,000	Sphere	Black
D-96	1010	986	1000	13,200,000	Sphere	Black
D-97	4240	1100	2160	467,000	Elongated	Black
D-98	1010	1230	1120	2,260,000	Sphere	Black

[redacted]

TABLE A.1 — (Continued)

Particle No.	Size, μ (a) Maximum diameter	(b) Diameter at right angles to maximum	(c) $\sqrt{ab}$	Gamma activity at H + 340 hr, counts/min	Shape	Color
D-99	1440	1200	1315	8,040,000	Sphere	Black
D-100	1480	1160	1310	397,000	Spheroidal	Black
D-101	1370	1130	1240	5,320,000	Sphere	Black
D-102	1090	1060	1050	5,300,000	Sphere	Black
D-103	1440	739	1030	231	Irregular angular	Black
D-104	1650	1270	1450	3,600	Irregular smooth	Black
D-105	1760	1230	1470	660,000	Irregular smooth	Black
D-107	915	915	915	4,250,000	Spheroidal	Black
D-108	1790	1580	1680	1,050,000	Irregular angular	Black
D-109	1580	739	1080	1,560,000	Elongated	Black
D-110	1370	1230	1290	963,000	Spheroidal	Black
D-111	1650	1230	1420	1,400,000	Irregular smooth	Black
D-112	1906	1350	1720	585,000	Sphere	Black
D-113	1340	1060	1190	467,000	Irregular angular	Black
D-114	1690	1340	1500	6,490,000	Irregular smooth	Black
D-116	2530	2430	2480	2,240,000	Sphere	Black
D-117	1620	1200	1390	1,180,000	Irregular smooth	Black
D-118	1620	1370	1290	1,330,000	Irregular angular	Black
D-119	3170	1440	2090	5,630,000	Irregular smooth	Black
D-120	3030	1410	2090	915,000	Elongated	Black
D-121	1720	1690	1700	421,000	Irregular angular	Black
D-123	950	880	900	906,000	Sphere	Black
D-124	950	845	900	998,000	Sphere	Black
D-125	1130	915	1105	2,600,000	Spheroidal	Black
D-126	2080	1090	1510	928,000	Elongated	Black
D-128	1510	1120	1300	677,000	Elongated	Black
D-129	950	816	877	1,970,000	Sphere	Black
D-130	950	880	910	729,000	Spheroidal	Black
D-131	845	810	827	1,090,000	Sphere	Black
D-132	1580	915	1200	5,010,000	Elongated	Black
D-133	669	669	669	835,000	Sphere	Black
D-134	915	880	900	564,000	Sphere	Black
D-135	880	704	787	787,000	Spheroidal	Black
D-136	880	810	845	1,280,000	Sphere	Black
D-137	1300	1160	1232	7,470,000	Spheroidal	Black
D-138	1370	845	1076	1,580,000	Irregular smooth	Black
D-139	1410	810	1069	1,430,000	Elongated	Black
D-140	915	880	900	964,000	Sphere	Black
D-141	1760	986	1175	2,260,000	Irregular smooth	Black
D-143	1550	915	1189	4,280,000	Elongated	Black
D-144	1550	1510	1530	1,140,000	Spheroidal	Black
D-145	880	845	848	3,860,000	Sphere	Black
D-146	1410	1130	1260	2,730,000	Elongated	Black
D-147	986	950	960	1,900,000	Sphere	Black
D-148	1160	810	970	985,000	Spheroidal	Black

TABLE A.1 — (Continued)

Particle No.	Size, μ (a) Maximum diameter	(b) Diameter at right angles to maximum	(c) $\sqrt{ab}$	Gamma activity at H + 340 hr, counts/min	Shape	Color
D-150	669	669	669	1,510,000	Sphere	Black
D-151	880	634	748	629,000	Spheroidal	Black
D-152	880	880	880	1,720,000	Spheroidal	Black
D-153	1510	880	1149	1,640,000	Elongated	Black
D-154	1340	1060	1190	800,000	Spheroidal	Black
D-155	704	704	704	3,130,000	Sphere	Black
D-156	563	563	563	501,000	Sphere	Black
D-157	1160	845	990	1,210,000	Spheroidal	Black
D-158	704	669	686	2,220,000	Sphere	Black
D-159	915	810	863	2,570,000	Spheroidal	Black
D-160	1690	880	1220	2,910,000	Elongated	Black
D-161	915	845	880	1,990,000	Sphere	Black
D-162	986	950	965	511,000	Spheroidal	Black
D-163	1760	880	1240	1,770,000	Elongated	Black
D-164	1232	915	1060	963,000	Spheroidal	Black
D-165	880	810	845	1,190,000	Sphere	Black
D-166	915	810	863	1,590,000	Sphere	Black
D-167	774	739	755	1,820,000	Sphere	Black
D-168	986	704	834	959,000	Spheroidal	Black
D-169	774	634	700	959,000	Sphere	Black
D-170	880	739	807	1,600,000	Spheroidal	Black
D-171	845	809	827	1,280,000	Sphere	Black
D-172	739	669	703	1,820,000	Sphere	Black
D-173	1302	739	981	1,240,000	Spheroidal	Black
D-174	704	704	704	752,000	Sphere	Black
D-175	1373	1197	1280	5,450,000	Spheroidal	Black
D-176	704	704	704	1,460,000	Sphere	Black
D-177	774	739	755	1,570,000	Sphere	Black
D-178	598	563	580	528,000	Sphere	Black
D-179	1021	774	890	200,000	Spheroidal	Black
D-180	1226	774	974	519,000	Irregular smooth	Black
D-181	810	774	791	1,380,000	Sphere	Black
D-182	774	634	701	1,410,000	Sphere	Black
D-183	1338	950	1130	708,000	Irregular smooth	Black
D-184	845	810	827	589,000	Sphere	Black
D-185	880	634	748	2,080,000	Spheroidal	Black
D-186	704	598	648	629,000	Sphere	Black
D-187	915	810	863	2,080,000	Sphere	Black
D-188	704	704	704	1,630,000	Sphere	Black
D-189	1197	739	940	638,000	Irregular smooth	Black
D-190	704	634	668	1,600,000	Sphere	Black
D-191	1162	886	1010	2,580,000	Spheroidal	Black
D-192	634	634	634	1,250,000	Sphere	Black
D-194	880	598	725	305,000	Spheroidal	Black
D-195	891	776	831	1,690,000	Spheroidal	Black

TABLE A.1 — (Continued)

Particle No.	Size, μ (a) Maximum diameter	(b) Diameter at right angles to maximum	(c) $\sqrt{ab}$	Gamma activity at H + 340 hr, counts/min	Shape	Color
D-196	1091	880	980	2,010,000	Sphere	Black
D-197	915	739	823	497,000	Sphere	Black
D-198	1338	950	1130	1,120,000	Irregular smooth	Black
D-199	908	825	865	1,270,000	Sphere	Black
D-200	1172	825	983	2,720,000	Spheroidal	Black
D-201	1023	891	955	1,870,000	Spheroidal	Black
D-202	825	743	783	629,000	Spheroidal	Black
D-203	990	858	920	2,790,000	Spheroidal	Black
D-204	673	660	667	520,000	Sphere	Black
D-205	1007	924	965	1,330,000	Sphere	Black
D-206	759	693	725	963,000	Sphere	Black
D-207	726	627	725	717,000	Spheroidal	Black
D-208	875	776	824	937,000	Sphere	Black
D-209	825	776	800	3,030,000	Sphere	Black
D-210	462	462	462	787,000	Spheroidal	Black
D-211	743	693	717	1,810,000	Sphere	Black
D-212	610	545	576	629,000	Irregular smooth	Black
D-213	809	776	692	2,010,000	Sphere	Black
D-214	941	908	925	1,420,000	Sphere	Black
D-215	924	759	838	1,310,000	Spheroidal	Black
D-216	1601	858	1170	1,140,000	Elongated	Black
D-217	776	776	776	624,000	Spheroidal	Black
D-218	990	908	894	2,660,000	Spheroidal	Black
D-219	759	743	750	1,720,000	Sphere	Black
D-220	908	842	876	1,580,000	Spheroidal	Black
D-221	825	825	825	844,000	Sphere	Black
D-222	743	693	717	752,000	Sphere	Black
D-224	877	825	870	3,180,000	Sphere	Black
D-225	776	693	725	1,730,000	Sphere	Black
D-226	1106	974	1040	1,870,000	Sphere	Black
D-227	726	726	726	2,030,000	Sphere	Black
D-228	1320	1056	1170	4,530,000	Irregular smooth	Black
D-229	908	875	891	1,160,000	Sphere	Black
D-230	924	858	891	1,660,000	Spheroidal	Black
D-231	990	941	965	1,530,000	Spheroidal	Black
D-232	858	842	850	5,360,000	Spheroidal	Black
D-233	1221	644	888	3,060,000	Elongated	Black
D-234	2605	1373	1880	1,300,000	Elongated	Black
D-235	1370	1155	1260	1,460,000	Irregular smooth	Black
D-236	710	677	694	1,980,000	Sphere	Black
D-237	677	660	668	2,440,000	Sphere	Black
D-238	1023	974	997	1,590,000	Sphere	Black
D-239	693	660	675	1,830,000	Sphere	Black
D-240	1155	759	936	3,830,000	Elongated	Black
D-241	1254	908	1070	2,380,000	Irregular smooth	Black

TABLE A.1 — (Continued)

Particle No.	Size, μ (a) Maximum diameter	(b) Diameter at right angles to maximum	(c) $\sqrt{ab}$	Gamma activity at H + 340 hr, counts/min	Shape	Color
D-242	957	776	860	1,390,000	Sphere	Black
D-243	792	759	775	1,620,000	Sphere	Black
D-244	739	704	720	655,000	Sphere	Black
D-245	693	693	693	1,800,000	Sphere	Black
D-246	726	726	726	1,270,000	Sphere	Black
D-247	1650	941	1250	1,900,000	Elongated	Black
D-248	704	669	686	1,220,300	Sphere	Black
D-249	990	627	770	1,400,000	Spheroidal	Black
D-251	710	627	667	44,800	Irregular angular	Black
D-252	660	644	652	536,000	Sphere	Black
D-253	990	611	776	951,000	Spheroidal	Black
D-254	578	528	550	1,250,000	Sphere	Black
D-255	809	792	800	2,770,000	Spheroidal	Black
D-256	627	627	627	3,580,000	Sphere	Black
D-257	825	660	738	1,780,000	Spheroidal	Black
D-258	594	561	577	2,240,000	Sphere	Black
D-259	545	545	545	578,000	Sphere	Black
D-260	660	627	643	867,000	Sphere	Black
D-263	578	545	562	2,290,000	Sphere	Black
D-264	611	611	611	3,110,000	Sphere	Black
D-265	677	594	635	569,000	Sphere	Black
D-266	644	627	583	2,000,000	Sphere	Black
D-267	627	561	594	739,000	Sphere	Black
D-268	611	561	585	523,000	Sphere	Black
D-269	677	644	660	945,000	Sphere	Black
D-270	1232	634	2120	818,000	Elongated	Black
D-271	660	611	635	551,000	Sphere	Black
D-273	644	545	352	1,400,000	Sphere	Black
D-274	974	875	954	147	Irregular angular	Black
D-276	809	759	785	840,000	Irregular smooth	Black
D-277	545	528	538	1,240,000	Sphere	Black
D-278	627	611	616	607,000	Sphere	Black
D-279	1007	627	790	972,000	Irregular smooth	Black
D-280	1188	462	735	339,000	Elongated	Black
D-283	677	644	660	361,000	Irregular smooth	Black
D-284	627	627	627	1,530,000	Sphere	Black
D-286	578	495	545	23,800	Irregular angular	Black
D-287	578	561	570	1,680,000	Sphere	Black
D-290	743	660	639	959,000	Irregular smooth	Black
D-291	726	660	692	405,000	Spheroidal	Black
D-293	825	660	738	288,000	Irregular angular	Black
D-297	704	598	648	89	Irregular angular	Black
D-298	528	495	510	1,070,000	Sphere	Black
D-300	446	347	393	24,000	Irregular smooth	Black
D-301	462	363	409	38,300	Spheroidal	Black

TABLE A.1 — (Continued)

Particle No.	Size, μ (a) Maximum diameter	(b) Diameter at right angles to maximum	(c) $\sqrt{ab}$	Gamma activity at H + 340 hr, counts/min	Shape	Color
D-304	363	330	346	181,600	Sphere	Black
D-305	314	297	305	46,600	Sphere	Black
D-306	627	578	602	89,100	Sphere	Black
D-308	528	458	490	1,600	Spheroidal	Black
D-309	415	248	405	21,600	Irregular angular	Black
D-310	710	330	485	100,000	Irregular smooth	Black
D-313	330	314	320	31	Irregular angular	Black
D-316	598	598	598	673,000	Sphere	Black
D-319	1060	530	750	15,600	Irregular angular	Black
D-320	875	776	825	2,480,000	Spheroidal	Black
D-321	825	792	810	2,360,000	Spheroidal	Black
D-322	759	759	759	1,290,000	Sphere	Black
D-323	774	598	680	589,000	Sphere	Black
D-324	759	759	759	739,000	Sphere	Black
D-325	825	908	865	314,000	Sphere	Black
D-326	810	774	790	1,710,000	Sphere	Black
D-327	704	669	686	1,060,000	Sphere	Black
D-328	842	792	816	906,000	Sphere	Black
D-329	396	396	396	994,000	Sphere	Black
D-330	845	704	770	1,070,000	Spheroidal	Black
D-331	1485	1056	1250	2,200,000	Spheroidal	Black
D-332	726	660	692	391,000	Sphere	Black
D-333	915	880	906	576,000	Spheroidal	Black
D-334	1021	915	966	1,190,000	Sphere	Black
D-335	776	743	759	1,180,000	Sphere	Black
D-336	1089	974	1060	2,280,000	Spheroidal	Black
D-337	3143	3070	3105	981,000	Sphere	Black
D-338	710	642	675	963,000	Sphere	Black
D-339	704	634	668	1,050,000	Sphere	Black
D-340	669	669	669	2,200,000	Sphere	Black
D-341	704	669	686	1,840,000	Sphere	Black
D-342	908	809	857	1,360,000	Sphere	Black
D-343	743	693	717	1,520,000	Sphere	Black
D-344	677	677	677	879,000	Sphere	Black
D-345	1469	974	1195	642,000	Irregular smooth	Black
D-346	380	347	363	532,000	Sphere	Black
D-347	669	634	652	1,820,000	Sphere	Black
D-348	660	660	660	950,000	Sphere	Black
D-349	1073	941	1005	3,980,000	Sphere	Black
D-350	1901	915	1315	1,220,000	Elongated	Black
D-523	2147	1162	1580	4,080,000	Elongated	Black
D-525B	1478	1267	1370	4,700,000	Sphere	Black
D-526	1232	1232	1232	4,970,000	Sphere	Black
D-527A	1478	986	1205	699,000	Irregular smooth	Black
D-527B	693	644	668	1,050,000	Sphere	Black

[redacted]

TABLE A.1 — (Continued)

Particle No.	Size, μ (a) Maximum diameter	(b) Diameter at right angles to maximum	(c) $\sqrt{ab}$	Gamma activity at H + 340 hr, counts/min	Shape	Color
D-527C	941	825	882	1,840,000	Irregular smooth	Black
D-527D	809	743	775	823,000	Spheroidal	Black
D-527E	726	693	710	1,310,000	Sphere	Black
D-527F	627	627	627	1,600,000	Sphere	Black
D-527G	704	598	650	2,070,000	Sphere	Black
D-528	986	845	913	2,200,000	Sphere	Black
D-530A	974	875	923	2,250,000	Spheroidal	Black
D-530B	880	845	848	336,000	Spheroidal	Black
D-530C	693	644	668	2,820,000	Spheroidal	Black
D-532	1373	1267	1320	4,030,000	Irregular smooth	Black
D-533X	246	246	246	1,200	Spheroidal	Black
D-535	891	825	858	1,910,000	Sphere	Black
D-539	710	660	685	620,000	Spheroidal	Black
D-542A	1443	1021	1215	137,000	Irregular smooth	Black
D-542B	704	669	686	1,030,000	Sphere	Black
D-542C	810	669	736	39,100	Spheroidal	Black
D-562	1267	1021	1140	60,200	Irregular smooth	Black
D-583	1760	1549	1650	2,110,000	Irregular smooth	Black
D-543A	594	594	594	1,060,000	Sphere	Black
D-543B	578	528	553	1,040,000	Spheroidal	Black
P-1	4825	4168	4510	102,000,000	Spheroidal	Black
P-2	7310	1462	3260	18,900,000	Elongated	Black
P-3	1584	1338	1460	2,770,000	Spheroidal	Black
P-4	1619	1514	1565	8,790,000	Sphere	Black
P-6	3436	1754	2450	21,900,000	Elongated	Black
P-7	1462	1462	1462	11,000,000	Sphere	Black
P-8	2147	1901	2020	10,700,000	Spheroidal	Black
P-9	1021	950	980	2,740,000	Sphere	Black
P-10	3070	1316	2010	12,100,000	Elongated	Black
P-12	4532	1754	2820	8,040,000	Irregular smooth	Black
P-13	2323	1478	1850	5,280,000	Irregular smooth	Black
P-14	1974	1901	1935	11,200,000	Sphere	Black
P-15	2147	1936	2040	9,900,000	Spheroidal	Black
P-16	3143	1243	1975	15,800,000	Elongated	Black
P-17	2851	2266	2545	15,200,000	Spheroidal	Black
P-18	1373	1338	1355	8,090,000	Sphere	Black
P-20	2042	1830	1935	10,600,000	Spheroidal	Black

TABLE A.2—CHARACTERIZATION OF RADIOACTIVE FALLOUT PARTICLES COLLECTED AT 1.3 MILES FROM GZ, SHOT PRISCILLA

Particle No.	Size, μ (a) Maximum diameter	(b) Diameter at right angles to maximum	(c) $\sqrt{ab}$	Gamma activity at H + 340 hr, counts/min	Shape	Color
20-A-A	3115	930	1720	Not counted	Elongated	Opaque, yellow-brown
20-A-B	1810	1020	1360	Not counted	Spheroidal	Cream opaque
20-A-C	2560	2560	2560	3,066	Irregular angular	Opaque, rose-grey
20-A-D	1440	1440	1440	24,626	Spheroidal	Transparent with black specks
20-A-E	2880	1900	2340	10,650	Spheroidal	Sand, semi-transparent
20-A-F	2320	2090	2200	9,318	Irregular angular	White, semi-transparent
20-A-G	1160	1160	1160	1,347	Sphere	Cream, semi-transparent
20-A-H	2930	2100	2480	24,894	Irregular angular	Sand opaque
20-A-I	1395	1350	1370	3,575	Spheroidal	White, semi-transparent
20-B-A	980	980	980	35,592	Sphere	Transparent, olive-green
20-B-B	2140	1630	1870	Not counted	Irregular angular	Sand opaque
20-B-C	1720	1580	1650	Not counted	Irregular angular	Cream-sand opaque
20-B-D	1400	1250	1320	Not counted	Irregular angular	Sand opaque
20-B-E	3720	1250	2160	Not counted	Elongated	White opaque
20-B-F	3720	2320	2940	56,831	Irregular smooth	White, semi-transparent
20-B-G	1670	1070	1340	4,887	Irregular smooth	White opaque
20-C-A	2240	980	1480	Not counted	Elongated	Cream opaque
20-C-B	2560	1400	1890	Not counted	Irregular angular	Cream-brown opaque
20-C-C	1860	1630	1740	Not counted	Irregular smooth	Cream, semi-transparent
20-C-D	1120	1120	1120	16,772	Sphere	Mottled amber, clear in spots
20-C-E	1160	1160	1160	1,589	Sphere	Mottled amber with clear spots
20-C-H	4650	1160	2300	Not counted	Elongated	Cream-brown semitransparent
20-C-I	1950	1630	1780	Not counted	Irregular angular	Rose opaque
20-C-J	2460	1540	1940	Not counted	Irregular angular	White opaque
30-A-A	1160	790	956	Not counted	Irregular smooth	Cream, transparent

TABLE A.2— (Continued)

Particle No.	Size, μ (a) Maximum diameter	(b) Diameter at right angles to maximum	(c) $\sqrt{ab}$	Gamma activity at H + 340 hr, counts/min	Shape	Color
30-A-B	930	930	930	1,575	Sphere	Mottled amber with clear spots
30-B-A	980	930	955	2,146	Sphere	Mottled amber with clear spots
30-B-B	1400	980	1170	Not counted	Spheroidal	Mottled amber with clear spots
30-B-C	840	790	813	Not counted	Irregular angular	White, semi-transparent
30-B-D	1210	880	1030	Not counted	Spheroidal	Mottled amber with clear spots
30-B-E	1630	1160	1370	Not counted	Irregular angular	Amber and milk color
30-B-F	980	980	980	8,484	Sphere	Mottled amber with clear spots
30-B-G	880	880	880	1,772	Sphere	Mottled amber with clear spots
30-B-H	1210	1120	1160	Not counted	Spheroidal	Cream opaque
30-B-J	1070	1070	1070	Not counted	Sphere	Mottled amber with clear spots
30-B-K	1400	880	1110	Not counted	Irregular smooth	Mottled amber with clear spots
30-B-L	930	930	930	Not counted	Sphere	Cream opaque
30-B-M	835	835	835	19,789	Sphere	Mottled amber with clear spots
30-C-A	1120	1120	1120	Not counted	Irregular angular	Whitish-grey
30-C-B	2100	1070	1500	Not counted	Irregular smooth	Amber, transparent
30-C-C	1070	930	1000	Not counted	Irregular angular	Sand opaque
30-C-D	1630	930	1230	Not counted	Irregular angular	Sand and black opaque
30-C-E	2320	930	1470	Not counted	Irregular smooth	Amber, transparent
30-C-F	1170	930	1040	Not counted	Irregular angular	Rose-sand opaque
30-C-G	930	930	930	5,524	Sphere	Black opaque
30-C-H	790	790	790	723	Sphere	Mottled amber with clear spots
30-C-I	1630	1160	1370	Not counted	Irregular smooth	White amber, transparent
30-C-J	1070	740	890	Not counted	Irregular angular	White opaque
30-C-K	1530	840	1130	Not counted	Irregular smooth	Amber, transparent
40-A-A	605	560	580	1,252	Spheroidal	Cream opaque
40-A-B	560	560	560	538	Irregular angular	Cream opaque
40-A-C	790	465	605	Not counted	Irregular smooth	Cream opaque

TABLE A.2— (Continued)

Particle No.	Size, μ (a) Maximum diameter	(b) Diameter at right angles to maximum	(c) $\sqrt{ab}$	Gamma activity at H+340 hr, counts/min	Shape	Color
40-A-D	745	465	589	Not counted	Irregular smooth	Cream opaque
40-A-E	1020	510	720	Not counted	Irregular smooth	Cream, semi-transparent
40-A-F	790	700	745	Not counted	Irregular angular	White opaque
40-A-G	840	790	815	Not counted	Irregular angular	White, semi-transparent
40-A-H	700	560	625	Not counted	Irregular angular	Cream, trans-parent
40-A-I	1020	600	782	Not counted	Irregular smooth	Cream, trans-parent
40-A-J	700	700	700	Not counted	Irregular smooth	Cream, trans-parent
40-A-K	1530	790	1100	Not counted	Irregular smooth	Cream, trans-parent
50-A-A	600	420	502	Not counted	Irregular smooth	Cream, trans-parent
50-A-B	650	510	575	Not counted	Irregular smooth	Whitish specky, transparent
50-A-C	700	465	570	Not counted	Irregular smooth	Amber, trans-parent
50-A-D	930	465	658	Not counted	Irregular angular	Rose-sand opaque
50-A-E	420	420	420	Not counted	Sphere	Cream opaque
50-A-F	840	465	625	Not counted	Irregular angular	Rose-cream opaque
60-A-A	790	232	427	Not counted	Elongated	Clear, trans-parent
60-A-B	465	280	361	Not counted	Irregular smooth	Clear, trans-parent
60-A-C	560	330	430	Not counted	Irregular angular	White opaque
60-A-D	510	330	410	Not counted	Irregular smooth	Amber, trans-parent
60-A-E	465	330	391	Not counted	Irregular smooth	Clear, trans-parent
100-A-A	280	230	254	Not counted	Irregular smooth	Cream opaque
100-A-B	465	185	293	Not counted	Irregular smooth	Dark opaque
100-A-C	280	140	198	Not counted	Irregular smooth	Clear, trans-parent
100-A-D	330	280	304	Not counted	Irregular angular	Yellow opaque
100-B-A	185	93	131	Not counted	Irregular angular	Cream opaque
100-B-B	325	185	246	Not counted	Irregular angular	Cream opaque

TABLE A.2— (Continued)

Particle No.	Size, μ (a) Maximum diameter	(b) Diameter at right angles to maximum	(c) $\sqrt{ab}$	Gamma activity at H+340 hr, counts/min	Shape	Color
100-B-C	280	185	227	Not counted	Irregular angular	Cream opaque
100-B-D	330	280	304	Not counted	Spheroidal	White opaque
140-A-A	375	375	375	Not counted	Irregular smooth	Cream opaque
140-A-B	93	93	93	Not counted	Spheroidal	Opaque
140-A-C	280	140	198	Not counted	Irregular smooth	Transparent
140-A-D	140	140	140	Not counted	Irregular smooth	Transparent
200-A-A	93	93	93	Not counted	Sphere	Amber, transparent
200-A-B	140	93	114	Not counted	Irregular smooth	Transparent
200-A-C	140	93	114	Not counted	Irregular smooth	Cream opaque
200-A-D	140	93	114	Not counted	Spheroidal	
200-B-A	93	46	65	Not counted	Spheroidal	Transparent
200-B-B	46	46	46	Not counted	Irregular smooth	Transparent
W-A	560	325	426	Not counted	Irregular smooth	Amber opaque
T-A	1300	1020	1150	Not counted	Spheroidal	Amber, transparent
T-B	232	185	207	Not counted	Spheroidal	Cream opaque
Y-A	600	325	441	Not counted	Irregular smooth	Cream opaque

TABLE A.3 — PARTICLE DENSITY MEASUREMENTS

Diablo Diameter-Mass Technique

Particle No.	Weight, μg	Shape	Diameter, μ	Apparent density, g/cm³
D-349	1214.8	Sphere	924	2.97
D-327	416.9	Sphere	650	2.92
D-305	39.3	Sphere	297	2.87
D-344	375.9	Sphere	637	2.80
D-227	459.9	Sphere	668	2.91
D-155	614.1	Sphere	733	2.86
D-322	550.9	Sphere	742	2.56
D-156	246.9	Sphere	537	3.17
D-95	965.0	Sphere	874	2.76
D-150	413.1	Sphere	660	2.74
D-348	403.3	Sphere	670	2.56
D-171	751.4	Sphere	818	2.61
D-145	918.8	Sphere	874	2.76
D-224	869.4	Sphere	860	2.59
D-192	365.3	Sphere	603	3.16
D-131	558.8	Sphere	818	1.95
D-332	376.0	Sphere	669	2.42
D-221	693.5	Sphere	828	2.36

Flotation Technique

Particle No.	Float, g/cm³	Sink, g/cm³	Apparent density, g/cm³	Shape
		Diablo		
P-6	1.5	1.0	1.25	Irregular
P-13	2.1	2.0	2.05	Irregular
P-19	1.5	1.0	1.25	Irregular
D-35	2.4		2.4	Irregular
D-48	2.1	2.0	2.05	Irregular
D-107	2.8	2.7	2.75	Irregular
D-151	2.5	2.4	2.45	Irregular
D-152	2.6	2.5	2.55	Irregular
D-279	2.6	2.5	2.55	Irregular
D-289	2.8	2.7	2.75	Irregular
		Priscilla		
Pr-2D	2.6	2.5	2.55	Sphere
Pr-3D	2.1	2.0	2.05	Sphere
Pr-4D	2.5	2.4	2.45	Sphere
Pr-5D	2.2	2.1	2.15	Sphere
Pr-6D	2.1	2.0	2.05	Sphere

TABLE A.3 — (Continued)

Particle No.	Float, g/cm^3	Sink, g/cm^3	Apparent density, g/cm^3	Shape
		Priscilla (Continued)		
Pr-7D	2.6	2.5	2.55	Sphere
Pr-8D	2.2	2.1	2.15	Sphere
Pr-9D	2.1	2.2	2.15	Sphere
Pr-10D	2.3	2.2	2.25	Sphere
Pr-11D			1.5	Irregular
Pr-12D			1.5	Irregular
Pr-13D	2.1	2.0	2.05	Irregular
Pr-14D	2.1	2.0	2.05	Irregular
Pr-15D	2.0	1.9	1.95	Irregular
Pr-16D	1.9		1.90	Irregular
Pr-17D	2.3	2.2	2.25	Irregular
Pr-18D	1.9	1.5	1.7	Irregular
Pr-19D	2.1	2.0	2.05	Irregular
Pr-20D	2.0	1.9	1.95	Irregular

TABLE A.4—IRON AND LEAD ANALYSIS

Particle No.	Weight, g	Total content, mg	
		Lead*	Iron
	Diablo		
1X	0.0022	0.019	0.15
2X	0.0048	0.023	0.42
3X	0.0073	0.041	0.43
4X	0.0022	0.028	0.14
5X	0.0031	0.036	0.17
6X	0.0029	0.0097	0.16
7X	0.0049	0.043	0.16
8X	0.0131	0.091	0.78
	Priscilla		
9X	0.0012	0.047	0.049
10X	0.0007	0.027	0.037
11X	0.0007	0.014	0.020
12X	0.0035	0.042	0.072
13X	0.0019	0.021	0.033
14X	0.0016	0.025	0.032

*Because of the difficulty in analyzing microgram quantities of lead, the accuracy of these values is questionable.

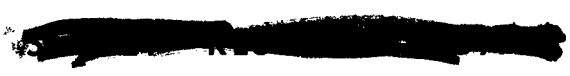

Appendix B

SAMPLE ANALYSES

B.1 INTRODUCTION

Fallout mass determinations, total radioactivity analyses, decay studies, and chemical analyses were performed on many Operation Plumbbob samples at USNRDL in support of Projects 32.3 and 32.4. This appendix contains the bulk of these data.

B.2 PROCEDURE

B.2.1 Sample Identification

Each sample and aliquot of a sample was identified by a number and letter. The first number of the designation refers to the shot. This is followed by an upper-case letter, which denotes the type of sample. After this, a number identifies a specific sample (first, second, third, etc.) of a given type and describes the sample location for OCC's and AOC's. This is followed by an upper-case letter designating an aliquot of the original sample. Finally, lower-case letters indicate sub-aliquots and sub-sub-aliquots. The following designators* were used:

Shot:	I, Priscilla; II, Diablo; IV, Shasta
Type:	A, open-close collector sample (OCC) B, always-open collector sample (AOC) C, incremental collector sample (IC) E, CWS filter sample from Project 32.3 shelter F, cloud-filter sample G, preshot surface-soil sample H, large air-duct filter sample from Project 32.3 shelter
Specific sample:†	1, first sample of type noted; also sample location designator for OCC's and AOC's 2, second sample of type noted, etc.

*Exceptions to the sample-type designation were made for the individual particles recovered following shot Diablo. These particles were simply designated D1 through D125.

†Specific samples of a given type were not designated by single numbers in two instances. These were (1) CWS filter samples from Diablo, which were designated IIEO1, IIEM1 to IIEM24, and IIED1 to IIED24, and (2) CWS filter samples from Shasta, which were designated IVEO1, IVEM1 to IVEM15, and IVED1 to IVED15.

Aliquots:	A, first aliquot of a specific sample B, second aliquot of a specific sample, etc.
Sub-aliquots:	a, first aliquot of an aliquot of a specific sample b, second aliquot of an aliquot of a specific sample, etc.

Two examples of this identification system are

IA2Aa, Priscilla; OCC sample; location 2; first aliquot; first sub-aliquot.

IIF1Bab, Diablo; cloud sample; first sample of this type; second aliquot; first sub-aliquot; second sub-sub-aliquot.

The primary exception to the use of the stated identification scheme was in the case of the IC samples. Diablo IC samples were designated IIC1,515 to IIC1,570, where IIC1,515 was the sample from the first tray exposed. Likewise, Shasta IC samples were designated IVC1,457 to IVC1,515.

Many of these sample analyses, specifically the filter-paper samples and air-duct filters, were a part of the support function of this project for Project 32.3. Reference to the application of these data can be found in the Project 32.3 report.

Field locations of all OCC and AOC samples can be found in the main body of this report. The preshot soil samples were obtained in the near vicinity of GZ, and the cloud filter samples were obtained by aircraft at early times.

B.2.2 Description of Counting Instruments

A variety of instruments was used to measure the radioactivity of the samples and aliquots of the samples. The instruments used were conventional and consisted of end-window gas-flow proportional beta counters, gamma well scintillation counters (WC counters), gamma end-on scintillation counters, and a single-channel gamma pulse-height analyzer. Two other instruments used were (1) a low-geometry gamma scintillation counter and (2) a high-pressure gamma-ionization chamber.

The low-geometry scintillation counter (colloquially termed the "doghouse" counter, and referred to in this report as the "DH counter") was employed to assay the large OCC and AOC fallout samples. The detector consists of a 1- by 1-in. NaI(Tl) crystal located approximately 36 in. from the floor where the collector tray was placed. Shielding consists of a 2-in.-thick lead cave, which surrounds the sample and detector. Readout is by means of a binary scaler (scale of 128) connected in tandem, with an additional scale of 128. The register is driven once for each 16,384 counts. Linear count rates are observed up to 10^6 counts/min. Higher rates (up to 5×10^6) are accommodated with suitable corrections for loss of resolution.

The high-pressure gamma-ionization chamber consists of a large steel chamber containing argon gas at 600 psig, with a $1\frac{3}{8}$-in.-diameter re-entrant cylinder extending from the top to approximately the geometrical center of the chamber. The chamber is equipped with a vibrating-reed electrometer to measure the voltage developed across suitable resistors of approximately 10^8, 10^9, 10^{10}, and 10^{11} ohms. The response of the chamber is 3.55×10^{-15} ma/dis/min for Co^{60}. Samples were placed in a Lusteroid tube (6 by $1\frac{1}{8}$ in.) and were lowered into the cylinder. Readout was via a Brown recorder. All readings were corrected to a 100-μg radium standard having a response of 560.10^{-9} ma. This instrument is hereafter referred to as the "GIC counter."

B.2.3 Analytical Procedures

Each sample received was assayed for total radioactivity. The plastic trays from the OCC's and AOC's were retained inside their aluminum trays and were placed on the bottom of the DH counter and counted; the aluminum cover was removed during counting. The mean of three successive counts was recorded on each sample. Surface-soil samples were generally counted by placing the sample in a plastic bag that was spread over the bottom of the DH

chamber. Again the mean of three successive counts was recorded. IC samples were counted in an end-on gamma counter. Filter-paper assays were obtained on the WC. Individual particles were assayed on the GIC.

A number of fallout samples from each shot was removed from the OCC's by brushing them into tared beakers. The trays were washed with distilled water. The wash water was removed from an individual tray, evaporated, and the residue remaining was added to the bulk fallout material. After this the beaker was weighed on an analytical balance. In some cases large sticks and pebbles were removed. These were assayed and found to be associated with insignificant amounts of radioactivity. In these instances the remaining material was considered to constitute the fallout mass; however, some of this material was found to be ground dust raised by the detonation shock wave.

The gamma radioactivity of a number of aliquots of separate fallout collections was measured in the GIC. It was found that the activity was not distributed uniformly throughout individual samples. Consequently each fallout sample was ground to a fine powder in a power-driven mortar and pestle. Analyses of the pulverized samples indicated homogeneity in radioactivity distribution. Weighed aliquots of the pulverized samples were taken for the following measurements:

(a) *Radioactive Decay.* Decay was followed in both the GIC and WC. In some cases for the WC measurements it was necessary to dilute the aliquots with background soil to reduce the activity levels. These dilutions were then made in all cases to maintain fairly constant self-absorption factors. All GIC samples were 25 g (or diluted to 25 g), and all WC samples were 2 g (or diluted to 2 g), except when indicated.

(b) *Total Fissions.* The number of fissions represented by the fallout samples was determined in the conventional manner by radiochemical analysis of Mo^{99} content. Molybdenum carrier was added directly to the soil before dissolution. The aliquot was dissolved by repeated digestion with HNO_3, HF, and $HClO_4$. The molybdenum was separated twice with α-benzoinoxime followed by suitable scavenging. The molybdenum was finally precipitated with $Pb(NO_3)_2$, weighed as $PbMoO_4$, and counted on a calibrated gas-flow proportional beta counter. After correction for chemical yield and decay back to zero time (assuming a 66.0-hr half life), total fissions were computed assuming a 6.1 per cent fission yield.

(c) *Capture to Fission.* Neptunium-239 capture to fission ratios were determined on the aliquots taken to measure decay in the WC. A single-channel gamma pulse-height analyzer was used in this work. The 140-kev Tc^{99m} and 105-kev Np^{239} photopeaks were measured, and the capture to fission ratios were computed by the method of McIsaac.[1]

(d) *Chemical Analyses.* X-ray-diffraction examinations and analyses for total lead, total iron, silicon dioxide, moisture content, and organic matter were carried out. Standard analytical procedures were employed.

B.3 MEASUREMENTS

The results of measurements made on the samples are grouped according to shot. The data have been compiled in various illustrative tables.

Total-activity-assay data have been corrected for decay to a common time after detonation for purposes of comparison. Total fissions have been computed for the assay data, using average instrument response factors obtained from the analysis of individual samples.

Times of measurements are given in terms of hours after detonation. For example, H + 56 equals 56 hr after detonation.

The data presented are of three distinct types. These are (1) weight determinations, (2) activity measurements (in terms of instrument response, e.g., milliamperes and counts), and (3) radiochemical determinations for total fissions and computed fissions.

Except for very small samples (less than 10 mg), the weight determinations were carried out with an accuracy and precision better than 1 per cent.

With few exceptions all determinations of activity by gamma well counting (WC) were carried out with a statistical precision (standard deviation) of ±3 per cent or better. Although a similar value would be expected for the low-geometry scintillation counter (DH), the non-uniform distribution of the fallout in the collector trays caused a decrease in the precision of these measurements to an estimated ±5 per cent. The ionization chamber measurements were made with a precision dependent upon the total activity. For samples reading greater than 10^{-8} ma, the precision was better than ±3 per cent and decreased from this value to approximately ±20 per cent for samples that gave readings of twice background (0.017×10^{-8} ma).

Radiochemical determinations for Mo^{99}, and thus total fissions, were carried out with an accuracy of approximately ±20 per cent for samples from shots Diablo and Shasta. Calculations of instrument-response factors in terms of fissions [e.g., fissions/(counts/min) DH and fissions/ma GIC] indicated a precision in these measurements of better than ±10 per cent. These data have been used to estimate an accuracy of at least ±25 per cent for reported values of computed fissions which were based on radiochemical analyses and calculated instrument-response factors. These considerations do not apply to samples received from Priscilla. The low total activity and large bulk of material created considerable difficulty in the radiochemical separations and caused low chemical yields and greater uncertainties. It is estimated that the reported fission values for samples from Priscilla should not be considered with an accuracy any greater than ±50 per cent.

B.3.1 Priscilla Shot

A total of nine samples was received. The samples consisted of seven OCC's, one pre-shot surface-soil sample, and one filter-paper cloud sample.

(a) *Fallout Samples.* The seven OCC samples received were designated IA1 to IA7 and were assayed in the DH counter. The sample materials of six OCC's were removed and

TABLE B.1—WEIGHT AND ACTIVITY OF OCC SAMPLES, SHOT PRISCILLA

Sample	Weight,* g	DH assay at H + 56 hr,† 10^4 counts/min	Total fissions ($\times 10^{12}$)	Np^{239} atoms / Fission
IA1	27.4648	1.01	1.04‡	
IA2	13.4789	1.08	0.849	0.078
IA3	56.6626	1.36	1.73	
IA4	50.9187	0.682	0.702‡	
IA5	14.0192	0.239	0.246‡	
IA6	0.8357	0.0017	0.0018‡	
IA7	21.3628	0.0012	0.0012‡	

*Not true fallout, includes shock-wave-raised dust.
†Computed from the decay of sample IA1 (Table B.2).
‡Computed from 1.03×10^8 fissions/DH counts/min at H+56 hr (based on results obtained on aliquots of samples IA2 and IA3).

weighed. Table B.1 lists the initial assay and weight measurements for each tray. Decay studies were carried out with the DH counter on the remaining OCC sample IA1. The decay data are summarized in Table B.2. Upon completion of the decay measurements, the material of this collector was removed and weighed. The total fissions represented by the radioactivity of trays IA1, IA4, IA5, IA6, and IA7 were computed on the basis of measurements of aliquots from OCC's IA2 and IA3.

Three fallout samples (IA2, IA3, and IA7) were selected for analysis. Table B.3 reports the mass and radioactivity of the aliquots prepared from these samples and includes the purpose for which each aliquot was taken. This table also lists the results of radiochemical determinations for total fissions and the measurements of product to fission ratios for Np^{239}

Initial radioactivity assays indicated that the collections were not homogeneous, and consequently the samples were pulverized as indicated previously. The decay data are tabulated in Tables B.4 and B.5. Results of X-ray-diffraction and chemical analysis are given in Tables B.6 and B.7.

TABLE B.2—DH DECAY DATA FOR OCC SAMPLE IA1

Time, H+hr	Activity, 10^4 counts/min	Time, H+hr	Activity, 10^4 counts/min
15.5	3.52	79.0	0.680
16.5	3.37	100	0.521
18.5	2.97	126	0.397
25.5	2.19	170	0.269
32.0	1.77	201	0.215
38.0	1.48	266	0.139
50.0	1.14	340	0.0941
59.5	0.938	415	0.0667

(b) *Filter Samples.* A portion of a Priscilla filter-paper cloud sample, designated IF1, was received and analyzed as shown in Table B.8. The decay of aliquots of IF1 was measured in the GIC (Table B.4) and in the WC (Table B.5).

(c) *Surface-soil Samples.* The surface-soil sample analyzed consisted of one preshot sample. The preshot surface-soil sample weighed 25 lb and was designated IG1. Twelve 2-g aliquots were removed and assayed in the WC. Results of these measurements are given in Table B.9. Aliquots were removed from two samples; these were designated IG1A and IG1E (X-ray analysis, Table B.6) and IG1H and IG1L (chemical analysis, Table B.7).

B.3.2 Diablo Shot

A total of 148 samples was received from this shot. These consisted of 5 OCC samples, 55 IC samples, 69 CWS filter-paper samples, 1 cloud filter-paper sample, and 1 preshot surface-soil sample.

(a) *Fallout Samples.* A large proportion of the OCC and IC samples was made up of relatively large pebbles and of straw. The specific activity of the remaining material was high, and many small (<0.5 mm) black spheres were observed.

The five OCC samples received from this shot were designated IIA1 to IIA5, assayed in the DH counter, and weighed, and the total fissions were determined. These results are given in Table B.10.

Sample IIA4 was retained for decay measurements in the DH counter. Data are given in Table B.11. The contents of tray IIA2 were transferred to a large Lusteroid tube, and decay measurements were taken in the GIC (Table B.12) and in the WC (Table B.13).

Additional analyses were performed on three fallout samples (IIA1, IIA3, and IIA5). The materials from the collector trays were first passed through a No. 10 sieve to remove the sticks and pebbles. The fine portions were then ground and aliquoted. The trays themselves were rinsed with water, and the residue was dried, weighed, and counted. Descriptions of the aliquots taken, and their amount, activity, and purpose are given in Table B.14. Total-fission determinations and measured product to fission ratios are also given in this table.

Decay rates obtained from the GIC and WC aliquots are presented in Tables B.12 and B.13. X-ray and chemical analyses data are given in Tables B.15 and B.16.

Fifty-six trays from the IC were received and designated IIC1,515 to IIC1,570. Sample IIC1,517 was the first sample tray exposed at H+20 sec. Each subsequent tray was exposed for a period of 1 min. The trays were assayed on the end-on gamma counter; the data obtained are given in Table B.17.

TABLE B.3—ALIQUOT DESIGNATION AND PURPOSE OF FALLOUT SAMPLES, SHOT PRISCILLA

Sample	Purpose	Weight, g	Activity at H+56 hr, 10^{-9} ma
	Sample IA2		
IA2	OCC sample; DH count = 1.08×10^4 counts/min at H+56 hr. Material removed from tray, and aliquots IA2A, B, and C removed prior to grinding. Remainder ground and aliquots IA2J, K, L, M, and N prepared	13.4789	
IA2A	Preliminary aliquot; aliquots IA2Aa and IA2Ab removed	1.2502	
IA2Aa	Preliminary aliquot; aliquots IA2Aad and IA2Aae (single particle) prepared	0.0553	
IA2Aad	Remainder of aliquot IA2Aa submitted to WC decay	0.0547	
IA2Aae	Particle removed from aliquot IA2Aa for WC decay	0.0006	
IA2Ab	Aliquot for radiochemistry; fissions = 5.74×10^{10}; product to fission ratio = 0.12	1.1949	
IA2B	Aliquot for radiochemistry; fissions = 1.09×10^{11}; product to fission ratio = 0.073	1.4143	
IA2C	Aliquot for GIC decay; diluted with 23.5 g of IG1	1.5127	25.2
IA2J	Aliquot for X-ray analysis	1.9346	15.0
IA2K	Aliquot for radiochemical analysis; fissions = 9.62×10^{10}	1.5281	12.4
IA2L	Aliquot for GIC decay	2.7838	21.5
IA2M	Aliquot for WC decay; product to fission ratio = 0.078	1.6232	13.0
IA2N	Aliquot for chemical analysis	2.0529	16.3
	Sample IA3		
IA3	OCC sample; DH count = 1.36×10^4 counts/min at H+56 hr. Material removed from tray, and aliquots IA3A, B, and C removed. Remainder ground and aliquots IA3D, E, F, G, and H removed	56.6626	
IA3A	Preliminary aliquot; aliquot IA3Aa removed	1.4983	3.29
IA3Aa	Aliquot for WC decay	0.2492	
IA3B	Aliquot for radiochemical analysis; fissions = 1.10×10^{11}	6.3232	
IA3C	Aliquot for GIC decay; diluted with 9.17 g of IG1	15.8264	37.5
IA3D	Preliminary aliquot; aliquot IA3Da removed	5.2471	15.2
IA3Da	Aliquot for WC decay	2.0017	
IA3E	Aliquot for X-ray analysis	5.5621	16.4
IA3F	Aliquot for GIC decay; diluted with 19.0 g of IG1	6.0406	17.9
IA3G	Aliquot for chemical analysis	6.6803	19.5
IA3H	Aliquot for radiochemical analysis; fissions = 1.39×10^{11}	4.5476	13.9

TABLE B.3 — (Continued)

Sample	Purpose	Weight, g	Activity at H + 56 hr, 10^{-9} ma
	Sample IA7		
IA7	OCC sample; DH count = 123 counts/min at H + 56 hr. Material removed from tray, and aliquots IA7A, B1, and C prepared. Remainder ground and aliquots IA7D, E, and F prepared	21.3628	
IA7A	Preliminary aliquot; no further treatment	1.1440	0.020
IA7B	Aliquot for GIC decay; diluted with 20.4 g of IG1	4.6341	0.09
IA7C	Aliquot for WC decay	2.0612	
IA7D	Aliquot for chemical analysis	1.6414	
IA7E	Aliquot for X-ray analysis	1.7941	
IA7F	Aliquot for WC decay	1.9375	

A large number of particles of varying size and shape were recovered from the Diablo GZ area at a later date. These individual particles were weighed and assayed in the GIC. The results are presented in Table B.18.

(b) *Filter Samples.* A large number of CWS filter-paper samples from the air-sampling devices were received and assayed. In addition, a portion of a Diablo cloud filter-paper sample and two large air-duct filters were analyzed.

The cloud sample consisted of a small piece of filter paper accompanied by the following information: Paper No. PW-2R, fission 9.5×10^{11}. This specimen was designated IIF1 and analyzed as shown in Table B.19. Portions were removed for decay studies; the values obtained are shown in Tables B.12 and B.13.

The CWS filter-paper samples were in the form of small pieces of filter cloth, which had been placed in separate paper envelopes after recovery in the field. Each sample was assayed by removing it from the envelope, rolling it in cellophane, doubling it, and placing it in a small Lusteroid tube (with the active portion at the bottom). Counting was carried out in the WC. Total fissions were computed for each sample; the results of these computations are summarized in Table B.20. Filter sample IIED3 was retained for decay studies.

Two large air-duct filter samples were received and designated IIH1 and IIH2. Because of their size, they were cut in half, and the separated halves were assayed in the DH counter. Total fissions were computed, and the results are given in Table B.21.

(c) *Surface-soil Sample.* The surface-soil sample from this shot consisted of a large sample of preshot soil. Twelve 2-g aliquots were removed from the preshot soil sample (IIG1) and were designated IIG1A to IIG1L. These were assayed in the WC; the results are listed in Table B.22. Samples IIG1A and IIG1F were submitted to X-ray-diffraction analysis, and samples IIG1K and IIG1L were chemically analyzed.

B.3.3 Shasta Shot

A total of 108 samples was received from this shot. These consisted of 12 OCC, 6 AOC, and 56 IC fallout samples; 31 CWS filter-paper samples, 1 roll of CWS filter cloth, and 2 large air-duct filter samples. No surface-soil samples were obtained after this shot. The mass of material collected in the individual fallout samples was relatively small by comparison to fallout samples from Priscilla and Diablo. Conversely, sample radioactivity was high. There were a large number of small black spheres present in the fallout.

(Text continues on page 100.)

TABLE B.4—GIC DECAY DATA FOR FALLOUT SAMPLES, SHOT PRISCILLA

Time, H+hr	OCC sample aliquots, 10^{-9} ma					Cloud sample aliquot, 10^{-9} ma
	IA2C	IA2L	IA3C	IA3F	IA7B	IF1Ac
11.3						
12.6						
13.3						
14.0						
15.4						
25.1						
29.5						
31.4	58.0		87.3		0.26	
32.7						
33.1	54.3		86.1		0.22	
49.5	31.3		46.1		0.17	
56.7	25.2		37.5		0.09	
73.5	17.2		26.0			
75.5					0.06	
80.6	15.3		22.9			
81.5						
97.7	11.8		17.6			
105	10.8	9.07	15.4			15.5
122	8.90	7.54	13.8			13.2
129	8.44	7.08	12.9	5.79		12.6
170	6.19	5.18	9.50	4.27		9.63
177	5.89	4.96	9.10	4.09		9.25
194	5.35	4.43	8.24	3.68		8.25
201	5.05	4.24	7.84	3.46		7.87
218	4.57	3.79	7.10	3.16		7.16
225	4.39	3.67	6.91	3.06		6.94
265	3.64	2.99	5.65	2.53		5.70
273	3.44	2.89	5.44	2.33		5.56
338	2.61	2.14	4.12	1.77		4.21
435	1.91	1.59	3.05	1.31		3.12
442	1.82		2.94			2.92
506	1.52		2.45			2.52
513	1.48		2.41			2.50
602	1.19		1.98			2.02
609	1.19		1.89			1.90
1010	0.57		0.97			1.01
1280	0.42		0.67			0.73
1615	0.29		0.46			0.52
2020	0.19		0.35			0.38
2530						0.27

TABLE B.5—WC DECAY DATA FOR FALLOUT SAMPLES, SHOT PRISCILLA

Time, H+hr	OCC sample aliquots, 10^4 counts/min							Cloud sample aliquot, 10^4 counts/min
	IA2Aad	IA2Aae	IA2M	IA3Aa	IA3Da	IA7C	IA7F	IF1Ab
13.4								
14.0								
15.4								
25.3								
29.3								
33.1	19.0	340		43.6		3.05		
49.6	11.7	249		29.5		2.05		
56.8	10.1	222		25.4		1.76		
73.7	7.53	177		19.5		1.35		
78.6								
81.0	6.85	165		17.8		1.23		
97.8	5.59	136		14.4		0.993		
105	5.17	129	315	13.4		0.876		59.3
110								57.6
115								
122	4.30	110	252	11.1		0.779		48.4
130	3.79	104	216	10.4	98.2	0.733		45.1
146								
153								
170		76.3	163	8.17	70.4	0.544		32.0
178	2.69	72.3	155	6.91	66.7	0.525		30.4
194	2.32	64.5	134	6.16	59.0	0.471		26.9
201	2.23	61.4	128	5.88	56.1	0.453		25.6
218	2.00	54.9	114	5.23	50.1	0.410		22.7
225	1.90	52.3	109	4.91	47.7	0.379		21.6
266	1.44	41.4	84.3	3.80	37.0	0.318		16.8
273	1.39	39.3	81.7	3.70	35.8	0.301		16.3
345	0.977	27.4	57.5	2.56	26.0	0.232		11.4
417	0.731	20.1	42.7	1.95	18.7	0.196	0.313	8.56
507	0.543	15.5	32.0	1.46		0.161	0.258	6.48
513		14.4	31.5				0.242	6.35
602	0.426	11.2	25.2				0.211	5.14
609		11.0	24.8				0.212	5.06
773		7.58	18.1				0.172	3.69
1010		4.86	12.6				0.151	2.75
1040		4.59					0.136	
1270		3.26	9.15					1.95
1610		2.18	6.75					1.43
2020		1.48	4.90					1.06
2520		0.956	3.51					0.770
2860		0.755	2.90					0.662
3220		0.584	2.39					0.552
3750		0.431	1.86					0.445
4060		0.353	1.61					0.389

TABLE B.6—X-RAY-DIFFRACTION ANALYSIS OF FALLOUT SAMPLES, SHOT PRISCILLA

	Sample*				
	IA2J	IA3E	IA7E	IG1A	IG1E
Quartz (SiO_2)	+	+	+	+	+
Feldspar [$(Na,K)AlSi_3O_8$]	+	+	+	+	+
Magnetite† (Fe_3O_4)	1½%	ND	2%	3%	2½%
Hematite (Fe_2O_3)	ND	ND	ND	ND	ND
Iron (Fe)	ND	ND	ND	ND	ND
Calcite ($CaCO_3$)	+	+	+	+	+
Dolomite [$(Ca,Mg)CO_3$]	+	+	+	+	+

*+, qualitatively identified; ND. not detectable.

†The very low magnetite content severely limited the accuracy of analysis. However, it was certain that magnetite constituted much less than 5 per cent of any sample.

TABLE B.7—CHEMICAL ANALYSIS OF FALLOUT SAMPLES, SHOT PRISCILLA

	Sample				
	IA2N	IA3G	IA7D	IG1H	IG1L
Weight, g	1.0007	1.0000	1.0003	1.0000	1.0000
Moisture, g	0.0171	0.0084	0.0107	0.0140	0.0158
Organic matter, g	0.1642	0.1674	0.1236	0.0444	0.0452
Milligrams of lead per gram of soil	0.13	0.077	0.070	0.059	0.050
Milligrams of iron per gram of soil	8.7	15	10	27	27
SiO_2, %		48.19			

TABLE B.8—ALIQUOT DESIGNATION AND PURPOSE OF CLOUD FILTER-PAPER SAMPLE, SHOT PRISCILLA

Sample	Purpose	Activity at H+56 hr, 10^{-9} ma
IF1	Cloud sample; DH count = 0.732 counts/min at H+56 hr	40.0
IF1A	Preliminary aliquot; subdivided into three portions (IF1Aa, b, and c)	19.7
IF1Aa	Aliquot for radiochemical analysis; fissions = 1.59×10^{11}	2.29
IF1Ab	Aliquot for WC decay	1.00
IF1Ac	Aliquot for GIC decay	15.9

TABLE B.9—WC ASSAY OF PRESHOT SURFACE-SOIL SAMPLES

Sample	Activity at H+170 hr, counts/min	Sample	Activity at H+170 hr, counts/min
IG1A	81	IG1G	41
IG1B	57	IG1H	47
IG1C	48	IG1I	63
IG1D	71	IG1J	126
IG1E	221	IG1K	67
IG1F	51	IG1L	245

TABLE B.10—WEIGHT AND ACTIVITY OF OCC SAMPLES, SHOT DIABLO

Sample	Weight,* g	DH assay at H+56 hr, 10^6 counts/min	Total fissions ($\times 10^{14}$)	Np^{239} atoms / Fission
IIA1	36.5424	1.98	4.90	0.151
IIA2	16.7597	2.22†	5.48‡	
IIA3	13.5905	1.70	4.23	0.137
IIA4	5.6663	1.68†	4.15‡	
IIA5	7.9961	1.61	3.71	0.138

*Not true fallout, includes shock-wave-raised dust.

†Computed from the decay of sample IIA4 (Table B.11).

‡Computed from 2.47×10^8 fissions/DH counts/min at H+56 hr (based on results obtained on aliquots of samples IIA1, IIA3, and IIA5).

TABLE B.11—DH DECAY OF OCC SAMPLE IIA4

Time, H+hr	Activity, 10^6 counts/min
16.8	3.85
19.8	3.55
23.0	3.15
30.5	2.71
35.0	2.38
53.5	1.71
59.0	1.56
77.8	1.20
99.7	0.910
107	0.841
171	0.437
219	0.293
250	0.234
340	0.137
390	0.109

TABLE B.12—GIC DECAY DATA FOR FALLOUT SAMPLES, SHOT DIABLO

Time, H+hr	OCC sample aliquots, 10^{-9} ma					Cloud sample aliquot, 10^{-9} ma
	IIA2	IIA1B	IIA3R	IIA3B	IIA5B	IIF1A
20.0	4780					
21.5	4440	1990				
27.4	3480	1560				
30.1			161			
31.5	2970	1320	154			
34.7	2660	1190	139		1030	71.3
52.5	1620	702	93.6	2870	716	45.5
59.2	1370	597	82.0	2470	612	39.8
75.7	980	431	62.9	1780	443	30.1
82.9	880			1590	393	27.5
99.3	680	305	46.9	1250	313	22.3
107	620	277	43.3	1150	286	20.4
172	370		25.6	654	168	11.9
179	351	162	24.2	623	161	11.4
187		156				
220	279	124	18.5	500	128	8.86
249	247	109	15.6	437	111	7.61
268	227	101	14.1	402	102	6.96
275	223		13.7	395	102	6.82
298		99.0				
341	178	80.0	10.2	317	81.9	5.19
414	144	65.2	7.77	256	67.0	3.99
532	112	50.5	5.55	200	51.6	2.92
583	103	46.2	4.91	182	47.1	2.60
682	87.0	39.0	4.08	153	39.8	2.17
750	78.2	34.9	3.52	134	35.8	1.92
1017	56.3	25.3	2.31	99.0	25.6	1.27
1280	42.6	19.1	1.70	75.9	19.5	0.92
1930	26.5	11.4	0.83	47.1	12.2	0.56
2240	22.6	9.92	0.71	40.2	10.2	0.36
2600	19.5	8.61	9.56	34.6	8.81	
3250	15.0	6.67	0.46	26.6	6.82	
4040	10.6	5.11	0.36	19.3	4.99	

TABLE B.13—WC DECAY DATA FOR FALLOUT SAMPLES, SHOT DIABLO

Time, H+hr	OCC sample aliquots, 10^4 counts/min				Cloud sample aliquots, 10^4 counts/min	
	IIA1Aa	IIA1Ab	IIA3Aa	IIA5Ca	IIF1Baa	IIF1Bab
22.1	213	320				
27.4	182	278				
31.0	171	250				
35.3	151	228		292	372	266
51.6	112	165		209	280	195
54.3			246			189
59.2	97.6	145	227	186	248	177
75.6	73.1	115	176	146	198	140
83.2	66.1	105	163	132	177	127
99.6	53.9	84.0	130	106	148	106
107	50.0	75.7	120	97.0	135	93.3
172	25.5	39.5	59.7	49.1	70.1	50.6
202	19.6	30.4	45.9	37.9	54.7	39.4
249	13.6	21.1	32.0	26.3	38.4	27.6
340	7.91	12.1	18.5	15.2	21.8	15.8
414	5.82	8.76	13.5	11.0	15.5	11.1
532	4.09	6.13	9.49	7.78	10.3	7.36
587	3.63	5.36	8.36	6.86	8.80	6.34
748	2.76	4.03	6.28	5.13	6.19	4.42
874						
1010	1.99	2.82	4.44	3.66	4.12	2.95
1250	1.57	2.20	3.51	2.95	3.09	2.20
1780	1.03	1.44	2.33	1.90	1.95	1.36
2240	0.818	1.11	1.80	1.49	1.43	1.01
2600	0.691	0.917	1.50	1.23	1.15	0.825
3250	0.514	0.679	1.11	0.913	0.858	0.598
4040	0.370	0.485	0.80	0.658	0.605	0.423

TABLE B.14—ALIQUOT DESIGNATION AND PURPOSE OF FALLOUT SAMPLES, SHOT DIABLO

Sample	Purpose	Weight, g	GIC activity at H+56 hr, 10^{-9} ma
	Sample IIA1		
IIA1	OCC sample; DH count = 1.98×10^6 counts/min at H+56 hr. Material removed from tray and sieved	36.5424	
	Residue, removed from tray by water spray. Set aside	0.3841	37.9
	Coarse fraction, failed to pass No. 10 sieve; DH count = 2370 counts/min at H+56 hr. Set aside	20.1446	167
	Fine fraction, passed through No. 10 sieve; ground and aliquots prepared. DH count = 1.89×10^6 counts/min at H+56 hr	16.0317	
IIA1A	Diluted with 24.0 g of IIG1; aliquots IIA1Aa and b removed	1.0920	1050
IIA1Aa	Aliquot of IIA1A after dilution for WC decay; diluted with 2.0 g of IIG1; product to fission ratio = 0.151	0.0247	1.14
IIA1Ab	Aliquot of IIA1A after dilution of WC decay sample; diluted with 2.0 g of IIG1	0.0343	1.68
IIA1B	Aliquot for GIC decay; diluted with 24.0 g of IIG1	0.6903	657
IIA1C	Aliquot for radiochemical analysis; fissions = 7.47×10^{12}	0.2443	
IIA1D	Aliquot for X-ray analysis		
	Sample IIA3		
IIA3	OCC sample; DH count = 1.70×10^6 counts/min at H+56 hr. Material removed from tray and sieved	13.5905	
	Residue, removed from tray by water spray; designated IIA3R and decayed in GIC	0.4941	74.9
	Coarse fraction, failed to pass No. 10 sieve; DH count = 379 counts/min at H+56 hr. Set aside	8.2493	2.33
	Fine fraction, passed through No. 10 sieve; ground and aliquots prepared; DH count = 1.72×10^6 counts/min at H+56 hr	4.8471	
IIA3A	Diluted with 24.0 g of IIG1; aliquot IIA3Aa removed	0.9999	2700
IIA3Aa	Aliquot after dilution for WC decay; diluted with 2.0 g of IIG1; product to fission ratio = 0.137	0.0235	2.75
IIA3B	Aliquot for GIC decay; diluted with 24.0 g of IIG1	1.0136	2710
IIA3C	Aliquot for radiochemical analyses; fissions = 2.20×10^{13}	0.2520	651
IIA3D	Aliquot for X-ray analysis		
IIA3E	Aliquot for chemical analysis		

TABLE B.14—(Continued)

Sample	Purpose	Weight, g	GIC activity at H+56 hr, 10^{-9} ma
	Sample IIA5		
IIA5	OCC sample; DH count = 1.55×10^6 counts/min at H+56 hr. Material removed from tray and sieved	7.9961	
	Coarse fraction, failed to pass No. 10 sieve. Set aside	1.4752	0.82
	Fine fraction, passed through No. 10 sieve; ground and aliquots prepared	5.5209	
IIA5A	Aliquot for radiochemical analysis; fissions = 6.66×10^{12}	0.09835	204
IIA5B	Aliquot for GIC decay; diluted with 24.0 g of IIG1	0.31960	673
IIA5C	Diluted with 24.0 g of IIG1; aliquot IIA5Ca removed	0.31102	645
IIA5Ca	Aliquot after dilution for WC decay; diluted with 2.0 g of IIG1; product to fission ratio = 0.138	0.08178	2.18
IIA5D	Aliquot for X-ray analysis		
IIA5E	Aliquot for chemical analysis		

TABLE B.15—X-RAY-DIFFRACTION ANALYSIS OF FALLOUT SAMPLES, SHOT DIABLO

	Sample*				
	IIA1D	IIA3D	IIA5D	IIG1A	IIG1F
Quartz (SiO_2)	+	+	+	+	+
Feldspar [$(Na,K)AlSi_3O_8$]	+	+	+	+	+
Magnetite† (Fe_3O_4)	2½%	2½%	3%	1½%	2%
Hematite (Fe_2O_3)	ND	ND	ND	ND	ND
Iron (Fe)	ND	ND	ND	ND	ND
Calcite ($CaCO_3$)	Trace	ND	ND	Trace	Trace
Dolomite [$(Ca,Mg)CO_3$]	Trace	ND	ND	+	+

*+, qualitatively identified; ND, not detectable.

†The very low magnetite content severely limited the accuracy of analysis. However, it was certain that magnetite constituted much less than 5 per cent of any sample. Values given represent upper limits of quantity. In some cases they may be high by as much as 50 per cent.

TABLE B.16—CHEMICAL ANALYSIS OF FALLOUT SAMPLES, SHOT DIABLO

	Sample				
	IIA1E	IIA3E	IIA5E	IIG1K	IIG1L
Weight, g	0.9989	0.9989	0.9982	1.0000	1.0005
Moisture, g	0.0102	0.0146	0.0176	0.0193	0.0170
Organic matter, g	0.0384	0.0890	0.1029	0.0464	0.0722
Total lead, mg	0.35	0.93	0.76	0.28	0.074
Total iron, mg	11	24	21	19	19

TABLE B.17—ASSAY OF IC SAMPLES, SHOT DIABLO

Sample	Activity at H+31.5 hr, counts/min	Cumulative activity, 10^6 counts/min	Sample	Activity at H+31.5 hr, counts/min	Cumulative activity, 10^6 counts/min
IIC1,515	23	0.000023*	IIC1,543	518,300	10.5
516	3	0.000026*	544	27	10.5
517		0.000026	545		10.5
518	13	0.000039	546	6	10.5
519	17	0.000056	547	10	10.5
520	14	0.000070	548	17	10.5
521		0.000070	549		10.5
522	97	0.000167	550		10.5
523	1,026,000	1.03	551		10.5
524	47	1.03	552		10.5
525	1,671,000	2.70	553	20	10.5
526	1,117,000	3.81	554		10.5
527	1,688,000	5.50	555		10.5
528	488,900	5.99	556	17	10.5
529	163	5.99	557	20	10.5
530	1,208,000	7.20	558	34	10.5
531	117	7.20	559	167	10.5
532	938,800	8.14	560	467	10.5
533	541,000	8.68	561	22,460	10.5
534	97	8.68	562		10.5
535	434,600	9.11	563		10.5
536	60	9.11	564		10.5
537	70	9.11	565		10.5
538	33	9.11	566		10.5
539	168,000	9.28	567		10.5
540	308,900	9.59	568	47	10.5
541	393	9.59	569	34	10.5
542	383,400	9.97	570	281	10.5

*Field notes indicate that these samples were exposed prior to event.

TABLE B.18—GIC ASSAY OF INDIVIDUALLY RECOVERED LARGE PARTICLES, SHOT DIABLO

Sample	Activity at H+850 hr, 10^{-9} ma	Weight, g	Specific activity, 10^{-9} ma/g
D1	215	1.58344	136
D2	67.2	2.08871	32.1
D3	100	0.69628	143
D4	32.4	0.07139	455
D5	11.4	0.02174	524
D6	85.7	0.15095	568
D7	57.5	0.17908	321
D8	90.4	0.22871	395
D9	36.5	0.03475	1050
D10	15.2	0.02209	688
D11	37.2	0.18611	200
D12	17.5	0.03471	504
D13	29.2	0.07894	370
D14	23.0	0.07745	297
D15	58.9	0.14677	401
D16	26.9	0.01565	1720
D17	102	0.16225	629
D18	109	0.81910	133
D19	6.7	0.01241	489
D20	35.0	0.02095	1670
D21	30.2	0.09531	317
D22	3.81	0.03337	114
D23	49.3	0.36353	136
D24	17.2	0.05160	333
D25	13.58	0.04314	315
D26	42.7	0.02615	1633
D27	25.2	0.12319	205
D28	38.6	0.07025	549
D29	50.7	0.24407	208
D30	23.8	0.04393	545
D31	26.7	0.14871	179
D32	35.1	0.16865	208
D33	169	0.23558	717
D34	27.2	0.16756	162
D35	41.6	0.39197	106
D36	15.2	0.03244	469
D37	45.5	0.04807	947
D38	44.1	0.05086	867
D39	79.4	0.09137	869
D40	18.6	0.50488	36.8
D41	48.9	0.06304	776
D42	40.6	0.03098	1311
D43	22.1	0.05458	405
D44	15.1	0.00838	1802
D45	45.1	0.03633	1241
D46	71.8	0.08056	891
D47	43.6	0.04150	1051
D48	92.4	0.04815	1920
D49	104	0.07325	1420
D50	1.11	0.01830	60.4

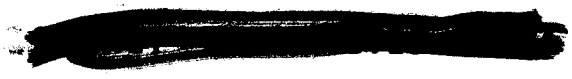

TABLE B.18 — (Continued)

Sample	Activity at H+850 hr, 10^{-9} ma	Weight, g	Specific activity, 10^{-9} ma/g
D51	74.0	0.05427	1364
D52	56.1	0.08075	695
D53	29.2	0.03121	934
D54	10.2	0.04270	239
D55	18.2	0.03604	506
D56	23.8	0.05450	437
D57	58.9	0.13585	434
D58	28.9	0.03044	950
D59	44.7	0.05158	867
D60	14.9	0.12899	116
D61	32.1	0.18481	174
D62	0.0281	0.01428	1.97
D63	86.9	0.63376	137
D64	106	0.49106	216
D65	6.54	0.03528	185
D66	10.7	0.02231	480
D67	18.0	0.01301	1385
D68	19.5	0.06165	317
D69	12.8	0.00910	1407
D70	51.3	0.65085	1009
D71	17.5	0.02085	839
D72	21.3	0.01382	1540
D73	3.14	0.01374	229
D74	27.6	0.21751	127
D75	166	0.23446	708
D76	57.2	0.45692	125
D77	83.0	0.04150	2000
D78	42.8	0.56415	75.9
D79	83.5	0.45220	185
D80	43.1	0.25943	166
D81	25.2	0.47170	53.5
D82	57.0	0.44835	127
D83	48.5	0.29992	162
D84	44.7	0.27643	162
D85	112	0.47056	239
D86	33.2	0.33141	100
D87	70.8	0.46770	151
D88	40.4	0.10960	370
D89	43.9	0.21319	206
D90	31.8	0.18556	171.3
D91	44.5	0.22023	202
D92	31.8	0.13071	232
D93	37.7	0.14253	264
D94	41.2	0.16098	256
D95	40.7	0.19490	209
D96	134	0.18370	729
D97	7.40	0.26074	36.8
D98	109	0.14427	756
D99	33.5	0.18454	181
D100	119	0.09242	1290

TABLE B.18 — (Continued)

Sample	Activity at H+850 hr, 10^{-9} ma	Weight, g	Specific activity, 10^{-9} ma/g
D101	12.2	0.00760	1605
D102	19.1	0.01753	1089.5
D103	60.4	0.03686	1640
D104	22.6	0.02120	1067
D105	20.4	0.01251	1633
D106	3.17	0.00420	755
D107	13.1	0.01557	839
D108	64.7	0.04581	1413
D109	37.2	0.04894	760
D110	53.6	0.02832	1899
D111	11.9	0.01173	1015
D112	16.8	0.01981	846
D113	15.1	0.01880	804
D114	3.58	0.00950	376
D115	23.0	0.02862	804
D116	5.88	0.01312	448
D117	75.1	0.05802	1294
D118	11.7	0.02503	468
D119	52.3	0.07151	732
D120	22.0	0.03030	724
D121	21.0	0.01184	1780
D122	46.3	0.03663	1266
D123	37.0	0.04667	796
D124	50.4	0.07032	716
D125	8.0	0.01530	523

TABLE B.19 — ALIQUOT DESIGNATION AND PURPOSE OF CLOUD FILTER-PAPER SAMPLE, SHOT DIABLO

Sample	Purpose	GIC activity at H+56 hr, 10^{-9} ma
IIF1	Cloud sample; DH count = 1.05×10^4 counts/min at H+56 hr	90.1
IIF1A	Aliquot for GIC decay	41.6
IIF1B	Preliminary aliquot; aliquots IIF1Ba, b, and c removed	48.5
IIF1Ba	Preliminary aliquot; aliquots IIF1Baa and b removed	5.33
IIF1Baa	Aliquot for WC decay	3.11
IIF1Bab	Aliquot for WC decay	2.20
IIF1Bb	Aliquot for radiochemical analysis; fissions = 4.68×10^{11}	26.2
IIF1Bc	Aliquot for radiochemical analysis; fissions = 3.09×10^{11}	17.0

TABLE B.20 — WC ASSAY OF CWS FILTER SAMPLES, SHOT DIABLO

Sample	Time of exposure, H+min	Fissions ($\times 10^{10}$)	Cumulative fissions ($\times 10^{10}$)
	Total Sample		
IIEO1	*	9.57	
	M6 Intake Sample		
IIEM1	7–9	0.0256	0.0256
2	10–12	0.549	0.575
3	13–15	1.09	1.67
4	16–18	0.581	2.25
5	19–21	0.481	2.73
6	22–24	0.373	3.10
7	25–27	0.107	3.21
8	28–30	0.0563	3.26
9	31–33	0.158	3.42
10	34–36	0.0162	3.44
11	37–39	0.0244	3.46
12	40–42	0.0133	3.48
13	43–45	0.102	3.58
14	46–48	0.0189	3.60
15	49–51	0.0140	3.61
16	52–54	0.0121	3.62
17	55–57	0.00849	3.63
18	58–60	0.00512	3.64
19	61–63	0.00705	3.64
20	64–66	0.00789	3.65
21	67–72	0.0127	3.66
22	73–78	0.0116	3.68
23	79–109	0.0474	3.72
24	240–260	0.0534	3.78
	Door Intake Sample		
IIED1	7–9	0.104	0.104
2	10–12	2.79	2.89
3	13–15	3.94	6.83
4	16–18	2.18	9.01
5	19–21	2.19	11.2
6	22–24	1.87	13.1
7	25–27	0.310	13.4
8	28–30	0.000542	13.4
9	31–33	0.00976	13.4
10	34–36	0.00894	13.4
11	37–39	0.00778	13.4
12	40–42	0.00850	13.4
13	43–45	0.254	13.7
14	46–48	0.00708	13.7
15	49–51	0.0137	13.7
16	52–54	0.00739	13.7

TABLE B.20 — (Continued)

Sample	Time of exposure, H+min	Fissions ($\times 10^{10}$)	Cumulative fissions ($\times 10^{10}$)
	Door Intake Sample (Continued)		
IIED17	55–57	0.00634	13.7
18	58–60	0.00588	13.7
19	61–63	0.00315	13.7
20	64–66	0.00393	13.7
21	67–72	0.00708	13.7
22	Missing		
23	79–94	0.00772	13.7
24	95–105	0.118	13.9
	Cyclic Air Sample		
†	*	0.0956	0.0956
IIE1		0.366	0.4606
2		0.994	1.46
3		1.583	3.04
4		2.338	5.38
5		0.822	6.20
6		0.946	7.14
7		0.860	8.00
8		0.269	8.27
9		0.152	8.43
10		0.0410	8.47
11		0.0151	8.48
12		0.168	8.50
13		0.00993	8.51
14		0.00923	8.52
15		0.00535	8.52
16		0.00983	8.53
17		0.312	8.84
18		0.0152	8.86
19		0.00503	8.86

*No information available.

†No identification. Comments on container: "Cyclic air samples; first sample in position at time of blast."

TABLE B.21 — ASSAY OF AIR-DUCT FILTER SAMPLES, SHOT DIABLO

Sample	DH activity at H+56 hr, 10^4 counts/min	Total fissions ($\times 10^{12}$)
IIH1	1.76	4.35
IIH2	1.71	4.22

(a) *Fallout Samples.* Twelve OCC's (designated IVA1 to IVA12) and six AOC's (designated IVB1 to IVB6) were recovered after shot Shasta. The initial DH assay values and weights of these samples are given in Table B.23.

TABLE B.22—WC ASSAY OF PRESHOT SURFACE-SOIL SAMPLES

Sample	Activity,* counts/min	Sample	Activity,* counts/min
IIG1A	472	IIG1G	238
IIG1B	95	IIG1H	77
IIG1C	432	IIG1I	101
IIG1D	150	IIG1J	113
IIG1E	326	IIG1K	1740
IIG1F	1152	IIG1L	474

*Measured 14 days prior to Diablo Shot.

TABLE B.23—WEIGHT AND ACTIVITY OF OCC AND AOC SAMPLES, SHOT SHASTA

Sample	Weight,* g	DH assay at H+56 hr,† 10^6 counts/min	Total fissions ($\times 10^{14}$)	Np^{239} atoms / Fission
IVA1	3.5981	2.80	7.61‡	0.133
IVA2		0.0337	0.0907	
IVA3		2.17	5.84	
IVA4	3.1862	2.75	7.47‡	0.142
IVA5		0.115	0.309	
IVA6	1.3207	2.54	6.90‡	0.138
IVA7		1.44	3.87	
IVA8		3.83	10.30	
IVA9	2.6848	4.37	11.76‡	0.140
IVA10		6.90	18.56	
IVA11		5.73	15.41	
IVA12	3.4417	6.54	17.59	0.139
IVB1		0.00134	0.00360	
IVB2		0.0635	0.171	
IVB3		0.00450	0.0121	
IVB4		0.000306	0.000823	
IVB5		0.000055	0.000148	
IVB6		0.000147	0.000395	

*Not true fallout, includes shock-wave-raised dust.

†Computed from the decay of sample IVA5 (Table B.24).

‡Fissions were measured directly on aliquots of these samples. The remaining fission values were computed from 2.69×10^8 fissions/DH counts/min at H+56 hr.

Samples IVA5 and IVB2 were retained intact. The decay rates of these samples were measured on the DH. Values obtained are shown in Tables B.24 and B.25.

Further analyses, as described in Table B.26, were performed on aliquots from samples IVA1, IVA4, IVA6, IVA9, and IVA12. One aliquot from each sample was periodically measured in the GIC to establish decay rates. These aliquots were designated IVA1B, IVA4A, IVA6A, IVA9A, and IVA12A. The results of the GIC measurements are listed in Table B.27. Additional

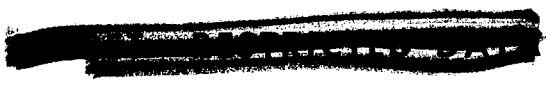

GIC aliquots from sample IVA1 were prepared to test the effect on measured decay rates of sealing samples. For these measurements aliquot IVA1D was sealed with paraffin prior to counting and compared with aliquot IVA1C (which was unsealed), as shown in Table B.27.

TABLE B.24—DH DECAY DATA FOR SAMPLE IVA5

Time, H+hr	Activity, 10^5 counts/min	Time, H+hr	Activity, 10^5 counts/min
40.2	1.55	249	0.152
44.0	1.44	318	0.111
51.7	1.23	387	0.0713
58.6	1.09	464	0.0544
80.2	0.784	627	0.0374
100	0.616	781	0.0286
130	0.434	968	0.0219
195	0.231	1200	0.0134

Decay rates were also measured in the WC. This was done with aliquots IVA1G and IVA9C (Table B.28). X-ray-diffraction analysis was carried out on aliquot IVA12C. Chemical analyses were made of aliquots IVA11, IVA4D, IVA9E, and IVA12D. Table B.29 records the results of the X-ray examinations; Table B.30 lists the chemical data.

Total fission measurements and product-to-fission evaluations were made on Shasta samples, as shown in Table B.26. Additional total fission values were computed (based on measurements of aliquots from samples IVA1, IVA4, IVA6, IVA9, and IVA12), and the results are given in Table B.23.

TABLE B.25—DH DECAY DATA FOR SAMPLE IVB2

Time, H+hr	Activity, 10^5 counts/min	Time, H+hr	Activity, 10^5 counts/min
36.3	9.06	249	0.830
44.3	7.68	318	0.602
55.5	6.69	387	0.382
57.8	5.96	464	0.292
80.3	4.32	627	0.195
100.2	3.33	781	0.153
130.3	2.38	968	0.120
195.3	1.29	1200	0.082

The 56 IC samples received were designated IVC1,457 to IVC1,512. Sample IVC1,462 was the first sample exposed at H+30 sec, and each subsequent tray was exposed for approximately 1 min. The trays were individually assayed on the end-on gamma counter. Results obtained are listed in Table B.31.

(b) *Filter Samples*. Several types of CWS filter samples were received. They were assayed in the manner dictated by their particular size and shape. No filter-paper cloud sample was received from this shot.

Thirty-one filter-paper samples (designated IVEO1, IVEM1 to IVEM15, and IVED1 to IVED15) plus one roll of filter tape from the cyclic air sampler were received. The individual samples were counted in the WC in the same manner as for the Diablo filter samples. Counting results are given in Table B.32.

TABLE B.26—ALIQUOT DESIGNATION AND PURPOSE OF FALLOUT SAMPLES, SHOT SHASTA

Sample	Purpose	Weight, g	GIC activity at H+56 hr, 10^{-9} ma
	Sample IVA1		
IVA1	OCC sample; DH count = 2.80×10^6 counts/min at H+56 hr. Material removed from tray, and ground and aliquots prepared	3.5981	
IVA1A	Aliquot for radiochemistry; fissions = 2.20×10^{13}; product to fission ratio = 0.133	0.1053	728
IVA1B	Aliquot for GIC decay; diluted with 25.0 g of IIG1	0.2004	1370
IVA1C	Aliquot for GIC decay; sample not diluted or sealed in order to compare with IVA1D	0.1984	1360
IVA1D	Aliquot for GIC decay; sample undiluted and sealed with paraffin in order to compare with IVA1C	0.1963	1350
IVA1E	Aliquot submitted to Nucleonics Division for gamma spectral measurements	0.1993	1450
IVA1F	Aliquot submitted to Nucleonics Division for gamma spectral measurements	0.0524	365
IVA1G	Aliquot for WC decay; diluted with 2.0 g of IIG1		1.63
IVA1I	Aliquot for chemical analysis		
	Sample IVA4		
IVA4	OCC sample; DH count = 2.75×10^6 counts/min at H+56 hr. Material removed from tray, and ground and aliquots prepared	3.1862	
IVA4A	Aliquot for GIC decay	0.2047	1480
IVA4B	Aliquot for radiochemical analysis; fissions = 1.91×10^{13}; product to fission ratio = 0.142	0.0898	621
IVA4D	Aliquot for chemical analysis		
	Sample IVA6		
IVA6	OCC sample; DH count = 2.54×10^6 counts/min at H+56 hr. Material removed from tray, and ground and aliquoted	1.3207	
IVA6A	Aliquot for GIC decay; diluted with 25.0 g of IIG1	0.0979	1530
IVA6B	Aliquot for radiochemical analysis; fissions = 3.11×10^{13}; product to fission ratio = 0.138	0.0583	905
	Sample IVA9		
IVA9	OCC sample; DH count = 4.37×10^6 counts/min at H+56 hr. Material removed from tray, and ground and aliquots prepared	2.6848	
IVA9A	Aliquot for GIC decay; diluted with 25.0 g of IIG1	0.1008	1500
IVA9B	Aliquot for radiochemical analysis; fissions = 2.41×10^{13}; product to fission ratio = 0.140	0.0504	721
IVA9C	Aliquot for WC decay; diluted with 2.0 g of IIG1		2.39
IVA9E	Aliquot for chemical analysis		

TABLE B.26 — (Continued)

Sample	Purpose	Weight, g	GIC activity at H+56 hr, 10^{-9} ma
	Sample IVA12		
IVA12	OCC sample; DH count = 6.54×10^6 counts/min at H+56 hr. Material removed from tray, and ground and aliquots prepared	3.4417	
IVA12A	Aliquot for GIC decay; diluted with 25.0 g of IIG1	0.1012	2120
IVA12B	Aliquot for radiochemical analysis; fissions = 3.37×10^{13}; product to fission ratio = 0.139	0.0468	994
IVA12C	Aliquot for X-ray analysis		
IVA12D	Aliquot for chemical analysis		

TABLE B.27—GIC DECAY DATA FOR FALLOUT SAMPLES, SHOT SHASTA

Time, H+hr	OCC samples, 10^{-9} ma						
	IVA1B	IVA4A	IVA6A	IVA9A	IVA12A	IVA1C	IVA1D
42.6	1880	1960					
43.7						1820	1810
44.5				1870		1770	1750
47.6	1590	1720	1820	1730	2600	1600	1560
51.4	1450	1540	1620	1570	2360	1460	1430
48.6	1220	1290	1360	1310	1990	1230	1200
75.6	839	883	934	903	1440	848	824
82.8	744	788	834	805	1275	754	735
101	578	612	650	628	952	587	572
124	451	478	507	491	743	458	446
131	427	452	478	463	703	433	422
196	273	288	308	298	451	278	272
244	214	225	238	230	351	218	213
291	175	183	195	188	290	177	173
384	127	137	143	137	215	131	126
461	106	114	121	114	177	110	108
580	88.0	92.5	95.0	94.1	143	88.8	87.6
800	59.7	62.8	66.5	63.9	96.0	61.3	59.4
965	48.1	51.5	54.0	51.7	78.6	49.6	48.5
1210	37.6	39.9	41.8	40.1	60.4	38.5	37.6
1520	28.7	30.5	31.6	30.4	45.8	29.5	28.6
1870	23.4	24.8	26.0	24.9	37.4	24.0	23.4
2300	19.2	20.0	21.1	20.2	30.4	19.6	18.9
2950	14.6	15.5	16.0	15.3	23.1	14.9	14.3
3450	11.6	12.4	13.3	12.6	19.0	11.9	11.6

TABLE B.28—WC DECAY DATA FOR FALLOUT SAMPLES, SHOT SHASTA

Time, H+hr	OCC samples, 10^4 counts/min		Filter sample, 10^4 counts/min
	IVA1G	IVA9C	IVEM8
44.1	157		
45.6		268	
47.8	144	253	
51.9	134	237	
75.8	93.0	162	
80.8			133
99.4	67.0	117	105
132	46.5	80.5	75.0
195	25.2	42.9	40.7
245	17.1	29.0	27.5
293	12.4	21.2	19.9
389	7.45	13.0	11.6
460	5.76	10.0	8.68
559		7.49	
580	4.26		5.90
772	3.01	5.21	3.82
965	2.33	4.12	2.81
1200	1.82	3.25	2.10
1550	1.36	2.41	1.51
1880	1.10	1.93	1.19
2280	0.867	1.55	0.925
2430	0.805	1.44	0.848
2980	0.632	1.12	0.663
3490	0.509	0.904	0.529

TABLE B.29—X-RAY-DIFFRACTION ANALYSIS OF FALLOUT SAMPLE IVA1C,* SHOT SHASTA

Quartz (SiO_2)	+
Feldspar [$(Na,K)AlSi_3O_8$]	+
Magnetite† (Fe_3O_4)	$3\frac{1}{2}$%
Hematite (Fe_2O_3)	ND
Iron (Fe)	ND
Calcite ($CaCO_3$)	ND
Dolomite [$(Ca,Mg)CO_3$]	+

*+, qualitatively identified; ND, not detectable.

†Value given represents upper limit of quantity; it may be too high by as much as 50 per cent.

TABLE B.30—CHEMICAL ANALYSIS OF FALLOUT SAMPLES, SHOT SHASTA

	Sample			
	IVA11	IVA4D	IVA9E	IVA12D
Weight, g	0.5040	0.4955	0.4996	0.5007
Moisture, g	0.0038	0.0036	0.0034	0.0026
Organic matter, g	0.0378	0.0321	0.0346	0.0340
Total lead, mg	1.16	1.17	2.91	3.96
Total iron, mg	15	17	25	32

TABLE B.31—ASSAY OF IC SAMPLES, SHOT SHASTA

Sample	Activity at H+77 hr, counts/min	Cumulative activity, 10^6 counts/min	Sample	Activity at H+77 hr, counts/min	Cumulative activity, 10^6 counts/min
IVC1,457	64	0.000064	IVC1,485	115	12.2
458	94	0.000158	486	165	12.2
460	389	0.000547	487	120	12.2
459	429	0.000976	488	200	12.2
461	159	0.00114	489	215	12.2
462	3	0.00114	490	280	12.2
463	23	0.00116	491	355	12.2
464	87	0.00125	492	220	12.2
465	970,000	0.971	493	180	12.2
466	2,390,000	3.36	494	175	12.2
467	2,160,000	5.52	495	125	12.2
468	4,300,000	9.82	496	180	12.2
469	830,000	10.7	497	165	12.2
470	420,000	11.1	498	175	12.2
471	176,000	11.2	499	135	12.2
472	630,000	11.9	500	225	12.2
473	135	11.9	501	210	12.2
474	1,210	11.9	502	195	12.2
475	126,850	12.0	503	160	12.2
476	75	12.0	504	195	12.2
477	40	12.0	505	180	12.2
478	5	12.0	506	135	12.2
479	110	12.0	507	185	12.2
480	202,000	12.2	508	80	12.2
481	135	12.2	509	85	12.2
482	95	12.2	510	145	12.2
483	115	12.2	511	50	12.2
484	125	12.2	512	65	12.2

TABLE B.32—WC ASSAY OF CWS FILTER SAMPLES, SHOT SHASTA

Sample	Time of exposure, H+min	Fissions ($\times 10^{10}$)	Cumulative fissions ($\times 10^{10}$)
	Total Sample*		
IVEO1	18–71	171	
	M6 Intake Sample*		
IVEM1	11.8–13.8	0.0304	0.0304
2	14.5–17.5	0.000787	0.0312
3	18.5–21.5	3.68	3.71
4	22.7–25.7	0.952	4.66
5	26.5–29.5	4.39	9.05
6	30.5–33.5	3.67	12.7
7	34.5–37.5	5.73	18.5
8†	38.5–41.5	7.53	26.0
9	42.5–45.5	6.80	32.8
10	46.5–49.5	8.09	40.9
11	51.5–54.5	5.23	46.1
12	55.5–58.5	3.37	49.5
13	59.5–62.5	2.80	52.3
14	63.5–66.5	2.45	54.7
15	68.0–71.0	1.89	56.6
	Door Intake Sample*		
IVED1	11.8–13.8	0.000303	0.0003
2	14.5–17.5	0.00352	0.0038
3	18.5–21.5	7.02	7.03
4	22.7–25.7	3.43	10.5
5	26.5–29.5	7.87	18.3
6	30.5–33.5	6.91	25.2
7	34.5–37.5	9.05	34.3
8	38.5–41.5	12.1	46.4
9	42.5–45.5	11.1	57.5
10	46.5–49.5	13.4	71.0
11	51.5–54.5	8.32	79.3
12	55.5–58.5	4.94	84.2
13	59.5–62.5	4.21	88.4
14	63.5–66.5	3.65	92.0
15	68.0–71.0	2.16	94.3
	Cyclic Air Sample*		
IVE1	No information	0.00475	0.0047
2		0.00239	0.0071
3		0.000786	0.0079
4		0.00518	0.0131
5		0.00799	0.0211
6		0.0117	0.0328
7		0.00188	0.0347
8		0.00211	0.0368
9		0.00802	0.0448
10		0.00234	0.0471
11		0.00633	0.0534
12		0.00470	0.0581
13‡		0.00696	0.0651
	Cyclic Air Sample* (Continued)		
IVE14	No information	0.0124	0.0775
15		0.0101	0.0876
16		5.02	5.10
17		0.00493	5.11
18		3.27	8.38
19		3.22	11.6
20		3.26	14.8
21		4.06	18.9
22		3.91	22.8
23		3.95	26.7
24		4.52	31.3
25		3.72	35.0
26		5.07	40.0
27		6.60	46.6
28		5.72	52.4
29		4.65	57.0
30		4.60	61.6
31		5.13	66.7
32		4.82	71.6
33		4.07	75.6
34		3.39	79.0
35		2.78	81.8
36		2.88	84.7
37		2.16	86.8
38		1.64	88.5
39		2.05	90.5
40		1.64	92.2
41		0.00355	92.2
42		0.0247	92.2
43		1.50	93.7
44		0.0376	93.7
45		0.0246	93.8
46		0.0203	93.8
47		0.00231	93.8
48		0.0219	93.8
49		0.00318	93.8
50		0.00404	93.8
51		0.00236	93.8
52		0.00205	93.8
53		0.00159	93.8
54		0.00179	93.8
55		0.000687	93.8
56		0.00137	93.8
57		0.000418	93.8
58		0.000597	93.8
59		0.00117	93.8
60		0.000587	93.8

*So designated in field.
†Assigned to WC decay.
‡Sample was bright red in color.

The roll of filter tape (cyclic air sample) was unwound from the spool, and the active portions were located with the aid of a survey-meter probe. The active sections were then cut from the tape and assayed in the WC. A total of 60 samples was removed from the tape in this manner. No further samples were removed, although approximately one-half the roll remained. The early samples were easily identified by a heavy layer of dust. Sample 13 was bright red in

TABLE B.33—DH ASSAY OF AIR-DUCT FILTER SAMPLES, SHOT SHASTA

Sample	DH activity at H+56 hr, 10^4 counts/min	Computed fissions* ($\times 10^{13}$)
IVH1	7.66	2.06
IVH2	6.32	1.70

*Computed from 2.69×10^8 fissions/DH counts/min at H+56 hr.

color, apparently from a dye material. Later samples were detectable only through their activity, the amount of dust being very low. The cyclic air samples were designated IVE1 to IVE60. Table B.32 lists the results obtained. The decay of filter sample IVEM8 was followed on the WC. The results are listed in Table B.28.

The two large air-duct filter samples were designated in IVH1 and IVH2 and assayed on the DH. The results are shown in Table B.33 together with computed total fission values.

REFERENCE

1. L. D. McIsaac, Determination of Np^{239}, Total Fissions, Mo^{99}, and Ce^{141} in Fission-product Mixtures by Gamma-ray Scintillation Spectrometry, U. S. Naval Radiological Defense Laboratory, Report TR-72.

Appendix C

ROENTGENS PER HOUR PER PHOTON AS A FUNCTION OF ENERGY

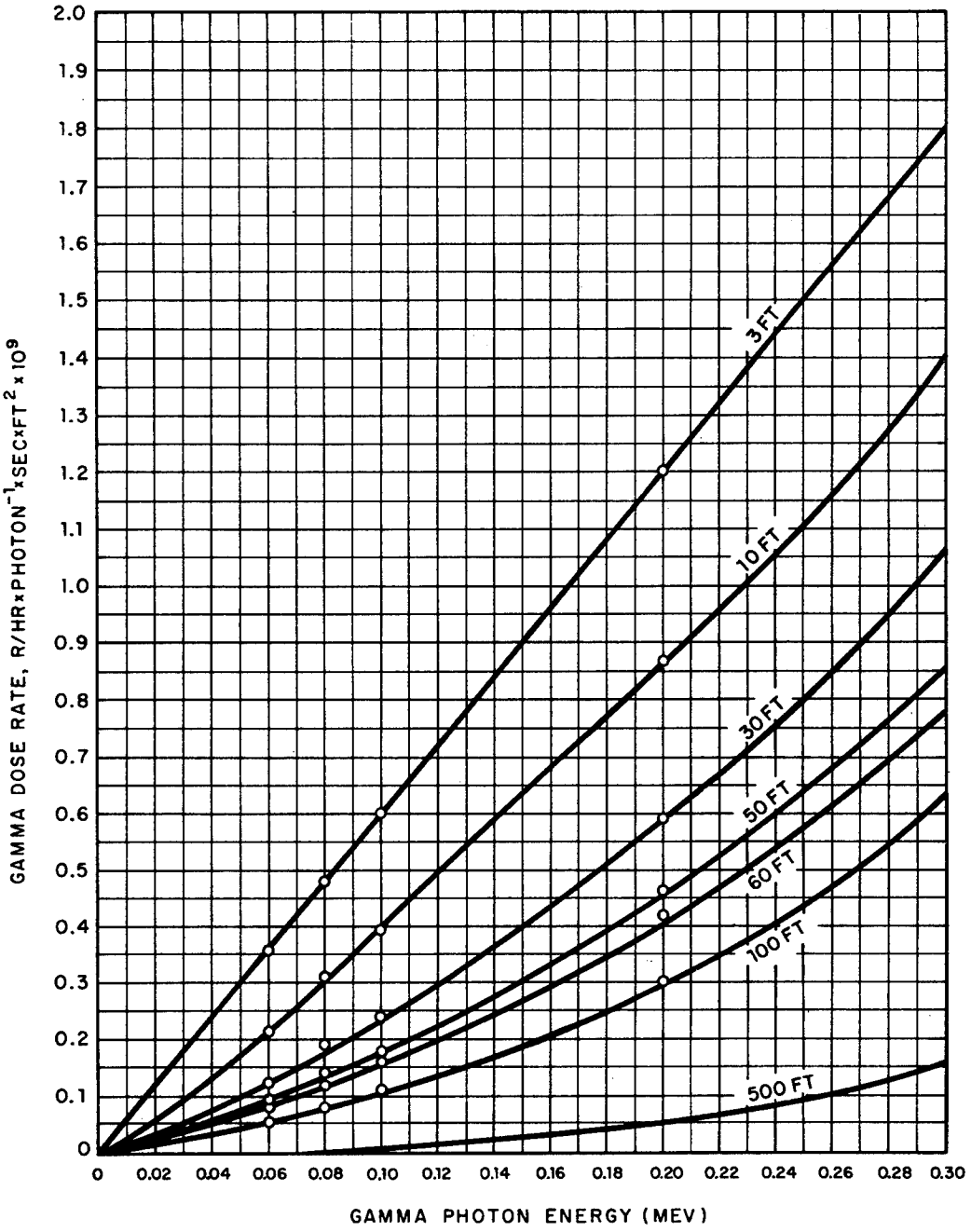

Fig. C.1—Gamma dose rate as a function of energy and height above an infinite smooth plane (0.0 to 0.30 Mev).

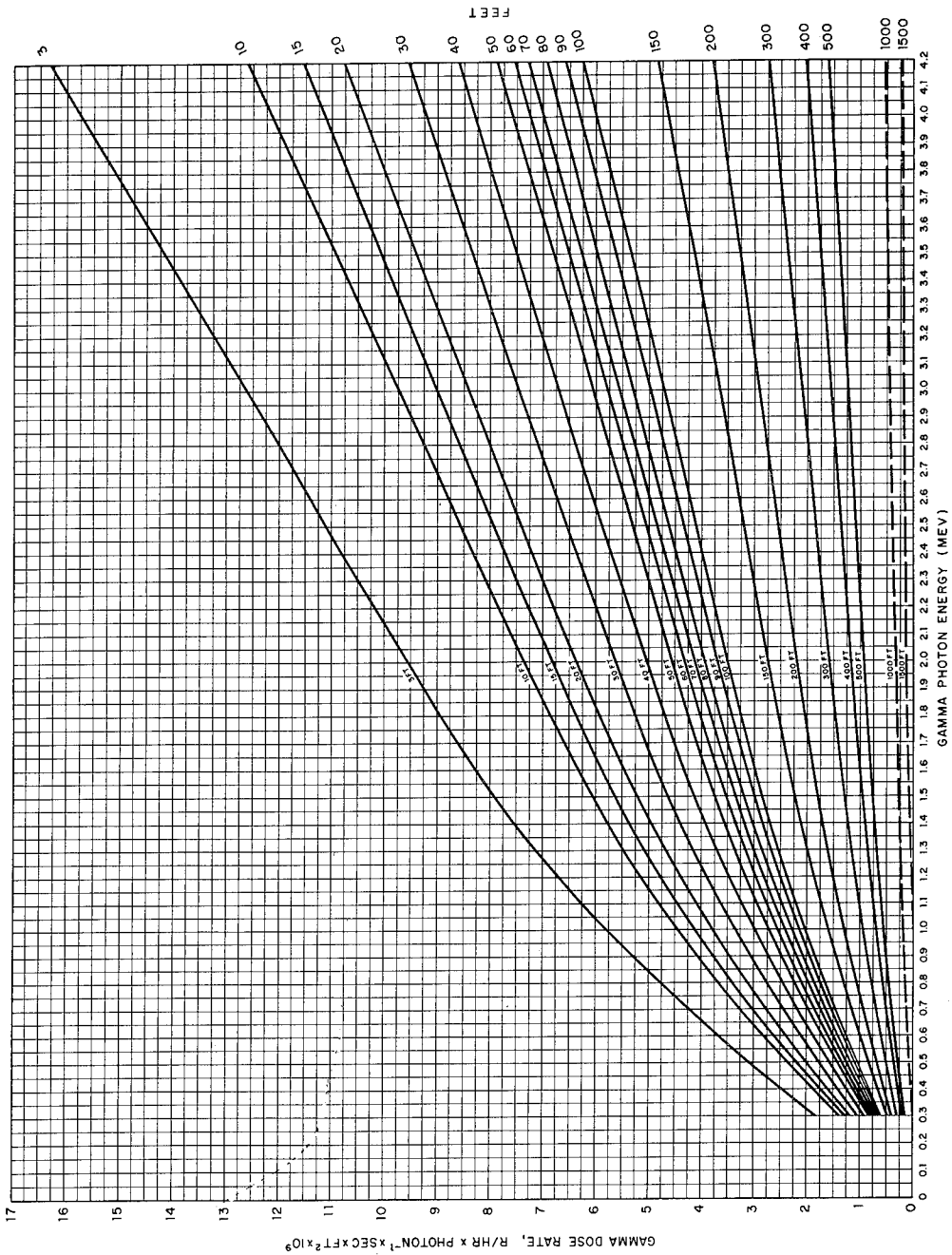

Fig. C.2—Gamma dose rate as a function of energy and height above an infinite smooth plane (0.3 to 4.2 Mev).

DISTRIBUTION

Military Distribution Category 26

ARMY ACTIVITIES

Deputy Chief of Staff for Military Operations, D/A, Washington 25, D. C. ATTN: Dir. of SW&R	1
Chief of Research and Development, D/A, Washington 25, D. C. ATTN: Atomic Div.	2
Assistant Chief of Staff, Intelligence, D/A, Washington 25, D. C.	3
Chief Chemical Officer, D/A, Washington 25, D. C.	4–5
Chief of Engineers, D/A, Washington 25, D. C. ATTN: ENGNB	6
Chief of Engineers, D/A, Washington 25, D. C. ATTN: ENGTB	7
Office, Chief of Ordnance, D/A, Washington 25, D. C. ATTN: ORDTN	8–9
Chief Signal Officer, D/A, Comb. Dev. and Ops. Div., Washington 25, D. C. ATTN: SIGCO-4	10
Chief of Transportation, D/A, Office of Planning and Int., Washington 25, D. C.	11
The Surgeon General, D/A, Washington 25, D. C. ATTN: MEDNE	12–13
Commanding General, U. S. Continental Army Command, Ft. Monroe, Va.	14–16
Director of Special Weapons Development Office, Headquarters CONARC, Ft. Bliss, Tex. ATTN: Capt. Chester I. Peterson	17
President, U. S. Army Artillery Board, U. S. Continental Army Command, Ft. Sill, Okla.	18
President, U. S. Army Air Defense Board, U. S. Continental Army Command, Ft. Bliss, Tex.	19
President, U. S. Army Aviation Board, Ft. Rucker, Ala. ATTN: ATBG-DG	20
Commanding General, First United States Army, Governor's Island, New York 4, N. Y.	21
Commanding General, Second U. S. Army, Ft. George G. Meade, Md.	22
Commanding General, Third United States Army, Ft. McPherson, Ga. ATTN: ACofS, G-3	23
Commanding General, Fourth United States Army, Ft. Sam Houston, Tex. ATTN: G-3 Section	24
Commanding General, Fifth United States Army, 1660 E. Hyde Park Blvd., Chicago 15, Ill.	25
Commanding General, Sixth United States Army, Presidio of San Francisco, San Francisco, Calif. ATTN: AMGCT-4	26
Commanding General, Military District of Washington, USA, Room 1543, Bldg. T-7, Gravelly Point, Va.	27
Commandant, Army War College, Carlisle Barracks, Pa. ATTN: Library	28
Commandant, U. S. Army Command & General Staff College, Ft. Leavenworth, Kans. ATTN: ARCHIVES	29
Commandant, U. S. Army Air Defense School, Ft. Bliss, Tex. ATTN: Dept. of Tactics and Combined Arms	30
Commandant, U. S. Army Armored School, Ft. Knox, Ky.	31
Commandant, U. S. Army Artillery and Missile School, Ft. Sill, Okla. ATTN: Combat Development Department	32
Commandant, U. S. Army Aviation School, Ft. Rucker, Ala.	33
Commandant, U. S. Army Infantry School, Ft. Benning, Ga. ATTN: C.D.S.	34
The Superintendent, U. S. Military Academy, West Point, N. Y. ATTN: Prof. of Ordnance	35
Commandant, The Quartermaster School, U. S. Army, Ft. Lee, Va. ATTN: Chief, QM Library	36
Commandant, U. S. Army Ordnance School, Aberdeen Proving Grounds, Md.	37
Commandant, U. S. Army Ordnance and Guided Missile School, Redstone Arsenal, Ala.	38
Commanding General, Chemical Corps Training Comd., Ft. McClellan, Ala.	39

[redacted]

Commandant, USA Signal School, Ft. Monmouth, N. J. 40
Commandant, USA Transport School, Ft. Eustis, Va. ATTN: Security and Info. Off. 41
Commanding General, The Engineer Center, Ft. Belvoir, Va. ATTN: Asst. Cmdt., Engr. School 42
Commanding General, Army Medical Service School, Brooke Army Medical Center, Ft. Sam Houston, Tex. 43
Director, Armed Forces Institute of Pathology, Walter Reed Army Med. Center, 625 16th St., NW, Washington 25, D. C. 44
Commanding Officer, Army Medical Research Lab., Ft. Knox, Ky. 45
Commandant, Walter Reed Army Inst. of Res., Walter Reed Army Medical Center, Washington 25, D. C. 46
Commanding General, QM R&D Comd., QM R&D Cntr., Natick, Mass. ATTN: CBR Liaison Officer 47–48
Commanding General, U. S. Army Chemical Corps, Research and Development Comd., Washington 25, D. C. 49–50
Commanding Officer, Chemical Warfare Lab., Army Chemical Center, Md. ATTN: Tech. Library 51–52
Commanding General, Engineer Research and Dev. Lab., Ft. Belvoir, Va. ATTN: Chief, Tech. Support Branch 53
Director, Waterways Experiment Station, P. O. Box 631, Vicksburg, Miss. ATTN: Library 54
Commanding Officer, Diamond Ord. Fuze Labs., Washington 25, D. C. ATTN: Chief, Nuclear Vulnerability Br. (230) 55
Commanding General, Aberdeen Proving Grounds, Md. ATTN: Director, Ballistic Research Laboratories 56–57
Commanding Officer, USA Signal R&D Laboratory, Ft. Monmouth, N. J. 58
Commanding General, U. S. Army Electronic Proving Ground, Ft. Huachuca, Ariz. ATTN: Tech. Library 59
Commanding General, USA Combat Surveillance Agency, 1124 N. Highland St., Arlington, Va. 60
Commanding Officer, USA Signal R&D Laboratory, Ft. Monmouth, N. J. ATTN: Tech. Doc. Ctr., Evans Area 61
Director, Operations Research Office, Johns Hopkins University, 6935 Arlington Rd., Bethesda 14, Md. 62
Commander-in-Chief, U. S. Army Europe, APO 403, New York, N. Y. ATTN: Opot. Div., Weapons Br. 63
Commanding General, Southern European Task Force, APO 168, New York, N. Y. ATTN: ACofS, G-3 64
Commanding General, Eighth U. S. Army, APO 301, San Francisco, Calif. ATTN: ACofS, G-3 65
Commanding General, U. S. Army Alaska, APO 942, Seattle, Wash. 66
Commanding General, U. S. Army Caribbean, Ft. Amador, C. Z. ATTN: Ordnance Officer 67
Commander-in-Chief, U. S. Army Pacific, APO 958, San Francisco, Calif. ATTN: Ordnance Officer 68
Commanding General, USARFANT & MDPR, Ft. Brooke, P. R. 69
Commander-in-Chief, EUCOM, APO 128, New York, N. Y. 70
Commanding Officer, 9th Hospital Center, APO 180, New York, N. Y. ATTN: CO, U. S. Army Nuclear Medicine Research Detachment, Europe 71

NAVY ACTIVITIES

Chief of Naval Operations, D/N, Washington 25, D. C. ATTN: OP-03EG 72
Chief of Naval Operations, D/N, Washington 25, D. C. ATTN: OP-36 73
Chief of Naval Operations, D/N, Washington 25, D. C. ATTN: OP-922G2 74
Chief of Naval Personnel, D/N, Washington 25, D. C. 75
Chief of Naval Research, D/N, Washington 25, D. C. ATTN: Code 811 76–77
Chief, Bureau of Aeronautics, D/N, Washington 25, D. C. 78–79
Chief, Bureau of Medicine and Surgery, D/N, Washington 25, D. C. ATTN: Special Wpns. Def. Div. 80–81
Chief, Bureau of Ordnance, D/N, Washington 25, D. C. 82
Chief, Bureau of Ships, D/N, Washington 25, D. C. ATTN: Code 423 83
Chief, Bureau of Yards and Docks, D/N, Washington 25, D. C. ATTN: D-440 84
Director, U. S. Naval Research Laboratory, Washington 25, D. C. ATTN: Mrs. Katherine H. Cass 85
Commander, U. S. Naval Ordnance Laboratory, White Oak, Silver Spring 19, Md. 86–87
Director, Material Lab. (Code 900), New York Naval Shipyard, Brooklyn 1, N. Y. 88

[redacted]

Director, USAF Project RAND, VIA: USAF Liaison Office, The RAND Corp., 1700 Main St., Santa Monica, Calif. 144–145
Assistant Chief of Staff, Intelligence, HQ., USAFE, APO 633, New York, N. Y. ATTN: Directorate of Air Targets 146
Commander, Alaskan Air Command, APO 942, Seattle, Wash. ATTN: AAOTN 147
Commander-in-Chief, Pacific Air Forces, APO 953, San Francisco, Calif. ATTN: PFCIE-MB, Base Recovery 148

OTHER DEPARTMENT OF DEFENSE ACTIVITIES

Assistant Secretary of Defense, Research and Engineering, DOD, Washington 25, D. C. ATTN: Tech. Library 149
Executive Secretary, Military Liaison Committee, P. O. Box 1814, Washington 25, D. C. 150
Director, Weapons Systems Evaluation Group, Room 1E880, The Pentagon, Washington 25, D. C. 151
Commandant, The Industrial College of the Armed Forces, Ft. McNair, Washington 25, D. C. 152
Commandant, Armed Forces Staff College, Norfolk 11, Va. ATTN: Secretary 153
Chief, Armed Forces Special Weapons Project, Washington 25, D. C. 154–161
Commander, Field Command, AFSWP, Sandia Base, Albuquerque, N. Mex. 162
Commander, Field Command, AFSWP, Sandia Base, Albuquerque, N. Mex. ATTN: FCTG 163
Commander, Field Command, AFSWP, Sandia Base, Albuquerque, N. Mex. ATTN: FCWT 164–168
Commander, JTF-7, Arlington Hall Station, Arlington 12, Va. 169
U. S. Documents Officer, Office of the United States National Military Representative, SHAPE, APO 55, New York, N. Y. 170

ATOMIC ENERGY COMMISSION ACTIVITIES

U. S. Atomic Energy Commission, Technical Library, Washington 25, D. C. ATTN: (for DMA) 171–173
Los Alamos Scientific Laboratory, Report Library, P. O. Box 1663, Los Alamos, N. Mex. ATTN: Helen Redman 174–175
Sandia Corporation, Classified Document Division, Sandia Base, Albuquerque, N. Mex. ATTN: H. J. Smyth, Jr. 176–180
University of California Lawrence Radiation Laboratory, P. O. Box 808, Livermore, Calif. ATTN: Clovis G. Craig 181–183
Weapon Data Section, Technical Information Service Extension, Oak Ridge, Tenn. 184
Technical Information Service Extension, Oak Ridge, Tenn. (surplus) 185–215

[redacted]